

Aus dem Biomedizinischen Centrum
Lehrstuhl: Physiologische Chemie
Institut der Ludwig-Maximilians-Universität München

Vorstand: Prof. Andreas Ladurner, PhD

**Functional dissection of the Tim17-Tim23 core of the mitochondrial
presequence translocase**

Dissertation
zum Erwerb des Doktorgrades der Naturwissenschaften
an der Medizinischen Fakultät der
Ludwig-Maximilians-Universität zu München

vorgelegt von
Umut Günsel

aus
Karabük, Türkei

Jahr
2020

Mit Genehmigung der Medizinischen Fakultät
der Universität München

Betreuerin: PD. Dr. rer. nat. Dejana Mokranjac

Zweitgutachter(in): Prof. Dr. rer. nat. Michael Kiebler

Dekan: Prof. Dr. med. dent. Reinhard Hickel

Tag der mündlichen Prüfung: 09.09.2020



"Hayatta en hakiki mürşit ilimdir, fendir"

M. Kemal ATATÜRK

TABLE OF CONTENTS

TABLE OF CONTENTS.....	I
1. INTRODUCTION.....	1
1.1 Protein translocation into mitochondria	1
1.2 The presequence translocase, TIM23 complex	3
1.2.1 Functional organization of the TIM23 complex.....	4
1.2.1.1 Receptors of the TIM23 complex receive incoming precursor proteins.....	5
1.2.1.2 Aqueous channel allows precursors to pass the IM	7
1.2.1.3 Import motor finalizes the import process	8
1.2.1.4 Lateral insertion by the TIM23 complex and regulatory subunits	10
1.3 The TIM23 complex and human diseases	12
1.4 Aim of the study.....	14
2. MATERIALS AND METHODS	15
2.1 Molecular Biology	15
2.1.1 Isolation of plasmid DNA from <i>E. coli</i>	15
2.1.1.1 Large scale plasmid isolation (Midiprep)	15
2.1.1.2 Small scale crude plasmid isolation (Miniprep)	15
2.1.2 Detection and analysis of DNA	16
2.1.2.1 Agarose gel electrophoresis.....	16
2.1.2.2 DNA extraction from the gel.....	16
2.1.2.3 Concentration measurement of DNA samples	17
2.1.3 Enzymatic modification of DNA.....	17
2.1.3.1 Restriction digestion	17
2.1.3.2 Ligation.....	17
2.1.4 Preparation of electrocompetent <i>E. coli</i>	17
2.1.5 Transformation of <i>E. coli</i> cells by electroporation.....	18
2.1.6 Plasmid constructs used in this work	18
2.1.7 Primer pairs used in this thesis.....	21
2.1.8 Amplification of DNA fragments and cloning procedure.....	25
2.1.8.1 Cloning (Cl.).....	25
2.1.8.2 Site directed mutagenesis (SDM).....	26
2.2 Yeast Genetics.....	27
2.2.1 Yeast strains used in this study.....	27
2.2.2 Transformation of yeast cells	29
2.2.3 Plasmid shuffling by 5FOA selection.....	30
2.3 Cell Biology	31
2.3.1 Bacterial culture	31
2.3.2 Yeast culture	31
2.3.3 Assays with yeast cells.....	32
2.3.3.1 Serial dilution spot assay.....	32
2.3.3.2 Preparation of total cell lysates	33
2.3.3.3 <i>In vivo</i> site-specific photocrosslinking (Total cell extracts and NiNTA pull down).....	33
2.3.3.4 Isolation of crude mitochondria.....	34

TABLE OF CONTENTS

2.3.3.5 Large-scale mitochondria isolation	35
2.4 Protein Biochemistry.....	36
2.4.1 Protein detection and analysis	36
2.4.1.1 SDS-PAGE	36
2.4.1.2 Western blotting	37
2.4.1.3 Determination of protein concentration	37
2.4.1.4 Coomassie Brilliant Blue (CBB) staining	38
2.4.2 <i>In vitro</i> import experiments.....	38
2.4.2.1 Preparation of radioactive precursors	38
2.4.2.2 Import of radioactive precursors into isolated mitochondria.....	39
2.4.3 $\Delta\Psi$ measurements.....	40
2.4.3.1 Measurement of mitochondrial $\Delta\Psi$	40
2.4.3.2 Measurement of $\Delta\Psi$ in liposomes	40
2.4.4 Co-immunoprecipitation assay.....	40
2.4.5 Chemical crosslinking.....	41
2.4.6 Blue Native PAGE (BN-PAGE).....	42
2.4.7 Purification of recombinant Tim17-Tim23 complex	42
2.4.7.1 Co-expression of Tim17 and Tim23.....	42
2.4.7.2 Isolation of <i>E.coli</i> membranes.....	43
2.4.7.3 Purification of recombinant membrane Tim17-Tim23 complex from isolated membranes	43
2.4.8 Reconstitution of recombinant Tim17-Tim23 in proteoliposomes	44
2.4.8.1 Na_2CO_3 extraction	45
2.4.8.2 Precursor binding to proteoliposomes	45
3. RESULTS.....	47
3.1 <i>In vivo</i> dissection of Tim23	47
3.1.1 Evolutionary conservation of Tim23	47
3.1.2 Deletion of the first 70 residues of Tim23 can be tolerated by yeast cells.....	48
3.1.3 Deletion of the first 30 residues of Tim23 reduces levels of Tim23 protein.....	50
3.1.4 Removal of the first 10 residues from Tim23 does not impair binding of Tim50 and Tim21 to the TIM23 complex	51
3.1.5 Protein import into mitochondria from $\Delta 10$ is slightly reduced.....	52
3.1.6 Alanine scanning mutagenesis of the region between amino acid residues 51 and 100 of Tim23 identifies three distinct functionally important regions	53
3.1.7 The region around amino acid residue 40 of Tim23 is in close proximity to Tom22.....	54
3.1.8 Tim50 binding region on Tim23 is larger than described previously.....	56
3.1.9 TIM23-mediated protein import is impaired in the <i>tim23L87A5</i> mutant	58
3.1.10 Interaction of Pam17 with Tim23 is reduced in <i>L87A5</i> mutant	60
3.1.11 Pam17 is in direct contact with Tim23 in the IMS	62
3.1.12 Negative charges at positions 95 and 96 are required for optimal cell growth	63
3.1.13 Protein import is impaired in <i>D95A2</i> and <i>D95K2</i> mutant mitochondria	63
3.1.14 Residues 95 and 96 alter conformation of Tim23 in the IMS	65
3.1.15 TMs 3 and 4 of Tim23 are not essential for cell viability	66
3.1.16 Import into ΔTM4 and $\Delta\text{TM3-4}$ is impaired.....	67
3.1.17 Last two transmembrane segments of Tim23 are important for stabilization of Tim23 interaction with Tim17	68

3.2	<i>In vivo</i> dissection of Tim17.....	71
3.2.1	TM of Tim17 is essential.....	71
3.2.2	Mutations in GxxxG motifs in the first 3 TMs of Tim17 result in defective import via the TIM23 complex	72
3.2.3	Mutations of GxxxG motifs in TM segments of Tim17 differently affect assembly of the TIM23 complex	74
3.2.4	N-terminal part of loop 3 of Tim17 is essential for cell viability.....	75
3.2.5	Conserved residue Arg105 is important for cell viability.....	75
3.2.6	Protein import via the TIM23 complex is defective in <i>R105A</i> mutant	76
3.2.7	Import motor interaction in <i>R105A</i> mutant is impaired.....	77
3.2.8	Loop 3 of Tim17 is in direct contact with Tim44	78
3.3	Purification and reconstitution of the recombinant Tim17-Tim23 core of the TIM23 complex.....	79
3.3.1	Expression and purification of the recombinant Tim17-Tim23 complex	79
3.3.2	Reconstitution of the recombinant Tim17-Tim23 complex in liposomes	81
3.3.3	Reconstituted Tim17 and Tim23 complex can specifically recognize presequences	82
3.3.4	Reconstituted proteoliposomes can generate membrane potential	83
4.	DISCUSSION	85
4.1	IMS domain of Tim23 does more than orchestrating the IMS part of the TIM23 complex	85
4.2	Last two TMs of Tim23 are required for stabilization of Tim17-Tim23 interaction	89
4.3	Tim17 has a role in coupling the import motor complex to the translocation channel of the TIM23 complex	90
4.4	The Tim17-Tim23 core of the TIM23 complex can be purified recombinantly and reconstituted in proteoliposomes	92
5.	SUMMARY	93
6.	ZUSAMENFASSUNG.....	95
7.	REFERENCES.....	97
	ABREVIATIONS.....	107
	PUBLICATIONS FROM THIS THESIS	111
	ACKNOWLEDGEMENTS	113
	CURRICULUM VITAE.....	115

1. INTRODUCTION

The most fascinating feature of eukaryotic cells is their intra-cellular compartmentalization. During evolution, membrane-enclosed structures, or organelles, were formed to allow more efficient metabolic processes to occur. Organelles contain their own specific sets of enzymes, metabolites, structural elements and, in some cases, even their own genetic material, distinct from the nuclear genome. Mitochondria are involved in various vital cellular processes including energy metabolism, synthesis of a number of different biomolecules and various signaling events. It is thus not surprising that dysfunction of mitochondria is associated with a myriad of human diseases (Herzig and Shaw, 2018; Nunnari and Suomalainen, 2012). Mitochondria are double membrane-surrounded organelles, resulting in formation of four different subcompartments: from outside to the inside, the outer membrane (OM), intermembrane space (IMS), inner membrane (IM) and the innermost matrix. Even though they contain their own genetic material and complete transcription and translation systems, only 8 out of ca. 1000 proteins in yeast and 13 out of ca. 1500 proteins in humans are encoded by the mitochondrial DNA (mtDNA). All other mitochondrial proteins are expressed from nuclear DNA (ncDNA), translated on cytosolic ribosomes and require specialized translocation machineries for their correct targeting, translocation and sorting within mitochondria (Blobel, 1980; Chacinska et al., 2009; Kang et al., 2018; Neupert, 2015; Wiedemann and Pfanner, 2017).

1.1 Protein translocation into mitochondria

Proteins destined to mitochondria are synthesized in the cytosol as precursor proteins with specific cleavable or internal targeting signals. These different mitochondrial targeting signals will guide the precursor proteins to their final destination within mitochondria (Figure 1.1) (Endo et al., 2011; Hansen and Herrmann, 2019; Mokranjac and Neupert, 2009; Wiedemann and Pfanner, 2017). Essentially all mitochondrial proteins use the TOM (translocase of the outer membrane) complex as a general gate for the passage through the OM and are subsequently handed over to the one of the downstream translocases. Below, the various mitochondrial protein translocation pathways are briefly described.

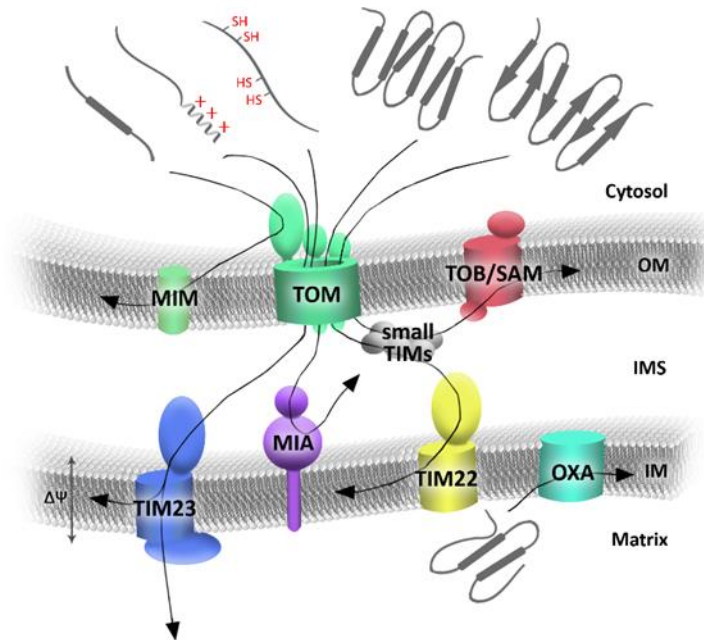


Figure 1.1 An overview of mitochondrial protein translocation pathways. See text for details. OM, outer membrane; IMS, intermembrane space; IM, inner membrane.

β -barrel proteins of the OM, such as porin, Tom40, Sam50/Tob55 and Mdm10, are initially translocated completely across the OM using the TOM complex. In the IMS, they are handled by the small TIM chaperones, which guide them to the TOB/SAM complex (topogenesis of mitochondrial OM β -barrel proteins/sorting and assembly machinery) for insertion into the OM from the IMS side. The single- and multi-spanning α -helical OM proteins use the TOM and MIM complexes for their insertion into the OM. Many small IMS proteins, including small TIMs, contain conserved cysteine motifs and undergo oxidative folding after they traverse the TOM complex. This process is mediated by the disulfide relay system, also called MIA (mitochondrial IMS assembly) pathway. Inner membrane proteins with multiple α -helical transmembrane segments (TMs), such as metabolite carriers and the core components of mitochondrial IM translocases, Tim23, Tim17 and Tim22, contain internal targeting signals and use the TIM22 complex (translocase of the inner membrane 22) for their insertion into the IM in a membrane potential ($\Delta\Psi$)-dependent manner. Like the clients of the TOB/SAM complex, the hydrophobic TIM22 substrates require small TIM proteins to chaperone them through the aqueous IMS from the TOM complex in the OM to the IM. Hydrophobic IM proteins that are encoded in the mtDNA and translated on mitochondrial ribosomes are inserted into the IM from the matrix side with the help of the OXA (oxidase

assembly) complex. The vast majority of mitochondrial proteins, however, follow the so-called presequence pathway. They contain N-terminal, cleavable presequences (also called matrix targeting signals) and are translocated by the TOM and TIM23 complexes across the OM and IM, respectively. The TIM23 complex utilizes the energy of $\Delta\Psi$ across the IM and ATP in the matrix to translocate proteins across and insert them into the IM. Some IM proteins are first completely translocated into the matrix by the TIM23 complex and then inserted into the IM from the matrix side by the OXA complex. An IM-localized AAA-ATPase Bcs1 inserts Rip1, Rieske Fe-S protein of the complex III of the respiratory chain, into the IM insertion from the matrix side (Wagener et al., 2011). Whether Rip1 is the only substrate of Bcs1 remains unknown.

My thesis deals with the TIM23 complex and therefore a more detailed description of this complex is given in the following sections.

1.2 The presequence translocase, TIM23 complex

The TIM23 complex tightly cooperates with the TOM complex during import of ncDNA-encoded mitochondrial proteins that have N-terminal presequences. Almost 70% of proteins targeted to mitochondria have this type of targeting signal (Vogtle et al., 2009). Presequences are usually 8 to 80 amino acid residues long and are typically found at the N-terminal end of a protein. They are characterized by the ability to form an amphipathic helix with a net positive charge (+3 to +6) on one side and a hydrophobic surface on the opposite side (von Heijne, 1986). Once in the matrix, presequences are usually cleaved by mitochondrial processing peptidase and, in some cases, peptidases such as mitochondrial intermediate peptidase and Icp55 can further process incoming proteins (Mossmann et al., 2012).

By default, presequences target precursor proteins into the matrix. However, the TIM23 complex can also open laterally and release precursor proteins into the IM, if an additional downstream, hydrophobic lateral sorting (also known as a 'stop-transfer') signal is present. Some of the laterally sorted precursor proteins are further processed by the inner membrane peptidase on the IMS side of the IM, releasing soluble proteins into the IMS. In

case of presequence containing precursor proteins with multiple TMs, some TMs can be laterally sorted and some completely translocated by the TIM23 complex (Bohnert et al., 2010; Hell et al., 1998; Meier et al., 2005b). The TIM23 complex can also import IM proteins with N-out, C-in topology, such as Bcs1 and Tim14. Here the amphipathic signal sequence was proposed to be formed by a tight hairpin structure between the TM and a positively charged patch directly behind it (Folsch et al., 1996). Besides import into the matrix, IM and IMS, the TIM23 complex was recently reported to be involved in an unusual import pathway of some OM proteins (Sinzel et al., 2016; Song et al., 2014; Wenz et al., 2014).

1.2.1 Functional organization of the TIM23 complex

The TIM23 complex can be functionally divided into the IMS-exposed receptors that recognize precursor proteins, the IM-integrated translocation channel through which the precursor proteins cross the IM in a $\Delta\Psi$ -dependent manner and the matrix-exposed import motor that uses the energy of ATP hydrolysis to provide unidirectionality to the transport into the matrix (Figure 1.2).

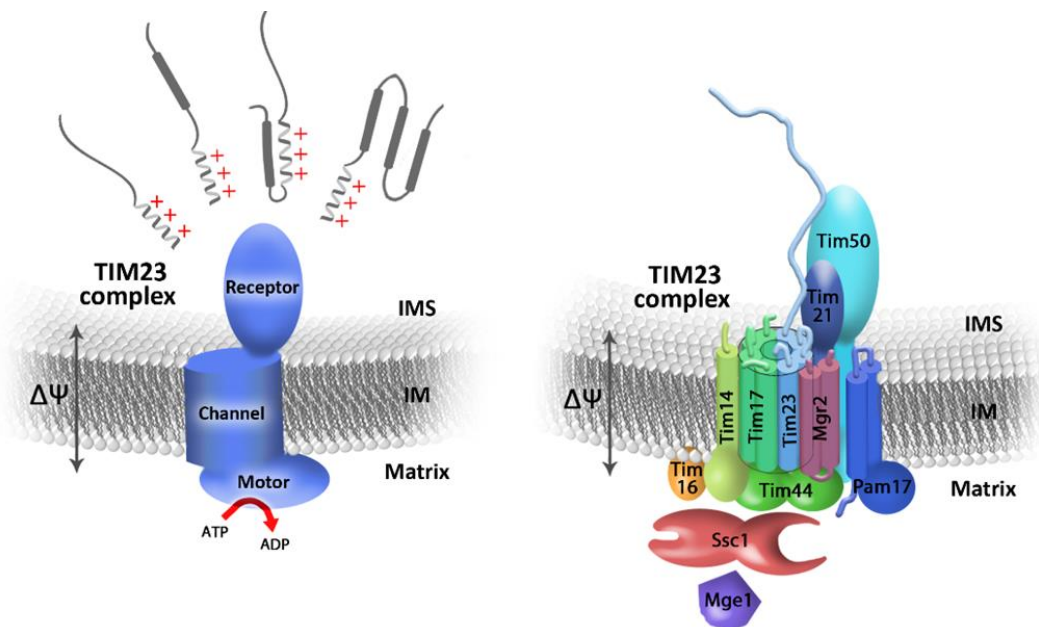


Figure 1.2 Schematic representation of the TIM23 complex. The TIM23 complex can be functionally divided into three functional units - receptors, translocation channel and import motor (left panel). Eleven subunits of the TIM23 complex were identified to date. These are Tim23, Tim17, Tim50, Tim44, Tim14, Tim16, mtHsp70 (Ssc1), Mge1, Tim21, Mgr2 and Pam17 (right panel). See text for details. IMS, intermembrane space; IM, inner membrane.

Genetic and biochemical studies, performed mainly with baker's yeast, *Saccharomyces cerevisiae*, showed that at least eleven, highly evolutionary conserved subunits form the TIM23 complex. Eight of them, Tim23, Tim17, Tim50, Tim44, Tim16 (Pam16), Tim14 (Pam18), mtHsp70 (Ssc1) and Mge1, are essential for yeast cell viability, demonstrating their essential roles in biogenesis of mitochondria. Deletions of the remaining three subunits, Tim21, Pam17 and Mgr2, which appear to modulate the import process, can be tolerated by yeast cells, at least under certain growth conditions.

1.2.1.1 Receptors of the TIM23 complex receive incoming precursor proteins

The first subunit of the TIM23 complex that recognizes presequences as they come from the TOM complex is the main receptor Tim50. It has a large C-terminal domain in the IMS, a single transmembrane segment in the IM and a short segment in the matrix (Geissler et al., 2002; Mokranjac et al., 2003a; Yamamoto et al., 2002). The C-terminal IMS domain of Tim50, that is sufficient to support the function of the full-length (FL) protein (Mokranjac et al., 2009), can be divided in two subdomains - a highly conserved core domain and a presequence binding domain (PBD) at the very C-terminus that appears to be fungi-specific. Tim50 is in close proximity of the TOM complex (Araiso et al., 2019; Shiota et al., 2011; Tamura et al., 2009; Waegemann et al., 2015) and recognizes presequences as soon as they appear at the outlet of the TOM complex (Mokranjac et al., 2003a; Mokranjac et al., 2009; Yamamoto et al., 2002). Both the core domain of Tim50 and the PBD were shown to bind to presequences (Lyrovchenko et al., 2013; Rahman et al., 2014). However, how the two cooperate during translocation of proteins into mitochondria is still unknown.

Tim50 cooperates with the IMS-exposed domain of Tim23 during recognition of presequences (Figure 1.3). Mutations that destabilize the interaction between Tim50 and Tim23 impair the receptor function of Tim50, reducing efficiency of import of proteins along the presequence pathway and impairing growth of yeast cells (Gevorkyan-Airapetov et al., 2009; Mokranjac et al., 2009; Tamura et al., 2009). Intriguingly, mutations of Tim50 that impair binding to Tim23 map to two distinct patches on Tim50 (Dayan et al., 2019; Qian et al., 2011; Tamura et al., 2009). Whether these two patches are directly involved in Tim23 binding remains unclear. The interaction between Tim50 and Tim23 is important for

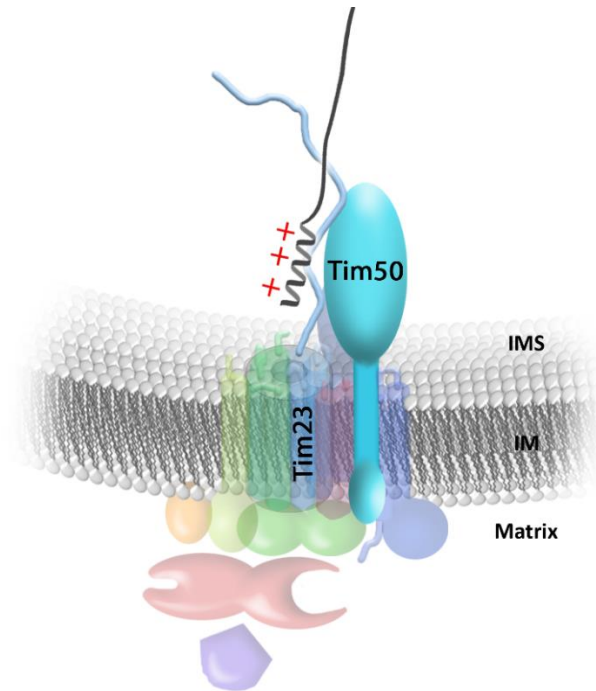


Figure 1.3 Receptor subunits of the TIM23 complex. The IMS domain of Tim23 (blue) and Tim50 (cyan) cooperate during initial recognition of presequences and convey them to the core channel.

maintaining the permeability barrier of the IM (Meinecke et al., 2006) and is also modulated by the lipid composition of the membrane (Malhotra et al., 2017). Moreover, cooperation of the two IMS domains is required for a proper communication between the TOM and TIM23 complexes (Tamura et al., 2009; Waagemann et al., 2015).

Like Tim50, the IMS exposed segment of Tim23 was also shown to directly bind presequences (Bauer et al., 1996; de la Cruz et al., 2010; Marom et al., 2011), suggesting a receptor function for this protein as well. Tim23 was also reported to dimerize in response to $\Delta\Psi$ and that the dimers dissociate in response to presequence binding (Bauer et al., 1996). Protease accessibility experiments with intact mitochondria demonstrated that around 20 residues at the very N-terminus of Tim23 can even extend outside of mitochondria (Donzeau et al., 2000). The exposure of Tim23 on the mitochondrial surface is regulated by Tim50, the TOM complex and the translocation activity of the TIM23 complex (Gevorkyan-Airapetov et al., 2009; Popov-Celeketic et al., 2008; Tamura et al., 2009; Waagemann et al., 2015). Besides with Tim50 and presequences, the intrinsically disordered Tim23_{IMS} was also shown to interact with Tim21, Tom22 and mitochondrial membranes. These various interactions were

shown, in most cases only, in *in vitro* experiments using recombinantly expressed and purified proteins (Bajaj et al., 2014a; Bajaj et al., 2014b; de la Cruz et al., 2010; Marom et al., 2011). Molecular details of all these interactions, their *in vivo* significance and their dynamics during transfer of precursor proteins from the TOM complex in the OM to the channel of the TIM23 complex in the IM still remain to be examined. It is, however, clear that a $\Delta\Psi$ dependent step is required to transfer the precursor protein to the translocation channel and initiate its translocation across the IM.

1.2.1.2 Aqueous channel allows precursors to pass the IM

The molecular nature of the translocation channel of the TIM23 complex is still unclear. Tim17 and the C-terminal domain of Tim23 belong to same protein family and have four predicted transmembrane segments, which embed the proteins in the IM (Figure 1.4). Electrophysiological measurements with recombinant Tim23, upon expression in inclusion bodies and subsequent refolding, showed that Tim23 alone can form an aqueous channel (Meinecke et al., 2006; Truscott et al., 2001). Whether Tim17 contributes to the formation of the translocation channel is still not clear. A more regulatory role was proposed for this protein in stabilizing the twin pore structure of the TIM23 channel and regulating its voltage gating (Martinez-Caballero et al., 2007; Ramesh et al., 2016). Unlike Tim23, Tim17 does not

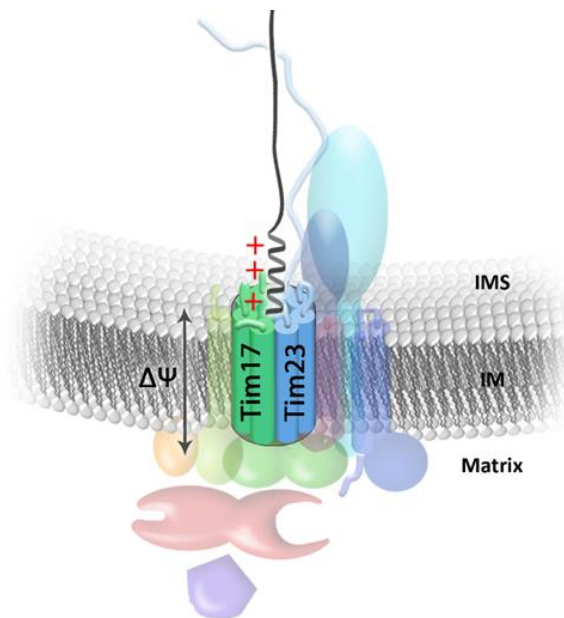


Figure 1.4 Core channel of the TIM23 complex. Membrane embedded subunits Tim17 (light green) and Tim23 (blue) likely form the translocation channel. Energy from $\Delta\Psi$ is required for translocation across the IM.

have a large N-terminal extension in the IMS. However, a ca. 10 amino acid long N-terminal extension of Tim17, which contains a conserved negatively charged motif, was reported to be important for gating of the TIM23 channel and thus for import of proteins (Meier et al., 2005a). Gating of the TIM23 channel is also dependent on two conserved cysteine residues in Tim17 that form a disulfide bond locking TM1 and TM2 together (Ramesh et al., 2016; Wrobel et al., 2016). Both Tim17 and Tim23 contain multiple GxxxG motifs in their TMs. In Tim23, these motifs play an important role in maintaining the structural integrity of the TIM23 complex and are thus likely involved in packing of the TMs (Demishtein-Zohary et al., 2015). TM1 and TM2 of Tim23 are in direct contact with translocating proteins (Alder et al., 2008a). TM2 and likely also TM1 are facing an aqueous environment and are hence likely directly forming the protein-conducting channel (Alder et al., 2008a). TM1 is in close proximity to Tim17 and Tim50 and, together with TM2, responds dynamically to the presence of $\Delta\Psi$ by undergoing conformation changes that likely lead to channel opening (Alder et al., 2008b; Malhotra et al., 2013). Intriguingly, TM3 and TM4 of Tim23 were reported to be dispensable for yeast cell viability (Pareek et al., 2013). The GxxxG motifs in Tim17 were not analyzed at the beginning of my work.

Membrane potential is required to activate the translocation channel of the TIM23 complex. Even though the true nature of the voltage sensor of the TIM23 complex remains unclear, this role has been attributed to the IMS domain of Tim23, which can dimerize in response to $\Delta\Psi$ (Bauer et al., 1996), and the conserved negatively charged residues in the N-terminal stretch of Tim17 (Meier et al., 2005a). Membrane potential was also suggested to generate an electrophoretic force that would pull positively charged presequences towards the matrix (Roise and Schatz, 1988). On the matrix side of the channel, presequences are recognized by the import motor of the TIM23 complex.

1.2.1.3 Import motor finalizes the import process

Complete translocation into the matrix requires the ATP-dependent action of the import motor of the TIM23 complex. Tim44 is a peripheral membrane protein that couples the import motor to the translocation channel. It is comprised of an N-terminal intrinsically disordered domain (Ting et al., 2017) and a C-terminal globular domain (Josyula et al., 2006).

The C-terminal domain engages Tim17 and Tim23 and the N-terminal domain recruits the import motor components (Banerjee et al., 2015; Schiller et al., 2008; Ting et al., 2017). Tim44 not only acts as a platform for recruitment of the import motor to the exit of the translocation channel, but it also interacts with presequences (Marom et al., 2011; Ting et al., 2017).

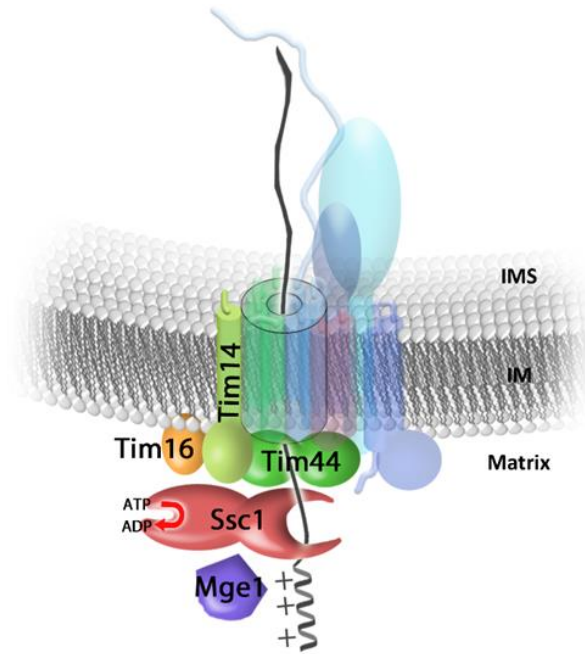


Figure 1.5 Import motor of the TIM23 complex. Multiple Hsp70 cycles mediate unidirectional transport of precursors. Tim44 (green) is a peripheral inner membrane protein that serves as a scaffold of the import motor. mtHsp70, Ssc1 (red), is the ATP-consuming subunit. Tim14 (light green) and Tim16 (orange) are J and J-like proteins, controlling the ATP hydrolysis. Mge1 (purple), the nucleotide exchange factor, resets the cycle by exchanging ADP with a new ATP molecule.

The import motor components are mitochondrial Hsp70 (mtHsp70, also known as Ssc1 in yeast) and its co-chaperones Tim14 (Pam18), Tim16 (Pam16) and Mge1 (Figure 1.5). The energy of ATP is used by mtHsp70 for further import of precursor proteins into the matrix in a process that is regulated by other subunits of the motor. mtHsp70 is a member of the conserved family of Hsp70 chaperones (Rosenzweig et al., 2019). Hsp70s are comprised of an N-terminal nucleotide-binding domain (NBD) which binds ATP and a C-terminal substrate-binding domain (SBD) which binds aggregation-prone stretches of hydrophobic amino acid residues that are exposed in unfolded proteins. When ATP is bound to the NBD, the SBD is in an open conformation, characterized by a low substrate affinity with high $k_{on/off}$ rates. When the ATPase activity is triggered, NBD hydrolyzes ATP to ADP and SBD closes, trapping the bound substrate. Upon ADP release and binding of a new molecule of ATP to NBD, the SBD

opens, releasing the bound substrate. Two types of co-chaperones, J-proteins and nucleotide exchange factors (NEFs), enable this cycle to progress in a regulated and efficient manner. J-proteins stimulate the ATPase activity of NBD and NEFs help the release of ADP, resetting the cycle by allowing a new ATP molecule to bind. In the TIM23 complex, Tim14 is the J-protein that stimulates the ATP hydrolysis by mtHsp70, and thus enables the tight binding of incoming proteins to mtHsp70 (D'Silva et al., 2003; Mokranjac et al., 2003b; Truscott et al., 2003). J-like protein Tim16 recruits Tim14 to the TIM23 complex and regulates the stimulatory activity of Tim14 (D'Silva et al., 2005; Frazier et al., 2004; Kozany et al., 2004; Li et al., 2004; Mokranjac et al., 2006). The molecular understanding of the function of the import motor is still missing. It is likely that, once the translocating protein is stably captured by mtHsp70 upon ATP hydrolysis, mtHsp70 is released from the channel into the matrix, taking along a segment of the translocating protein and leaving space for another molecule of mtHsp70 to bind to the next incoming segment of the translocating protein. In the matrix, the nucleotide exchange factor Mge1 exchanges the ADP molecule with an ATP, releasing the captured protein from mtHsp70 and resetting the cycle. mtHsp70 not only has a role during the import process, but is also important for folding of precursor proteins, which arrive in an unfolded state in the matrix.

1.2.1.4 Lateral insertion by the TIM23 complex and regulatory subunits

The TIM23 complex can import precursor proteins into the matrix and sort them laterally into the IM. The unique feature of the TIM23 complex among protein translocases in the cell is that it can discriminate between *bona fide* transmembrane segments. It can open laterally to release 'stop-transfer' signals into the IM but it can also translocate some transmembrane segments completely into the matrix. The latter ones are then inserted into the IM from the matrix side by the OXA complex. In comparison to the TMs that are translocated by the TIM23 complex, the TMs that are laterally sorted are slightly more hydrophobic, lack proline residues and are flanked by charged residues (Meier et al., 2005b). Which subunits of the TIM23 complex recognize lateral sorting signals and form the lateral gate and how TMs are laterally inserted into the IM remains unclear. Certain mutations of Tim17 specifically impaired lateral insertion and had no effect on translocation of proteins

into the matrix (Chacinska et al., 2005). In addition to stimulating the ATPase activity of Ssc1, Tim14 seems to have an additional active role during lateral insertion (Popov-Celeketic et al., 2011; Schendzielorz et al., 2018).

The roles of the three nonessential subunits of the TIM23 complex, Tim21, Pam17 and Mgr2 (Figure 1.6), also appear to be in differential sorting of proteins. Deletion of Mgr2 promoted lateral insertion and its upregulation delayed it (Ieva et al., 2014). One model of function of the TIM23 complex proposed that lateral insertion is mediated by a Tim21-containing, but motor-free TIM23 complex (Chacinska et al., 2005). However, subsequent experiments revealed that the import motor associates with the channel irrespective of the translocation activity of the TIM23 complex (Popov-Celeketic et al., 2008; Tamura et al., 2006). These findings led to a proposal that the TIM23 complex functions as a single entity that is actively remodeled to translocate proteins across or insert them into the IM membrane (Popov-Celeketic et al., 2008). According to this model, conformational changes underlie differential sorting of proteins and they are driven by recognition of targeting signals in the translocating proteins and modulated by an antagonistic behavior of Tim21 and Pam17.

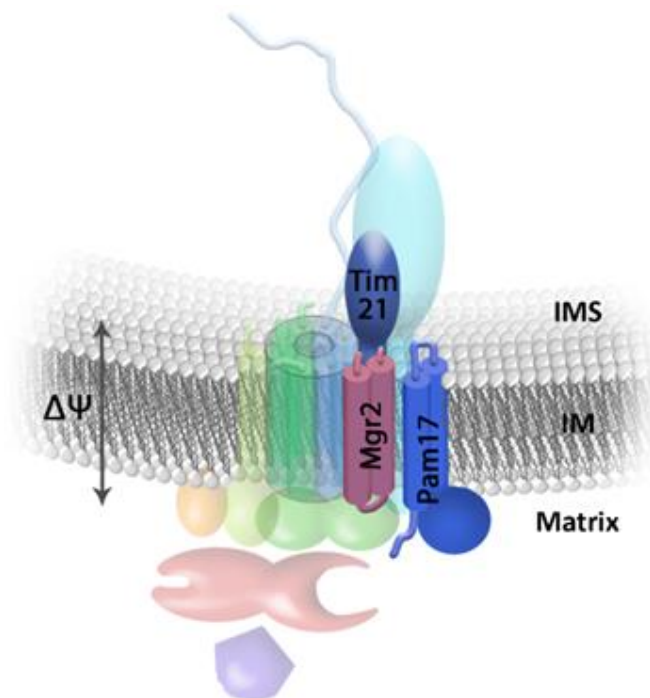


Figure 1.6 Regulatory subunits of the TIM23 complex. Non-essential subunits of the TIM23 complex are required for optimal import activity. Tim21 (dark blue), Pam17 (indigo) and Mgr2 (fuchsia).

Tim21 was also found to bind very efficiently to the TOM complex *in vitro* (Chacinska et al., 2005; Mokranjac et al., 2005a), however, the *in vivo* significance of this finding appears limited (Waegemann et al., 2015). The IMS-exposed domain of Tim21 seems to modulate the interactions among the receptors of the TIM23 complex and their interplay with the presequences (Lytovchenko et al., 2013). Tim21 may also improve energetics of the TIM23 complex by coupling it to the respiratory chain complexes (van der Laan et al., 2006). Pam17 was recently reported to promote translocation of $\Delta\Psi$ -hypersensitive precursor proteins into the matrix (Schendzielorz et al., 2017). These proteins appear to require $\Delta\Psi$ not only for translocation of their presequences but also of their mature parts.

1.3 The TIM23 complex and human diseases

Inspection of the sequenced eukaryotic genomes showed that the components of the TIM23 complex are highly conserved over the course of evolution, suggesting that the structure and function of the complex are equally conserved. Direct analyses of the human TIM23 complex are still in their very early stages. The data available so far revealed only very few differences between yeast and human TIM23 complexes (Demishtein-Zohary and Azem, 2017; Kang et al., 2018). Whereas in yeast all components are encoded by single genes (except for Tim14 that has a paralog Mdj2 (Mokranjac et al., 2005b)), human genome encodes for three different Tim17 (hTim17A, hTim17B1 and hTim17B2) and two different Tim14 (DnaJC15 and DnaJC19) proteins. All other subunits have one corresponding homolog in humans, though an equivalent of Pam17 has not been identified yet. In addition, unlike its yeast counterpart, hTim50 was reported to possess a phosphatase activity (Guo et al., 2004), the role of which still needs to be resolved. So far, three distinct TIM23 complexes in human mitochondria were identified. Tim17A appears to associate only with DnaJC15 and Tim17B1 and B2 with DnaJC19. Tim17B-containing complexes are essential for protein import into the matrix and, thus, cell viability, whereas the TIM23 complex containing Tim17A appears dispensable for cell growth (Sinha et al., 2014).

Concerning the essential nature of the majority of the TIM23 components for biogenesis of mitochondria and viability of yeast cells, it has been assumed that loss-of-

function mutations in TIM23 components would be embryonically lethal in humans. Indeed, homozygous Tim23 knockout is lethal in mice and heterozygous mice have neurological phenotypes and reduced life span (Ahting et al., 2009). It has therefore come as a surprise when point mutations and alteration in expression of different essential subunits of the TIM23 complex were identified in patients with different disorders. Mutations in hTim50 are associated with microcephaly, encephalopathy, epilepsy, delayed growth, vision loss, breast cancer and 3-methylglutaconic aciduria (Gao et al., 2016; Reyes et al., 2018; Shahrour et al., 2017). hTim44 is linked to oncocytic thyroid carcinoma and diabetes (Bonora et al., 2006; Wang et al., 2015). hTim16 (Magmas) and hmtHsp70 (Mortalin) are found mutated in skeletal dysplasia (Mehawej et al., 2014; Royer-Bertrand et al., 2015). Mortalin is also linked to EVEN-PLUS syndrome and Parkinson's disease (Burbulla et al., 2010; Royer-Bertrand et al., 2015). Loss of DNAJC19 has been found in patients with DCMA syndrome (Davey et al., 2006). Certain cancer types showed changes in the expression levels of Tim17A, Tim50, Magmas, DnaJC15 and Mortalin (Gao et al., 2016; Jubinsky et al., 2005; Lu et al., 2011; Xu et al., 2010). Recently, it has been shown that mutant huntingtin protein, which causes Huntington's disease, clogs the TIM23 channel and thereby prevents import of endogenous matrix proteins (Yablonska et al., 2019). In general, it is likely that any problem in the function of the TIM23 complex will cause problems in biogenesis of mitochondria and will thus result in malfunctioning mitochondria. Why mutations identified so far display such specific phenotypes and tissue specificity remains to be determined.

Gene complementation assays with different subunits of the TIM23 complex revealed remarkable similarities between yeast and human complexes. hTim16 (Magmas) and DnaJC15 can complement the functions of yTim16 and yTim14, respectively (Schusdziarra et al., 2013; Sinha et al., 2010). Moreover, a homozygous mutation of Magmas associated with early lethal skeletal dysplasia causes a temperature sensitive growth phenotype in yeast (Mehawej et al., 2014). On the other hand, hTim50 cannot rescue the function of yTim50 and the mutations in hTim50 that were identified in patients with encephalopathy, did not reveal any obvious growth defect when analyzed in yeast (Shahrour et al., 2017). A point mutation in Tim44 found in patients with oncocytic carcinoma (Bonora et al., 2006) similarly did not

cause a growth defect in yeast, but a reduction in protein stability was observed in this case (Banerjee et al., 2015). Thus, the analysis of the structure and function of the TIM23 complex in a simple eukaryote such as baker's yeast not only contributes towards understanding the basic principles of function of eukaryotic cells but also provides important insights into molecular mechanisms of human diseases.

1.4 Aim of the study

The aim of this study was to gain new molecular insight into the structure and function of the TIM23 complex. Two homologous proteins, Tim23 and Tim17, were to be dissected *in vivo* using yeast as a model system. A reconstitution of the Tim17-Tim23 complex from recombinantly expressed proteins was to be attempted.

2. MATERIALS AND METHODS

2.1 Molecular Biology

2.1.1 Isolation of plasmid DNA from *E. coli*

2.1.1.1 Large scale plasmid isolation (Midiprep)

Isolation of plasmid DNA from *E. coli* was done using Pure Yield Plasmid Midiprep kit (Promega). Single colony was picked and inoculated into 40 ml of LB medium (see section 2.3.1) containing 100 µg/ml of ampicillin. The culture was grown overnight at 37°C with vigorous shaking (150 rpm). Next morning, the cells were pelleted by centrifugation at 10,000 x g for 10 min at RT. Then, the cells were resuspended with 6 ml of 'Resuspension buffer' (50 mM Tris-HCl (pH 7.5), 10 mM EDTA (pH 8.0) and 100 µg/ml RNase A) followed by addition of 6 ml of 'Lysis buffer' (0.2M NaOH, 1% (w/v) SDS). After mixing by gently inverting the tube 3 to 5 times, the cells were incubated for additional 2 min for lysis at RT. Ten ml of 'Neutralization solution' (4.09M guanidine hydrochloride (pH 4.2), 759 mM potassium acetate, 2.12M glacial acetic acid) was added, the solution was gently mixed by inverting the tube 3-5 times and then incubated for additional 2 min. Precipitated genomic DNA and aggregated proteins were removed by centrifugation at 27,000 x g for 10 min at RT. The supernatant was passed, by application of vacuum, through two columns, first through Cleaning and then through Binding column. The Cleaning column was subsequently discarded and the Binding column was first washed with 5 ml of 'Endotoxin Removal Wash' solution followed by 20 ml of 'Column wash solution' (162.8mM potassium acetate, 22.6mM Tris-HCl (pH 7.5), 0.109mM EDTA (pH 8.0)). Vacuum application for 30 s was done for removal of residual EtOH. Finally, the plasmid DNA was eluted using 600 µl of sterile distilled water and stored at -20°C until use.

2.1.1.2 Small scale crude plasmid isolation (Miniprep)

Colonies from LB+Amp plates were inoculated into 2 ml of LB+Amp and grown overnight at 37°C with vigorous shaking. Next day, cells were harvested at 16,100 x g for 1 min and resuspended in 400 µl of E1 buffer (50 mM Tris-HCl, 10 mM EDTA, pH 8). Then, cells

were lysed by adding 400 µl of E2 (0.2 M NaOH, 1 % (w/v) SDS) and mixing by inverting the tube 10 times. The solutions were neutralized by adding 400 µl of E3 (3.1 M KAc in 99% acetic acid) and mixing as in the previous step. Lysates were clarified by centrifugation at 16,100 x g for 10 min at RT. To precipitate plasmid DNA, 850 µl of the supernatants were added to 600 µl of isopropanol. After mixing thoroughly, the tubes were incubated for 2 min and centrifuged for 20 min at 16,100 x g. The supernatants were discarded and the pellets were washed with 200 µl of ice-cold 70% EtOH without resuspending the pellets. A 5 min centrifugation step was applied at 16,100 x g at RT. Finally, the pellets were resuspended in 20 µl of sterile distilled water containing 0.1 mg/ml RNase and shaken for 15 min at RT. Plasmid DNA was subsequently stored at -20°C.

2.1.2 Detection and analysis of DNA

2.1.2.1 Agarose gel electrophoresis

DNA fragments from PCR reactions or restriction enzyme digestions were analyzed by agarose gel electrophoresis. Agarose solution was prepared by weighing 0.8 g of agarose per 100 ml of TAE buffer (40 mM Tris-acetate, 20 mM Na-acetate, 1 mM EDTA, pH 7.5) and boiling in a microwave oven until a clear solution was obtained. When the 0.8% agarose solution cooled to about 65°C, it was poured into a cast and 0.5 µg/ml of EtBr was added. After mixing with the pipette tip, a comb was inserted and the agarose solution was allowed to solidify after cooling under fume hood.

DNA samples, mixed with Gel Loading Dye (6X concentrate from NEB: 15% Ficoll®-400, 60mM EDTA, 19.8mM Tris-HCl, 0.48% SDS, 0.12% Dye1 (pink/red), 0.006% Dye2 (blue), pH 8), were loaded into the wells and the gel was run at constant voltage, 100-180V depending on the length of the gel. DNA fragments were visualized on a UV screen (366 nm).

2.1.2.2 DNA extraction from the gel

‘mi-Gel Extraction Kit’ from Metabion was used to extract DNA fragments from agarose gels. Using a scalpel, desired DNA fragment, visualized under UV light, was carefully cut out from the gel and placed into a 2 ml microcentrifuge tube. ‘GEX buffer’ (500µl per 50-200 mg gel piece) was added into the tube and the gel was dissolved by vigorous shaking at

60°C for 5-10 minutes. When the gel piece was dissolved completely, the solution was passed through 'GP column' by centrifuging at 10,000 x g for 30 s. The column was washed with 500 µl of 'WN buffer' followed by 500 µl of 'WS buffer'. After a spin at 16,100 x g for 1 min to remove residual EtOH, the DNA fragment was eluted with 20-30 µl of sterile distilled water at 16,100 x g for 1-2 minutes. The eluted DNA was used immediately for further experiments.

2.1.2.3 Concentration measurement of DNA samples

The concentration of DNA samples was done by measuring absorbance at 260 nm using NanoDrop. One optical unit corresponds to 50 µg/ml of double stranded DNA.

2.1.3 Enzymatic modification of DNA

2.1.3.1 Restriction digestion

Restriction enzymes from NEB were used for analysis or manipulation of DNA samples. Typically, 0.1 µg to 3 µg of DNA was digested with 10-20 units of enzyme per µg of DNA. Reaction buffer and temperature were chosen for each enzyme according to the instructions of the manufacturer (NEB). Following digestion reactions, DNA samples were analyzed by agarose gel electrophoresis.

2.1.3.2 Ligation

The vectors and the inserts, used for generation of plasmids used in this study, were digested with appropriate restriction enzymes to form DNA fragments with sticky ends, which provide desired directionality in the ligation procedure. After their extraction from the gel, about 100 ng of linearized vector was mixed with 5-10 molar excess of cut insert fragment in a ligation reaction with 10 U of T4 DNA ligase (NEB) and T4 ligase buffer (50 mM Tris-HCl, 10 mM MgCl₂, 1 mM ATP, 10 mM DTT, pH 7.5). Ligation reaction was incubated for 2 h at 25°C or overnight at 16°C. Then, 0.5-1 µl of the reaction was used to transform electrocompetent *E. coli* (MH1) cells.

2.1.4 Preparation of electrocompetent *E. coli*

Bacterial cells were cultured in 50 ml of LB medium and grown overnight at 37°C with vigorous shaking (150-160 rpm). Next day, 2 ml of the overnight culture was diluted into 1 L

of fresh LB medium and grown at 37°C until OD₆₀₀ reached 0.5-0.6. The culture was cooled on ice for 30 min, and then centrifuged at 4,400 x g for 5 min at 4°C. Pellet was resuspended in 400 ml of 10% glycerol and the solution centrifuged again as above. This step was repeated twice, first using 200 ml and then 50 ml of 10% glycerol. Finally, the cells were resuspended in 1 ml of 10% glycerol, aliquoted in 45 µl aliquots and stored at -80°C until use.

Table 2.1 *E. coli* strains used in this study.

<i>E. coli</i> Strain	Used for	Reference
MH1	Cloning	(Casadaban and Cohen, 1980)
C43(DE3)	Membrane prot. expression and purification	(Miroux and Walker, 1996)

2.1.5 Transformation of *E. coli* cells by electroporation

An aliquot of electrocompetent cells was taken from -80°C freezer and put immediately on ice. Once the cells were thawed, 0.5 – 1 µl of plasmid DNA or ligation mixture was mixed with the cells. Then, the mix was transferred into an ice-cold electroporation cuvette and high voltage pulse (2500 V) was applied using Eporator (Eppendorf). Transformed cells were resuspended in 1 ml of LB, transferred into a microfuge tube and incubated for 15-20 min at 37°C with shaking at 150-160 rpm. Lastly, the cells were either directly diluted into liquid LB-Amp medium or plated on LB-Amp agar plates for overnight growth.

2.1.6 Plasmid constructs used in this work

Table 2.2 List of plasmid constructs used in this study. The constructs were named from p1 to p77 for simplicity and linked with the list of primers in Table 2.3.

#	Construct	Vector	Reference
p1	prom-Tim23-flank	pRS315	(Gevorkyan-Airapetov et al., 2009)
p2	prom-Tim23Δ10-flank	pRS315	This thesis
p3	prom-Tim23Δ20-flank	pRS315	This thesis
p4	prom-Tim23Δ24-flank	pRS315	This thesis
p5	prom-Tim23Δ30-flank	pRS315	This thesis
p6	prom-Tim23Δ40-flank	pRS315	This thesis
p7	prom-Tim23Δ50-flank	pRS315	(Waegemann et al., 2015)
p8	prom-Tim23Δ60-flank	pRS315	This thesis

p9	prom-Tim23Δ70-flank	pRS315	This thesis
p10	prom-Tim23Δ80-flank	pRS315	This thesis
p11	prom-Tim23Δ90-flank	pRS315	This thesis
p12	Tim23Δ30	p415 GPD	This thesis
p13	prom-Tim23-flank	pRS314	(Waegemann et al., 2015)
p14	prom-Tim23M51A7-flank	pRS314	This thesis
p15	prom-Tim23L58A5-flank	pRS314	This thesis
p16	prom-Tim23G63A5-flank	pRS314	This thesis
p17	prom-Tim23V68A-flank	pRS314	This thesis
p18	prom-Tim23V68A5-flank	pRS314	This thesis
p19	prom-Tim23V68A/D72A-flank	pRS314	This thesis
p20	prom-Tim23E69A-flank	pRS314	This thesis
p21	prom-Tim23E69A2-flank	pRS314	This thesis
p22	prom-Tim23E69A/L71A-flank	pRS314	This thesis
p23	prom-Tim23E69A3-flank	pRS314	This thesis
p24	prom-Tim23Y70A-flank	pRS314	(Gevorkyan-Airapetov et al., 2009)
p25	prom-Tim23Y70A2-flank	pRS314	(Gevorkyan-Airapetov et al., 2009)
p26	prom-Tim23L71A-flank	pRS314	(Gevorkyan-Airapetov et al., 2009)
p27	prom-Tim23D72A-flank	pRS314	This thesis
p28	prom-Tim23L73A5-flank	pRS314	This thesis
p29	prom-Tim23L78A5-flank	pRS314	This thesis
p30	prom-Tim23L81A5-flank	pRS314	This thesis
p31	prom-Tim23S84A5-flank	pRS314	This thesis
p32	prom-Tim23L87A5-flank	pRS314	This thesis
p33	prom-Tim23S90A5-flank	pRS314	This thesis
p34	prom-Tim23G92A3-flank	pRS314	This thesis
p35	prom-Tim23D95A2-flank	pRS314	This thesis
p36	prom-Tim23D95K2-flank	pRS314	This thesis
p37	prom-Tim23L97A3-flank	pRS314	This thesis
p38	Tim23-His ₉	p415 GPD	This thesis
p39	Tim23W3Bpa-His ₉	p415 GPD	This thesis
p40	Tim23K8Bpa-His ₉	p415 GPD	This thesis
p41	Tim23T11Bpa-His ₉	p415 GPD	This thesis
p42	Tim23N15Bpa-His ₉	p415 GPD	This thesis

MATERIALS AND METHODS

p43	Tim23V18Bpa-His ₉	p415 GPD	This thesis
p44	Tim23Q21Bpa-His ₉	p415 GPD	This thesis
p45	Tim23K25Bpa-His ₉	p415 GPD	This thesis
p46	Tim23L29Bpa-His ₉	p415 GPD	This thesis
p47	Tim23Q33Bpa-His ₉	p415 GPD	This thesis
p48	Tim23F37Bpa-His ₉	p415 GPD	This thesis
p49	Tim23N40Bpa-His ₉	p415 GPD	This thesis
p50	Tim23F37Bpa/L58A5-His ₉	p415 GPD	This thesis
p51	Tim23N40Bpa/L58A5-His ₉	p415 GPD	This thesis
p52	Tim23F37Bpa/Y70A2-His ₉	p415 GPD	This thesis
p53	Tim23N40Bpa/Y70A2-His ₉	p415 GPD	This thesis
p54	Tim23Q85Bpa-His ₉	p415 GPD	This thesis
p55	Tim23L87Bpa-His ₉	p415 GPD	This thesis
p56	Tim23I88Bpa-His ₉	p415 GPD	This thesis
p57	Tim23R91Bpa-His ₉	p415 GPD	This thesis
p58	prom-Tim23ΔTM4-flank	pRS315	This thesis
p59	prom-Tim23ΔTM3-4-flank	pRS315	This thesis
p60	prom-Tim17-flank	pRS314	(Demishtein-Zohary et al., 2017)
p61	prom-Tim17 ΔTM1-2-flank	pRS314	This thesis
p62	prom-Tim17ΔTM3-4-flank	pRS314	This thesis
p63	prom-Tim17G25L-flank	pRS314	(Demishtein-Zohary et al., 2017)
p64	prom-Tim17G29L-flank	pRS314	(Demishtein-Zohary et al., 2017)
p65	prom-Tim17G62L-flank	pRS314	(Demishtein-Zohary et al., 2017)
p66	prom-Tim17G66L-flank	pRS314	(Demishtein-Zohary et al., 2017)
p67	prom-Tim17G95L-flank	pRS314	(Demishtein-Zohary et al., 2017)
p68	prom-Tim17G99L-flank	pRS314	(Demishtein-Zohary et al., 2017)
p69	prom-Tim17V104A5-flank	pRS314	This thesis
p70	prom-Tim17R109A5-flank	pRS314	This thesis
p71	prom-Tim17R105A-flank	pRS314	This thesis
p72	prom-Tim17R105K-flank	pRS314	This thesis
p73	Tim17-His ₉	p415 GPD	This thesis
p74	Tim17G106Bpa-His ₉	p415 GPD	This thesis
p75	Tim17R105A/G106Bpa-His ₉	p415 GPD	This thesis
p76	pBpa2-PGK1 + 3SUP4-tRNACUA	-	(Chen et al., 2007)

p77	pET-Duet1- Tim23 _{his9} - Tim17 _{strep}	pET-Duet1	This thesis
p78	pET-Duet1- Tim23 _{TEV-his9} - Tim17 _{strep}	pET-Duet1	This thesis

2.1.7 Primer pairs used in this thesis

Table 2.3 List of primer pairs used in this thesis. The sequences of primers were listed as pairs of forward (FP) and reverse (RP) from 5' to 3' end. Restriction enzymes used in the cloning method, template DNA used in the PCR reaction and the final construct were stated for each pair. Cl.- Cloning (section 2.1.8.1), SDM- Site directed mutagenesis (section 2.1.8.2).

Mutation		Primers (5'→3')	Rest. Enz.	Method	Template	Final Construct
Tim23 Δ10	FP	CCCGGATCCATGACCGATGATGCGAATGCTGCC	BamHI	Cl.	p1	p2
	RP	CCCAAGCTTTCATTTTCAAGTAGTCTTTCTTGACAC	HindIII			
Tim23 Δ20	FP	CCCGGATCCATGCAAGATACAACCAAGCCTAAGG	BamHI	Cl.	p1	p3
	RP	Same as Tim23Δ10-RP	HindIII			
Tim23 Δ24	FP	CCCGGATCCATGAAGCCTAAGGAACTATCGTTG	BamHI	Cl.	p1	p4
	RP	Same as Tim23Δ10-RP	HindIII			
Tim23 Δ30	FP	CCCGGATCCATGTTGAAGCAGAGTTTAGGTTTCG	BamHI	Cl.	p1	p5
	RP	Same as Tim23Δ10-RP	HindIII			
Tim23 Δ40	FP	CCCGGATCCATGATCAATAACATAATATCAGGTC	BamHI	Cl.	p1	p6
	RP	Same as Tim23Δ10-RP	HindIII			
Tim23 Δ60	FP	CCCGGATCCATGTTGGCTGGTCTAGACAAGGG	BamHI	Cl.	p1	p8
	RP	Same as Tim23Δ10-RP	HindIII			
Tim23 Δ70	FP	CCCGGATCCATGTTAGATCTGGAAGAAGAACAAC	BamHI	Cl.	p1	p9
	RP	Same as Tim23Δ10-RP	HindIII			
Tim23 Δ80	FP	CCCGGATCCATGTTAGAAGGCTCACAGGGTCTG	BamHI	Cl.	p1	p10
	RP	Same as Tim23Δ10-RP	HindIII			
Tim23 Δ90	FP	CCCGGATCCATGCGTGGGTGGACCGATGACCTATG	BamHI	Cl.	p1	p11
	RP	Same as Tim23Δ10-RP	HindIII			
Tim23 M51A7	FP	AGCTGCCGCTGCGCTGCATCCTTGGCTGGTC	PvuII site added	SDM	p13	p14
	RP	GCAGCCGCTCCACCAGGACCTGATATTATG				
Tim23 L58A5	FP	CAGCTGCTGGTCTAGACAAGGGTGTGGAG	PvuII site added	SDM	p13	p15
	RP	CAGCCGCCCTAGCGGTGTCGACATGCATTCC				

MATERIALS AND METHODS

Tim23 G63A5	FP	TGCGGCTGTGGAGTATTTAGATCTGGAAG	PvuII site added	SDM	p13	p16
	RP	GCTGCAGCAGCCAAAGGATGCAGCCTAGCG				
Tim23 V68A	FP	GCGGAGTATTTAGACCTGGAAGAAG	BglII site removed	SDM	p13	p17
	RP	ACCCTTGTCTAGACCAGCCAAAGG				
Tim23 V68A5	FP	TGCAGCACTGGAAGAAGAACAACATCCTC	PvuII site added	SDM	p13	p18
	RP	GCTGCTGCACCCTTGTCTAGACCAGCCAAAG				
Tim23 V68A/D72A	FP	GCGGAGTATTTAGCCCTGGAAGAAG	BglII site removed	SDM	p13	p19
	RP	Same as V68A-RP				
Tim23 E69A	FP	TATTTAGACCTGGAAGAAGAACAAC	BglII site removed	SDM	p13	p20
	RP	CGCCACACCCTTGTCTAGACCAGCC				
Tim23 E69A2	FP	CTTTAGACCTGGAAGAAGAACAAC	BglII site removed	SDM	p13	p21
	RP	CTGCCACACCCTTGTCTAGACCAGCC				
Tim23 E69A/L71A	FP	TATGCAGACCTGGAAGAAGAACAAC	BglII site removed	SDM	p13	p22
	RP	Same as E69A-RP				
Tim23 E69A3	FP	CTGCAGATCTGGAAGAAGAACAACATC	PvuII site added	SDM	p13	p23
	RP	Same as E69A2-RP				
Tim23 D72A	FP	GTGGAGTATTTAGCCCTGGAAGAAG	BglII site removed	SDM	p13	p27
	RP	Same as V68A-RP				
Tim23 L73A5	FP	CTGCAGCACTATCCTCGTTAGAAGGCTC	PvuII site added	SDM	p13	p28
	RP	CTGCTGCATCTAAATACTCCACACCCTTG				
Tim23 L78A5	FP	GCAGCAGCAGGCTCACAGGGTCTGATCCC	PvuII site added	SDM	p13	p29
	RP	AGCTGCTTGTCTCTTCCAGATCTAAATAC				
Tim23 L81A5	FP	CTGCAGCGGGTCTGATCCCTTCCCGTGGG	PvuII site added	SDM	p13	p30
	RP	CTGCTGCCGAGGATAGTTGTTCTTCTTCC				
Tim23 S84A5	FP	TGCAGCCCCTTCCCGTGGGTGGACCG	PvuII site added	SDM	p13	p31
	RP	GCTGCTGCGCCTTCTAACGAGGATAGTTG				
Tim23 L87A5	FP	GCTGCAGCTGGGTGGACCGATGACCTATG	PvuII site added	SDM	p13	p32
	RP	TGCCGCACCCTGTGAGCCTTCTAACG				
Tim23 S90A5	FP	GCAGCTGCAGATGACCTATGTTACGGTACC	PvuII site added	SDM	p13	p33
	RP	TGCGGCAGGGATCAGACCCTGTGAGC				
Tim23 G92A3	FP	Same as Tim23S90A5-FP	PvuII site added	SDM	p13	p34
	RP	ACGGGAAGGGATCAGACCCTG				
Tim23 D95A2	FP	GGACAGCTGCCCTATGTTACGGTACCGG	PvuII site added	SDM	p13	p35
	RP	ACCCGCGGGAAGGGATCAGACCCTG				

Tim23 D95K2	FP	GGACCAAGAAGCTTTGTTACGGTACCGG	HindIII site added	SDM	p13	p36
	RP	Same as Tim23D95A2-RP				
Tim23 L97A3	FP	CTGCAGGTACCGGTGCCGTCTACC	PvuII site added	SDM	p13	p37
	RP	CTGCGTCATCGGTCCACCCACGGG				
Tim23 W3Bpa	FP	TAGCTTTTTGGAGATAAGACACCTAC	BamHI site removed	SDM	p38	p39
	RP	CGACATTGATCCACTAGTTCTAGAATC				
Tim23 K8Bpa	FP	TGGCTTTTTGGAGATTAGACACCTAC	BamHI site removed	SDM	p38	p40
	RP	Same as Tim23W3Bpa-RP				
Tim23 T11Bpa	FP	TAGGATGATGCGAATGCTGCAGTGGG	PstI site added	SDM	p38	p41
	RP	AGGTGTCTTATCTCCAAAAGCCAC				
Tim23 N15Bpa	FP	ACCGATGATGCGTAGGCTGCAGTGGG	PstI site added	SDM	p38	p42
	RP	Same as Tim23T11Bpa-RP				
Tim23 V18Bpa	FP	TAGGGTGGCCAAGATACAACCAAG	MscI site added	SDM	p38	p43
	RP	GGCAGCATTCGCATCATCGGTAGGTG				
Tim23 Q21Bpa	FP	CCTAAGGAACTAAGCTTGAAGCAG	HindIII site added	SDM	p38	p44
	RP	CTTGGTTGTATCCTAGCCGCCAC				
Tim23 K25Bpa	FP	Same as Tim23Q21Bpa-FP	HindIII site added	SDM	p38	p45
	RP	CTAGGTTGTATCTTGGCCGCCAC				
Tim23 L29Bpa	FP	AGCCTAGGTTTCGAGCCAAACATC	AvrII site added	SDM	p38	p46
	RP	CTGCTTCAACGACTATTCCTTAGGC				
Tim23 Q33Bpa	FP	Same as Tim23L29Bpa-FP	AvrII site added	SDM	p38	p47
	RP	CTACTTCAACGATAGTTCCTTAGGC				
Tim23 F37Bpa	FP	TAGGAGCCAAACATCAATAACATAATATC	AvrII site added	SDM	p38	p48
	RP	ACCTAGGCTCTGCTTCAACGATAGTTC				
Tim23 N40Bpa	FP	TTCGAGCCATAGATCAATAACATAATATC	AvrII site added	SDM	p38	p49
	RP	Same as Tim23F37Bpa-RP				
Tim23 F37Bpa/ L58A5	FP	Same as Tim23L58A5-FP	PvuII site added	SDM	p48	p50
	RP	Same as Tim23L58A5-RP				
Tim23 N40Bpa/ L58A5	FP	Same as Tim23L58A5-FP	PvuII site added	SDM	p49	p51
	RP	Same as Tim23L58A5-RP				
Tim23 F37Bpa/ Y70A2	FP	Same as Tim23F37Bpa-FP	PvuII site added	SDM	p25	p52
	RP	Same as Tim23F37Bpa-RP				
Tim23 N40Bpa/ Y70A2	FP	Same as Tim23F40Bpa-FP	PvuII site added	SDM	p25	p53
	RP	Same as Tim23F37Bpa-RP				

MATERIALS AND METHODS

Tim23 Q85Bpa	FP	GATCCCTTCCCGTGGGTGGACCGATGACC	None	SDM	p38	p54
	RP	AGACCCTATGAGCCTTCTAACGAGG				
Tim23 L87Bpa	FP	Same as Tim23Q85Bpa-FP	None	SDM	p38	p55
	RP	TAACCCTGTGAGCCTTCTAACGAGG				
Tim23 l88Bpa	FP	GTAGCCTTCCCGTGGGTGGACCGATGACC	None	SDM	p38	p56
	RP	AGACCCTGTGAGCCTTCTAACGAGG				
Tim23 R91Bpa	FP	GATCCCTTCCTAGGGGTGGACCGATGACC	AverII site added	SDM	p38	p57
	RP	Same as Tim23l88Bpa-RP				
Tim23 ΔTM4	FP	AAAGGATCCATGTCGTGGCTTTTGGAGA	BamHI	Cl.	p1	p58
	RP	GGGAAGCTTTCATGAAGACTTGAACAAAGCGCCCG	HindIII			
Tim23 ΔTM3-4	FP	Same as Tim23ΔTM4-FP	BamHI	Cl.	p1	p59
	RP	GGGAAGCTTTCATAGTGCATCTATTGTAGAATTG	HindIII			
Tim17 ΔTM1-2	FP	CCCGGATCCATGGATTGCGCTGTGAAGGCCG	SacI	Cl.	p60	p61
	RP	GGGCTGCAGCTAAGCTTGCAGAGGTTGAG	PstI			
Tim17 ΔTM3-4	FP	CCCAGCTCCAATACCATTGCGGTTATACTG	SacI	Cl.	p60	p62
	RP	GGGCTGCAGTCAGTCCTCTCTTTCTAACGG	PstI			
Tim17 V104A5	FP	GCTGCTAGGCATACAAGGAACAGTTCG	SacII site added	SDM	p60	p69
	RP	AGCCGCGGCAGCTAAAGCGCCACCAAGTG				
Tim17 R109A5	FP	GCTGCTAGTTCGATCACGTGTGCTTG	SacII site added	SDM	p60	p70
	RP	AGCCGCGGCCCAACCACCTCTTACAGCTAAAG				
Tim17 R105A	FP	GCAGGTGGTTGGAGGCATACAAGG	NheI site added	SDM	p60	p71
	RP	TACAGCTAGCGGCCACCAAGTG				
Tim17 R105K	FP	AAAGGTGGTTGGAGGCATACAAGG	NheI site added	SDM	p60	p72
	RP	Same as Tim17R105A-RP				
Tim17 G106Bpa	FP	GTAAGATAGGGTTGGAGGCATACAAG	NheI site added	SDM	p73	p74
	RP	AGCTAGCGGCCACCAAGTGAAAAAC				
Tim17 R105A/ G106Bpa	FP	GTAGCATAGGGTTGGAGGCATACAAGGAAC	NheI site added	SDM	p73	p75
	RP	Same as Tim17G106Bpa-RP				
Tim23 _{his9} for pET- Duet1	FP	GGGCCATGGCATGGCTTTTTGGAGATAAGAC	NcoI	Cl.	p1	p77
	RP	CCCAAGCTTTCAGTGATGGTGATGGTGATGGTGATGGTGTT TTTCAAGTAGTCTTTCTTG	HindIII			
Tim17 _{strep} for pET- Duet1	FP	GGAATTGCATATGTCAGCCGATCATTCGAG	NdeI	Cl.	p60	
	RP	GGGCTCGAGCTATTTCTCAAATTGAGGGTGAGACCAACCAG AAGCTTGCAGAGGTTGAGAGG	XhoI			

2.1.8 Amplification of DNA fragments and cloning procedure

Polymerase chain reaction (PCR) was used to amplify DNA fragments. In this thesis, two types of PCR reactions were used (see sections 2.1.8.1 and 2.1.8.2). The primer pairs and the template DNA used in the PCR reaction and the type of PCR reaction together with the final product arose from the PCR reaction are summarized in Table 2.3 (Section 0).

2.1.8.1 Cloning (Cl.)

DNA fragment to be inserted into a vector was amplified in a PCR reaction consisting of 10 μ l of 10X Taq buffer (NEB), 2.5 U Taq polymerase (NEB), 0.8 μ l of dNTPs (10 mM each), 2.5 μ l of each forward and reverse primers (20 μ M each), 20 ng of template DNA and sterile distilled water to a final volume of 100 μ l. The following PCR program was used for amplification:

	Temperature	Time
Initial denaturation	95°C	3 min
PCR cycle:	30 cycle	
Denaturation	95°C	30 sec
Annealing	50°C	30 sec
Extension	72°C	1 min/kb
Final extension	72°C	5 min
Hold	8°C	∞

Following amplification by PCR, the PCR reaction was run on an agarose gel, the DNA fragment of the correct size excised and eluted from the gel and then cut (section 2.1.3.1) with the respective restriction enzymes shown in Table 2.3. In parallel, the vector was cut with the same enzymes. Both reactions were run on an agarose gel. After DNA extraction from the gel (section 2.1.2.2), they were ligated together (section 2.1.3.2), transformed into *E. coli* cells and the cells were plated on LB+Amp plate (section 2.3.1) for overnight growth. Two colonies from the plate were chosen for plasmid DNA isolation (section 2.1.1). Isolated plasmids were tested via restriction digestion (section 2.1.3.1) and positive clones were sent for sequencing for sequence confirmation.

2.1.8.2 Site directed mutagenesis (SDM)

Site-directed mutagenesis was done using primers designed to modify the DNA sequence in order to introduce the desired mutation (see section 0). Additionally, the primers contained a silent mutation, which either added or removed a restriction site to help in identification of positive clones. Each primer used for SDM was first phosphorylated in a reaction containing 2 μ l of 10X PNK buffer (NEB), 1 μ l of T4 PNK (NEB), 7 μ l of primer (100 μ M), 2 μ l of ATP (10 mM) and 8 μ l of sterile distilled water. The reactions were incubated for 1 h at 37°C and then stopped by heating at 95°C for 5 min. The concentration of the primers was adjusted to 10 μ M by adding 50 μ l of sterile distilled water. Since the PCR products are directly ligated in this protocol, phosphorylation of the primers is required for efficient ligation reaction.

In this method, instead of amplifying a small fragment of a plasmid, the whole plasmid was amplified using Phusion-HF (NEB) enzyme using phosphorylated primers. Each reaction contained 2 μ l of 5X Phusion-HF buffer, 0.1 μ l of Phusion-HF, 2-4 ng of template plasmid DNA, 0.6 μ l of each primer (10 μ M) and sterile distilled water to a final volume of 10 μ l. 5% DMSO was sometimes added, especially in case of high GC content. A gradient annealing step was used for most of the constructs in order to get the PCR products as clean as possible. The following PCR program was used for amplification:

	Temperature	Time
Initial denaturation	95°C	5 min
PCR cycle:	25 cycle	
Denaturation	95°C	30 sec
Annealing	50→70°C	30 sec
Extension	72°C	1 min/kb
Final extension	72°C	10 min
Hold	8°C	∞

PCR reactions were analyzed by agarose gel electrophoresis and 2-5 μ l of the cleanest PCR reaction were used directly for ligation. Alternatively, if all PCR reactions contained nonspecific bands, agarose gel separation followed by gel extraction were applied to get a

clean DNA fragment. Following ligation, *E. coli* cells were transformed and the cells were plated on LB+Amp plate (section 2.1.5) for overnight growth. Several colonies per plate were picked and inoculated for minipreps (section 2.1.1.2). Plasmid DNA isolated by miniprep was analyzed by restriction digestion for initial screening of positive colonies (section 2.1.3.1). Positive clones were inoculated for plasmid DNA isolation protocol (section 2.1.1), rechecked by restriction digestion and the mutations confirmed by sequencing.

2.2 Yeast Genetics

2.2.1 Yeast strains used in this study

Table 2.4 Yeast strains used. Yeast strains, plasmids used to generate the strains (Table 2.2) and the parent strains are listed below.

Name of the Strain/Mutant	Used plasmid(s)	Parent strain	Reference
YPH499	-	-	(Sikorski and Hieter, 1989)
Tim23 shuffling strain	-	YPH499ΔTIM23::KAN + pVT-102U-Tim23	(Gevorkyan-Airapetov et al., 2009)
Tim23 (WT)	p1	YPH499ΔTIM23::KAN	(Gevorkyan-Airapetov et al., 2009)
<i>tim23Δ10</i>	p2	YPH499ΔTIM23::KAN	This thesis
<i>tim23Δ20</i>	p3	YPH499ΔTIM23::KAN	This thesis
<i>tim23Δ24</i>	p4	YPH499ΔTIM23::KAN	This thesis
<i>tim23Δ30</i>	p5	YPH499ΔTIM23::KAN	This thesis
<i>tim23Δ40</i>	p6	YPH499ΔTIM23::KAN	This thesis
<i>tim23Δ50</i>	p7	YPH499ΔTIM23::KAN	(Waegemann et al., 2015)
<i>tim23Δ60</i>	p8	YPH499ΔTIM23::KAN	This thesis
<i>tim23Δ70</i>	p9	YPH499ΔTIM23::KAN	This thesis
<i>tim23Δ80</i>	p10	YPH499ΔTIM23::KAN	This thesis
<i>tim23Δ90</i>	p11	YPH499ΔTIM23::KAN	This thesis
<i>tim23Δ30</i> ↑	p12	YPH499ΔTIM23::KAN	This thesis
Tim23 (WT)	p13	YPH499ΔTIM23::KAN	(Waegemann et al., 2015)
<i>tim23M51A7</i>	p14	YPH499ΔTIM23::KAN	This thesis
<i>tim23L58A5</i>	p15	YPH499ΔTIM23::KAN	This thesis
<i>tim23G63A5</i>	p16	YPH499ΔTIM23::KAN	This thesis

MATERIALS AND METHODS

<i>tim23V68A</i>	p17	YPH499Δ <i>TIM23::KAN</i>	This thesis
<i>tim23V68A5</i>	p18	YPH499Δ <i>TIM23::KAN</i>	This thesis
<i>tim23V68A/D72A</i>	p19	YPH499Δ <i>TIM23::KAN</i>	This thesis
<i>tim23E69A</i>	p20	YPH499Δ <i>TIM23::KAN</i>	This thesis
<i>tim23E69A2</i>	p21	YPH499Δ <i>TIM23::KAN</i>	This thesis
<i>tim23E69A/L71A</i>	p22	YPH499Δ <i>TIM23::KAN</i>	This thesis
<i>tim23E69A3</i>	p23	YPH499Δ <i>TIM23::KAN</i>	This thesis
<i>tim23Y70A</i>	p24	YPH499Δ <i>TIM23::KAN</i>	(Gevorkyan-Airapetov et al., 2009)
<i>tim23Y70A2</i>	p25	YPH499Δ <i>TIM23::KAN</i>	(Gevorkyan-Airapetov et al., 2009)
<i>tim23L71A</i>	p26	YPH499Δ <i>TIM23::KAN</i>	(Gevorkyan-Airapetov et al., 2009)
<i>tim23D72A</i>	p27	YPH499Δ <i>TIM23::KAN</i>	This thesis
<i>tim23L73A5</i>	p28	YPH499Δ <i>TIM23::KAN</i>	This thesis
<i>tim23L78A5</i>	p29	YPH499Δ <i>TIM23::KAN</i>	This thesis
<i>tim23L81A5</i>	p30	YPH499Δ <i>TIM23::KAN</i>	This thesis
<i>tim23S84A5</i>	p31	YPH499Δ <i>TIM23::KAN</i>	This thesis
<i>tim23L87A5</i>	p32	YPH499Δ <i>TIM23::KAN</i>	This thesis
<i>tim23S90A5</i>	p33	YPH499Δ <i>TIM23::KAN</i>	This thesis
<i>tim23G92A3</i>	p34	YPH499Δ <i>TIM23::KAN</i>	This thesis
<i>tim23D95A2</i>	p35	YPH499Δ <i>TIM23::KAN</i>	This thesis
<i>tim23D95K2</i>	p36	YPH499Δ <i>TIM23::KAN</i>	This thesis
<i>tim23L97A3</i>	p37	YPH499Δ <i>TIM23::KAN</i>	This thesis
<i>tim23ΔTM4</i>	p58	YPH499Δ <i>TIM23::KAN</i>	This thesis
<i>tim23ΔTM3-4</i>	p59	YPH499Δ <i>TIM23::KAN</i>	This thesis
Tim17 shuffling strain	-	YPH499Δ <i>TIM17::HIS3</i> + pVT-102U-Tim17	(Demishtein-Zohary et al., 2017)
Tim17 (WT)	p60	YPH499Δ <i>TIM17::HIS3</i>	This thesis
<i>tim17ΔTM1-2</i>	p61	YPH499Δ <i>TIM17::HIS3</i>	This thesis
<i>tim17ΔTM3-4</i>	p62	YPH499Δ <i>TIM17::HIS3</i>	This thesis
<i>tim17G25L</i>	p63	YPH499Δ <i>TIM17::HIS3</i>	(Demishtein-Zohary et al., 2017)
<i>tim17G29L</i>	p64	YPH499Δ <i>TIM17::HIS3</i>	(Demishtein-Zohary et al., 2017)
<i>tim17G62L</i>	p65	YPH499Δ <i>TIM17::HIS3</i>	(Demishtein-Zohary et al., 2017)
<i>tim17G66L</i>	p66	YPH499Δ <i>TIM17::HIS3</i>	(Demishtein-Zohary et al., 2017)
<i>tim17G95L</i>	p67	YPH499Δ <i>TIM17::HIS3</i>	(Demishtein-Zohary et al., 2017)
<i>tim17G99L</i>	p68	YPH499Δ <i>TIM17::HIS3</i>	(Demishtein-Zohary et al., 2017)
<i>tim17V104A5</i>	p69	YPH499Δ <i>TIM17::HIS3</i>	This thesis

<i>tim17R109A5</i>	p70	YPH499Δ <i>TIM17::HIS3</i>	This thesis
<i>tim17R105A</i>	p71	YPH499Δ <i>TIM17::HIS3</i>	This thesis
<i>tim17R105K</i>	p72	YPH499Δ <i>TIM17::HIS3</i>	This thesis

Strains for *in vivo* site-specific photocrosslinking

Tim23 (WT)	p38, p76	YPH499Δ <i>TIM23::KAN</i>	This thesis
<i>tim23W3Bpa</i>	p39, p76	YPH499Δ <i>TIM23::KAN</i>	This thesis
<i>tim23K8Bpa</i>	p40, p76	YPH499Δ <i>TIM23::KAN</i>	This thesis
<i>tim23T11Bpa</i>	p41, p76	YPH499Δ <i>TIM23::KAN</i>	This thesis
<i>tim23N15Bpa</i>	p42, p76	YPH499Δ <i>TIM23::KAN</i>	This thesis
<i>tim23V18Bpa</i>	p43, p76	YPH499Δ <i>TIM23::KAN</i>	This thesis
<i>tim23Q21Bpa</i>	p44, p76	YPH499Δ <i>TIM23::KAN</i>	This thesis
<i>tim23K25Bpa</i>	p45, p76	YPH499Δ <i>TIM23::KAN</i>	This thesis
<i>tim23L29Bpa</i>	p46, p76	YPH499Δ <i>TIM23::KAN</i>	This thesis
<i>tim23Q33Bpa</i>	p47, p76	YPH499Δ <i>TIM23::KAN</i>	This thesis
<i>tim23F37Bpa</i>	p48, p76	YPH499Δ <i>TIM23::KAN</i>	This thesis
<i>tim23N40Bpa</i>	p49, p76	YPH499Δ <i>TIM23::KAN</i>	This thesis
<i>tim23F37Bpa/L58A5</i>	p50, p76	YPH499	This thesis
<i>tim23N40Bpa/L58A5</i>	p51, p76	YPH499	This thesis
<i>tim23F37Bpa/Y70A2</i>	p52, p76	YPH499	This thesis
<i>tim23N40Bpa/Y70A2</i>	p53, p76	YPH499	This thesis
<i>tim23Q85Bpa</i>	p54, p76	YPH499Δ <i>TIM23::KAN</i>	This thesis
<i>tim23L87Bpa</i>	p55, p76	YPH499Δ <i>TIM23::KAN</i>	This thesis
<i>tim23I88Bpa</i>	p56, p76	YPH499Δ <i>TIM23::KAN</i>	This thesis
<i>tim23R91Bpa</i>	p57, p76	YPH499Δ <i>TIM23::KAN</i>	This thesis
Tim17 (WT)	p73, p76	YPH499Δ <i>TIM17::HIS3</i>	This thesis
<i>tim17G106Bpa</i>	p74, p76	YPH499Δ <i>TIM17::HIS3</i>	This thesis
<i>tim17R105A/G106Bpa</i>	p75, p76	YPH499Δ <i>TIM17::HIS3</i> + pVT-102U-Tim17	This thesis

2.2.2 Transformation of yeast cells

Overnight culture of yeast cells was diluted to OD₆₀₀ ~0.1 in 50 ml of YPD medium and grown until OD₆₀₀ of 0.5-0.6. Cells were harvested at 3,000 x g for 5 min at RT and resuspended in 25 ml of sterile deionized water for washing. Centrifugation step was repeated and the supernatant was discarded. Cells were resuspended in 1 ml of 0.1 M lithium

acetate (LiAc) and transferred into a microfuge tube. Cells were harvested at 16,000 x g for 30 s and resuspended with 400 µl of 0.1 M LiAc (final volume ~500 µl). Cell suspension was split into microfuge tubes using 50 µl of cell suspension per transformation reaction. The cells were pelleted by centrifugation at 3,000 x g for 5 min. The supernatants were discarded and the cells were overlaid with 240 µl of 50% (w/v) PEG without disturbing the cell pellet. The following solutions were then added carefully on top of the PEG solution, without disturbing the cell pellet, in the given order: 36 µl of 1 M LiAc, 5 µl of 10 mg/ml ssDNA (boiled for 5 min at 95°C and chilled quickly on ice prior to use), 60 µl of sterile water and 5 µl of plasmid DNA (0.1- 1 µg). Afterwards, tubes were vortexed rigorously for about 1 min and then incubated at 30°C for 30 min with vigorous shaking (~1,000 rpm). The incubation temperature was increased to 42°C and the samples incubated for additional 20-25 minutes. Transformed cells were pelleted at 4,000-6,000 x g for 30 s and the supernatant was discarded. Finally, the cells were resuspended in 150 µl of sterile water and plated on SD plates (see section 0) with required selection markers.

2.2.3 Plasmid shuffling by 5FOA selection

The ability of the various mutants of Tim23 and Tim17 to support the *in vivo* function of the wild type proteins was analyzed by plasmid shuffling in yeast. The yeast shuffling strains used in this thesis (section 2.2.1) are based on the haploid yeast strain YPH499. They contain a chromosomal deletion of the essential gene under study (*TIM23* or *TIM17*) and are viable due to the presence of a *URA3* plasmid (pVT-102U) encoding the wild type copy of the respective essential gene.

For the analysis, shuffling strains were transformed (section 0) with plasmids encoding mutant versions of the protein (section 2.1.6) as well as with the empty plasmid and the plasmid encoding the wild type version of the protein which served as negative and positive controls, respectively. Transformation reactions were plated on SD plates with required markers to keep both of the *URA3* and the other plasmid. Transformants, which appeared on selective plates after 2-3 days of growth at 30°C, were picked and streaked for single colonies on fresh SD plates. Single colonies were then amplified on the same type of selective plates

and then transferred to nonselective YPD plates (see section 2.3.2). Finally, the cells were plated on medium containing 5-fluoroorotic acid (5-FOA). Because *URA3* gene encodes orotidine-5'-monophosphate decarboxylase which converts 5-FOA to toxic 5-fluoro uracil, only cells which lost the *URA3* plasmid and contain the other plasmid with a functional copy of the essential gene survive on this medium.

2.3 Cell Biology

2.3.1 Bacterial culture

E. coli cells were cultured in LB medium which contains 5 g/L yeast extract, 10 g/L bacto-tryptone and 10 g/L NaCl. The medium was sterilized by autoclaving and kept at RT. For the plates, 20 g/L bacto-agar was added prior to autoclaving.

For preparation of LB-Amp medium, ampicillin was added to a sterile LB medium a final concentration of 100 µg/ml from a 100 mg/ml filter-sterilized stock. When preparing LB-Amp plates, ampicillin is added when the medium cooled down to about 50°C. LB-Amp medium is stable for few weeks at 4°C.

2.3.2 Yeast culture

To prepare non-selective medium for yeast culture, YP medium (10 g/L yeast extract, 20 g/L bacto-peptone, pH 5.0) was supplemented with 2% (w/v) glucose or galactose from autoclaved stock solutions (40% (w/v) glucose and 30% (w/v) galactose) to make YPD and YPGal media, respectively. To prepare YPLac medium, 2% lactic acid was added from 90% stock before pH adjustment. For the plates, complete medium was prepared with the addition of 2% (w/v) bacto-agar prior to autoclaving. For isolation of mitochondria, yeast cells were typically grown on Lactate medium (3 g yeast extract, 1 g KH₂PO₄, 1 g NH₄Cl, 0.5 g CaCl₂·2H₂O, 0.5 g NaCl, 1.1 g MgSO₄·6H₂O, 0.3 ml 1% FeCl₃ and 22 ml of 90% lactic acid for 1 L medium and pH adjusted to 5.5 using KOH) supplemented with 0.1% glucose.

SD medium was used to keep a selective pressure on yeast cells to keep plasmids. SD medium was made by diluting the required stock solutions (Table 2.5) to a final 1X concentration and glucose (from 40% stock) to a final concentration of 2% (w/v) with sterile

water. All stock solutions were sterilized by autoclaving, except tryptophan, which was filter-sterilized. SD plates were made by mixing 500 ml of 4% (w/v) bacto-agar (pre-cooled to 65°C after autoclaving) and 500 ml of 2X SD medium with required markers before pouring the medium in Petri dishes. Plates were stored at 4°C until use.

Table 2.5 Stock solutions for selective medium

5X Synthetic minimal medium (5XS)	8.5 g yeast nitrogen base, 25 g (NH ₄) ₂ SO ₄ in 1 L
500X Histidine	10 mg/ml
333X Leucine	10 mg/ml
333X Lysine	10 mg/ml
100X Uracil	2 mg/ml
100X Adenine	2 mg/ml
500X Tryptophan	10 mg/ml

For 5-FOA plates, 1 g of 5-FOA was dissolved in 500 ml of 2X concentrated SD medium with required markers by shaking at 30°C and filter sterilized before mixing with autoclaved agar.

For medium with 1 mM Bpa (p-benzoyl-L-phenylalanine), required amount of Bpa was dissolved in 1 M filter sterilized NaOH. Dissolved Bpa solution was added into SD medium, which was pre-heated to 65°C, dropwise with constant stirring to prevent precipitation of Bpa and the same volume of sterile 1 M HCl was subsequently added to the medium. Bpa containing medium was kept in the dark because of its reactivity in the presence of UV.

2.3.3 Assays with yeast cells

2.3.3.1 Serial dilution spot assay

Growth of yeast cells was analyzed by serial dilution spot assay. Yeast strains to be analyzed were grown overnight in 20 ml of YPD or YPGal medium at 30°C with shaking at 160 rpm. Next day, the cultures were diluted to OD₆₀₀ 0.1 and grown until they reached to OD₆₀₀ ~0.5. Then, 0.5 OD₆₀₀ of cells (1 ml for OD₆₀₀ 0.5) were transferred into a sterile tube and the cells pelleted at 3,000 x g for 5 min. The cells were resuspended in 500 µl of sterile water (1 OD₆₀₀/ml) and five times 10-fold serial dilutions were made. Finally, 2 µl of each cell

suspensions were spotted on YPD and YPLac plates and plates were incubated at different temperatures (24°C, 30°C and 37°C) for 2-5 days.

2.3.3.2 Preparation of total cell lysates

Yeast cells, grown overnight, were diluted in fresh medium and grown until they reach OD₆₀₀ ~0.5 as for serial dilution spot assay (section 2.3.3.1). Three OD₆₀₀ of cells were harvested in 15 ml falcon tube by centrifuging the culture at 3,000 x g for 5 min. Cell pellet was resuspended in 1 ml of water and transferred into a microcentrifuge tube followed by centrifugation at 16,000 x g for 1 min. The pellet was resuspended with 100 µl of water and 100 µl of 0.2 M NaOH was added. Samples were vortexed and kept for 5 min at 25°C. The samples were centrifuged at 16,000 x g for 2 min and the pellets resuspended in 200 µl of 2X Laemmli buffer (120 mM Tris-HCl pH 6.8, 20% (v/v) glycerol, 4% (w/v) SDS, 0.02% (w/v) bromophenol blue) containing β-Mercaptoethanol (see section 2.4.1.1). After 5 min heating at 95°C, samples were centrifuged at 16,000 x g for 20-30 s and 10-20 µl was loaded on an SDS-PA gel, taking care not to disturb the pellet fraction.

2.3.3.3 *In vivo* site-specific photocrosslinking (Total cell extracts and NiNTA pull down)

In vivo site-specific photocrosslinking is used to determine protein-protein interactions *in vivo*. For this, non-natural, photo-reactive amino acid, Bpa (p-benzoyl-L-phenylalanine), is incorporated into a specific position in a protein by changing the codon for that position into a premature stop codon, TAG (see section 0 and 2.1.8.2). Then, the mutated plasmid and an engineered plasmid encoding tRNA_{CUA}/aminoacyl-tRNA_{CUA} synthetase pair, for incorporation of Bpa into the premature stop codon, were transformed into yeast cells (see section 0). Yeast cells were grown in SD medium containing required selection markers and 1 mM Bpa until OD₆₀₀ reached about 0.8. Typically, 40 ml of culture was grown for total cell extracts and 200 ml culture for NiNTA pull-down. Cells were harvested by centrifugation at 3,000 x g for 10 min at 4°C (60-80 OD₆₀₀ per sample). Then, the cells were resuspended in 10 ml of ice-cold SD medium and split into two halves. One half was exposed to UV light (365 nm, 100 W, 230 V) for 1 h on ice while the other half was kept in dark. The cells were re-collected by

centrifugation at 3,000 x g for 10 min at 4°C. At this point, they were either flash frozen in liquid N₂ and stored at -80°C until use or analyzed directly.

To prepare total cell extracts of Bpa mutants, cells pellets were resuspended in 300 µl of water and 300 µl of 0.2 M NaOH was added. Samples were vortexed and kept for 5 min at 25°C. The samples were centrifuged at 16,000 x g for 3 min and the pellets resuspended in 200 µl of 2X Laemmli buffer (120 mM Tris-HCl pH 6.8, 20% (v/v) glycerol, 4% (w/v) SDS, 0.02% (w/v) bromophenol blue) containing β-Mercaptoethanol (see section 2.4.1.1). After 5 min heating at 95°C, samples were centrifuged at 16,000 x g for 20-30 s and 20 µl was loaded on an SDS-PA gel, taking care not to disturb the pellet fraction.

To bind His-tagged protein and its crosslinked products to NiNTA-Agarose beads, a NiNTA pull down was done. The cells were resuspended 500 µl of water and 500 µl of 0.2 M NaOH was added. The samples were kept for 5 min at RT and centrifuged at 16,100 x g for 3 min. The pellets were resuspended in 300 µl of solubilization buffer (50 mM Tris, 150 mM NaCl, 1% (w/v) SDS, pH 8) and, after adding PMSF to a final concentration of 1 mM, the samples were cooked for 5 min at 95°C. Following centrifugation at 16,100 x g for 30 s, 20 µl of samples were taken for totals. The rest of the supernatants were diluted with 3 ml of 50 mM Tris, 300 mM NaCl, 0.5% (v/v) triton X-100, 20 mM imidazole, 1 mM PMSF and added to 50 µl of NiNTA-Agarose beads (beads were previously washed twice with water and equilibrated with the same buffer). Samples were incubated at 4°C for 30 min using an overhead shaker. The beads were pelleted at 1,000 x g for 1.5 min at 4°C, transferred into microfuge tubes and washed three times with 300 µl of wash buffer (50 mM Tris, 300 mM NaCl, 0.1% (v/v) triton X-100, 20 mM imidazole, pH 8). Bound proteins were finally eluted with 60 µl of Laemmli buffer containing β-mercaptoethanol (see section 2.4.1.1) and 300 mM imidazole by incubating at 95°C for 5 min. The samples were split into two and loaded on two SDS-PA gels.

2.3.3.4 Isolation of crude mitochondria

Eight OD₆₀₀ of yeast cells, in the exponential growth phase (see section 2.3.3.1), were transferred to a falcon tube and centrifuged at 3,000 x g at RT for 5 min. Following a wash

step with water, cells were resuspended in 300 μ l of SHK buffer (0.6 M Sorbitol, 20 mM HEPES-KOH, pH 7.2, 80 mM KCl) and PMSF was added to a final concentration 1 mM. After addition of 0.3 g of glass beads (diameter 0.3 mm), the cells were lysed mechanically by vigorous vortexing four times 30 s with 30 s intervals on ice. Glass beads were removed by centrifugation at 1,000 x g for 3 min at 4°C. The supernatant, containing lysed yeast cells, was transferred to a new tube and crude mitochondria were collected by centrifugation at 18,000 x g for 10 min. Mitochondrial pellet was resuspended in Laemmli buffer with β -mercaptoethanol (see section 2.4.1.1). To analyze proteins that remain in the cytosolic fraction, 10 μ l of 72% trichloroacetic acid (TCA) were added to 50 μ l of the supernatant. Samples were mixed thoroughly and then incubated at -20°C for 20 min. Precipitated proteins were collected by centrifugation at 36,700 x g for 20 min at 4°C. The pellet was washed with 200 μ l of ice-cold acetone and the centrifugation step repeated for 10 min. Precipitated proteins from the cytosolic fraction were resuspended in Laemmli buffer with β -mercaptoethanol. Following a 5 min incubation at 95°C, both cytosolic and mitochondrial fractions were loaded on an SDS-PA gel.

2.3.3.5 Large-scale mitochondria isolation

Yeast cells, grown until OD₆₀₀ of about 0.8, were pelleted at 4,400 x g for 5 min at RT and washed with distilled water. The pellet was resuspended in DTT buffer (100 mM Tris-SO₄, 10 mM DTT, pH 9.4) to a final concentration of 0.5 g of yeast cells/ml buffer. The suspension was incubated with shaking at 30°C (or 24°C when temperature sensitive mutants were used) for 10 min. The cells were harvested by centrifugation at 4,400 x g for 5 min. Following a wash step with 100 ml of 1.2 M sorbitol, the cells were resuspended in sorbitol buffer (6.6ml of 1.2 M sorbitol, 20 mM potassium phosphate-KOH, pH 7.5 per gram of cells). To digest the cell wall, 4 mg Zymolyase, per gram of cells, were added to the cell suspension and the suspension was incubated with shaking for 30-45 min at 30 or 24°C. Spheroplasts formation was determined by diluting 50 μ l of cell suspension once into 2 ml of dH₂O and once into 1.2 M sorbitol and measuring OD₆₀₀. As spheroplasts burst in water, 80-90% reduction of OD₆₀₀ of the solution in water, compared to the sorbitol one, confirms the formation of spheroplasts. Spheroplasts were harvested at 3,000 x g for 5 min at 4°C, resuspended at 0.15 g/ml in

homogenization buffer (0.6 M sorbitol, 10 mM Tris-HCl, 1mM EDTA, 0.2% (w/v) BSA, 1 mM PMSF, pH 7.4) and homogenized by ten strokes in Dounce-homogenizer. The cell debris was removed by centrifuging twice at 1,900 x g at 4°C for 5 min. The supernatant was transferred into a new tube and centrifuged at 17,400 x g for 12 min at 4°C. Pelleted mitochondria were resuspended in SH buffer (20 mM HEPES-KOH, 0.6 M sorbitol, pH 7.2) to a final concentration of 10 mg/ml and aliquoted. Aliquots were then flash frozen and stored at -80°C.

2.4 Protein Biochemistry

2.4.1 Protein detection and analysis

2.4.1.1 SDS-PAGE

Protein samples were analyzed via SDS-PAGE as published previously (Laemmli, 1970). SDS-PA gels consist of two layers - separating gel at the bottom is overlaid with a stacking gel on top. Composition of the gels and buffers is given below.

Separating gel: 8-16% (w/v) acrylamide:bis-acrylamide mix (37.5:1), 375 mM Tris-Cl (pH 8.8), 0.1% (w/v) SDS, 0.05% (w/v) APS, 0.05% (v/v) TEMED.

Stacking gel: 5% (w/v) acrylamide:bis-acrylamide mix (37.5:1), 60 mM Tris-Cl (pH 6.8), 0.1% (w/v) SDS, 0.07% (w/v) APS, 0.35% (v/v) TEMED.

Running buffer: 50 mM Tris-Cl, 384 mM glycine, 0.1% (w/v) SDS, pH 8.3 without adjustment.

2X Laemmli buffer: 120 mM Tris-Cl (pH 6.8), 20% (v/v) glycerol, 4% (w/v) SDS, 0.02% (w/v) bromophenol blue.

Samples resuspended in Laemmli buffer (at least 1X final concentration) with or without 3% β -mercaptoethanol were cooked for 95°C for 3-5 min and loaded into the wells of the SDS-PA gel, which was assembled in the chamber and filled with the running buffer. After loading, 35 mA constant current was applied for big gels (14x9x0.1 cm) for ca. 1 h 40 min and 25 mA for small gels (10x5.5x0.075 cm) for ca. 50 min.

2.4.1.2 Western blotting

Following SDS-PAGE, the proteins were transferred to a nitrocellulose membrane (0.2 μm pore size) by semi-dry blotting method. Transfer was done for big gels at 250 mA constant current for 1 h (or 1 h 15 min for crosslinked products).

Transfer buffer: 20 mM Tris, 150 mM glycine, 20% (v/v) methanol and 0.02% SDS.

After the blotting procedure, the membrane was stained with Ponceau S (0.2% (w/v) Ponceau S in 3% (w/v) TCA) in order to evaluate the transfer efficiency and to cut the strips for immunodetection of different proteins. Membrane strips were completely destained in water and TBS (50 mM Tris-Cl, 150 mM NaCl, pH 7.5) and blocked with 5% (w/v) milk powder in TBS for at least 30 min at RT. The blocking solution was removed and the membranes incubated with primary antibodies, diluted 100-1000 fold in 5% milk in TBS, 1.5-3 h at RT or overnight in cold room. Membranes were washed once with TBS, once with TBS with 0.05% (v/v) Triton X-100 and once again with TBS for 10 min each. Membranes were then incubated with HRP-labeled secondary antibody, diluted 1:10,000 in 5% milk in TBS, for 1-2 h at RT. The washing steps were repeated and proteins visualized via chemiluminescence using X-ray films for signal detection. Chemiluminescent substrate of peroxidase was prepared by mixing equal volumes of ECL1 and ECL2 solutions.

ECL1: 100 mM Tris-Cl, pH 8.5, 440 $\mu\text{g}/\text{mL}$ luminol, 65 $\mu\text{g}/\text{mL}$ p-coumaric acid.

ECL2: 100 mM Tris-Cl, pH 8.5, 0.6% hydrogen peroxide.

Antibodies used in this project are taken from the library of PD. Dr. Dejana Mokranjac.

2.4.1.3 Determination of protein concentration

Amount of proteins in samples were determined using Bradford assay (Bradford, 1976). Five protein standards were prepared by serially diluting a 1.4 mg/ml IgG (Bio-Rad) stock solution to get 24 μg , 12 μg , 6 μg , 3 μg and 0 μg (as standard and also blank) of proteins per tube. Protein solutions of unknown concentrations were analyzed in parallel. 1 ml of 1:5 diluted Bradford reagent (Bio-Rad) was added into each tube. The samples were incubated

for 10 min at RT and absorbance was measured at 595 nm. Protein concentration in the samples was calculated from the standard curve.

2.4.1.4 Coomassie Brilliant Blue (CBB) staining

Purified proteins were visualized via CBB staining. Ingredients of staining and destaining solution were given below.

CBB staining solution: 0.1% (w/v) CBB R-250, 40% methanol, 10% glacial acetic acid

CBB destaining solution: 40% methanol, 10% glacial acetic acid

SDS-PA gel was incubated in CBB staining solution for 30 min by shaking at RT. After briefly rinsing with dH₂O, excess CBB was removed using CBB destaining solution by shaking, until protein bands were clearly visible.

2.4.2 *In vitro* import experiments

2.4.2.1 Preparation of radioactive precursors

Precursor proteins to be translated *in vitro* in this thesis are under the control *Sp6* promotor in pGEM vectors, which were taken from the library of PD. Dr. Dejana Mokranjac.

a) Transcription of RNA

20 µl of 5X transcription buffer (200 mM Tris-HCl, pH 7.5, 50 mM NaCl, 30 mM MgCl₂, 10 mM spermidine), 10 µl of 0.1 M DTT, 4 µl RNAsin (40 U/µl), 20 µl rNTPs (10 mM each), 5.2 µl m⁷G(5')ppp(5')G, 3 µl *Sp6*-polymerase, 27 µl deionized water and 10 µl plasmid DNA were mixed in 100 µl of reaction mix. After incubation for 1 h at 37°C, 10 µl of 10 M LiCl and 300 µl of ethanol were added. Reaction mix was kept for 30 min at -20°C and RNA was pelleted at 36,700 x g for 20 min. Pellet was washed with 70% (v/v) ice-cold ethanol and resuspended in 100 µl H₂O containing 1 µl RNAsin, and then stored at -80°C until use. (Modified from Melton et al. (1984)).

b) *In vitro* translation

A reaction mix comprised of 100 µl of lysate, 3.5 µl amino acid mix (1 mM from each except methionine), 20 U RNAsin, 7 µl of 15 mM Mg-acetate, 12 µl of ³⁵S-methionine and 25

μ l of RNA (section 2.4.2.1a) was incubated at 30°C for 1 h. 12 μ l of 58 mM cold methionine and 24 μ l of 1.5 M sucrose were added to the reaction. Cold methionine stops incorporation of radiolabeled methionine into polypeptide chain. Ribosomes and aggregated proteins were removed by centrifugation at 125,900 x g for 30 min at 4°C. Supernatant was split as single use aliquots and stored at -80°C. (Pelham and Jackson, 1976).

c) TNT coupled reticulocyte lysate system

Promega TNT coupled transcription/translation system was used as an alternative to above mentioned transcription and translation protocols.

25 μ l TNT rabbit reticulocyte lysate, 2 μ l of TNT reaction buffer, 1 μ l of TNT *Sp6* RNA polymerase, 1 μ l of amino acid mix, 2 μ l of ³⁵S-methionine, 1 μ l RNasin (40 U/ μ l) and 2 μ l of plasmid DNA (~0.5 μ g/ μ l) were mixed to have a 50 μ l of reaction mix. After 1.5 h at 30°C, aggregated proteins and ribosomes were removed by centrifugation at 125,900 x g for 30 min at 4°C. Supernatant was split as single use aliquots and stored at -80°C.

2.4.2.2 Import of radioactive precursors into isolated mitochondria

Isolated mitochondria were resuspended at 0.5 mg/ml in SI buffer (50 mM HEPES-KOH, 0.6 M sorbitol, 75 mM KCl, 10 mM Mg(Ac)₂, 2 mM KH₂PO₄, 2.5 mM EDTA, 2.5 mM MnCl₂, pH 7.2) supplemented with 2.5 mM ATP, 3.75 mM NADH, 10 mM phosphocreatine, 0.1 mg/ml creatine kinase and 0.5 mg/ml BSA. After a pre-incubation step at 25°C for 3 min, ³⁵S-labeled precursor protein was added to the import reaction and the reaction incubated further at 25°C. Import reaction was stopped at indicated time points by removing 90 μ l of the reaction mix and diluting them into 810 μ l of ice cold SH buffer (20 mM HEPES-KOH, 0.6 M sorbitol, pH 7.2) supplemented with 1 μ M valinomycin. Two probes were taken out per each time point. One of the duplicates was treated with 35 μ g/ml of proteinase K (PK) and the other one was kept as is. After 15 min incubation on ice, 5 μ l of 0.2 M PMSF was added to stop PK. Mitochondria were collected by centrifugation at 18,000 x g for 10 min at 4°C and dissolved in Laemmli with β -mercaptoethanol. The samples were cooked for 5 min at 95°C and analyzed by SDS-PAGE and autoradiography.

2.4.3 $\Delta\Psi$ measurements

Membrane potential in isolated mitochondria was measured with the potentiometric, fluorescent dye, DiSC₃(5) (3,3'-dipropylthiadicarbocyanine iodide). Fluorescence of the samples was measured using excitation and emission wavelengths of 622 nm and 670 nm, respectively. For the fluorescence measurements, Fluorolog-3 (Horiba Scientific, Jobin Yvon Technologies) was used.

2.4.3.1 Measurement of mitochondrial $\Delta\Psi$

1.5 ml of SI buffer (50 mM HEPES-KOH, 0.6 M sorbitol, 75 mM KCl, 10 mM Mg(Ac)₂, 2 mM KH₂PO₄, 2.5 mM EDTA, 2.5 mM MnCl₂, pH 7.2) was mixed with 15 μ l of 0.2 M NADH and 3 μ l of 250 μ M DiSC₃(5) and the fluorescent signal measured in real time. After 1 minute, 20 μ g of isolated mitochondria were added to the reaction and the measurement continued. Finally, after 8 minutes, 3 μ l of 1 mM valinomycin were added to the reaction. Mitochondria take up the dye in a $\Delta\Psi$ -dependent manner and this can be observed as a decrease in fluorescence. Valinomycin dissipates the $\Delta\Psi$, resulting an increase in the fluorescence.

2.4.3.2 Measurement of $\Delta\Psi$ in liposomes

See section 2.4.8 for preparation of liposomes. 1.5 ml of Na⁺-import buffer (20 mM HEPES-NaOH, 100 mM NaCl, pH 7.5) was mixed with 3 μ l of 250 μ M DiSC₃(5) and the fluorescent signal measured in real time. After 1 minute, 2.5 μ l of liposome suspension was added and, 2 minutes later, 3 μ l of 5 μ M Valinomycin (10 nM final) was added to generate $\Delta\Psi$. By the addition of 50 μ l of 1 M KCl, the $\Delta\Psi$ was dissipated. Prior to addition of KCl, 50 μ l of 1 M NaCl was used, as a control, to show that addition of Na⁺ do not affect the generated $\Delta\Psi$.

2.4.4 Co-immunoprecipitation assay

Co-immunoprecipitation assay was used to analyze protein complexes in solubilized mitochondria. For this, Protein A Sepharose CL-4B (PAS) beads were first washed with water and equilibrated with TBS (50 mM Tris-HCl, 150 mM NaCl, pH 7.5). Then, affinity purified antibodies to a protein of interest were added to the beads and incubated on an overhead shaker for 1 h or longer. Antibodies present in a preimmune serum were used as a negative

control. Unbound antibodies were removed with two washing steps with TBS and the beads equilibrated in 20 mM Tris-HCl, 80 mM KCl, 10% (v/v) glycerol, pH 8.0, containing 0.05% (w/v) digitonin.

Isolated mitochondria, stored in SH buffer (20 mM HEPES-KOH, 0.6 M sorbitol, pH 7.2), were diluted with 500 μ l SH buffer and reisolated by centrifugation at 18,000 x g for 10 min at 4°C. After removal of the supernatant, mitochondria were solubilized, at 1 mg/ml, in 20 mM Tris-HCl, 80 mM KCl, 10% (v/v) glycerol, pH 8.0, containing 1% (w/v) digitonin and 2 mM PMSF for 15 min in cold room. Non-solubilized material was removed by centrifugation at 124,500 x g for 20 min at 4°C. Solubilized mitochondria (200 μ l) were added to the antibodies prebound to the PAS beads and incubated for 30 min at 4°C for binding. Then, the beads were washed three times 5 min at 4°C with 200 μ l 20 mM Tris-HCl, 80 mM KCl, 10% (v/v) glycerol, pH 8.0, containing 0.05% (w/v) digitonin. Finally, bound proteins were eluted with 60 μ l of 2X Laemmli buffer by cooking at 95°C for 3 min, samples split into 2 equal aliquots and loaded on two SDS-PAGE gels.

2.4.5 Chemical crosslinking

DSG (disuccinimidyl glutarate) crosslinking was used to analyze the molecular environment of Tim23 in intact mitochondria. DSG is a homobifunctional, amine-reactive crosslinker with 7.7 Å spacer arm. Isolated mitochondria (0.5 mg/ml) in SI buffer (50 mM HEPES-KOH, 0.6 M Sorbitol, 75 mM KCl, 10 mM Mg(Ac)₂, 2 mM KH₂PO₄, 2.5 mM EDTA, 2.5 mM MnCl₂, pH 7.2) supplemented with 2.5 mM ATP, 3.75 mM NADH, 10 mM phosphocreatine and 0.1 mg/ml creatine kinase, were pre-incubated at 25°C for 3 min and then put on ice. To one sample, DSG was added, to a final concentration of 200 μ M, from a freshly made 100x stock in DMSO and, to the other, DMSO was added as a negative control. Reactions were kept on ice for 30 min. Excess of crosslinker was quenched by the addition glycine (pH 8.8) to a final concentration of 100 mM and a further 10 min incubation on ice. After addition of 500 μ l of SH buffer, the samples were centrifuged at 18,000 x g for 10 min and mitochondria were dissolved in Laemmli containing β -mercaptoethanol, cooked for 5 min and the samples analyzed by SDS-PAGE and Western Blotting.

2.4.6 Blue Native PAGE (BN-PAGE)

Mitochondria were solubilized at 2mg/ml in 20 mM Tris-HCl, 80 mM KCl, 10% (v/v) glycerol, pH 8.0, containing 1% (w/v) digitonin and 2 mM PMSF by rotating on an overhead shaker for 15 min at 4°C. Insoluble material was removed by centrifugation at 124,500 x g for 20 min at 4°C. Supernatant (40 µl) was mixed with 2 µl of NativePAGE 5% G-250 Sample Additive (Life Technologies). Then 10 µl of sample per lane was loaded on 4–16% Native PAGE Bis-Tris Gel (Life Technologies) which was assembled in gel running chamber. In the beginning, gels were run at 150 V for 30 min at 4°C with 1X NativePAGE dark blue cathode buffer and 1X NativePAGE anode buffer. Voltage was increased to 250 V and run until dye reaches ca. 1/3 of the gel. Then, cathode buffer was changed with 1X NativePAGE light blue cathode buffer and gel was run until the dye reaches to the bottom of the gel. The proteins were transferred to a PVDF membrane at 130 mA, 7 V for 1 h. Finally, the proteins were visualized by Western blotting (section 2.4.1.2).

For 1X NativePAGE anode buffer, 30 ml of 20X Native PAGE Anode Buffer (Life Technologies) was diluted to 600 ml with deionized water.

For 1X NativePAGE dark blue cathode buffer, 10 ml of 20X Native PAGE Anode Buffer and 10 ml of 20X NativePAGE Cathode Additive (Life Technologies) were diluted to 200 ml with deionized water.

For 1X NativePAGE light blue cathode buffer, 10 ml of 20X Native PAGE Anode Buffer and 1 ml of 20X NativePAGE Cathode Additive were diluted to 200 ml with deionized water.

2.4.7 Purification of recombinant Tim17-Tim23 complex

2.4.7.1 Co-expression of Tim17 and Tim23

E. coli C43(DE3) cells were transformed with pET-Duet1 vector construct carrying Tim23_{his9} and Tim17_{strep} (section 2.1.5). Transformed cells were diluted in 120 ml of LB-Amp medium and grown overnight at 37°C, 160rpm. Next day, the overnight culture was diluted in 6 L of LB-Amp prewarmed at 30°C. The culture was grown until OD₆₀₀ reached ~0.6-0.7 and expression of proteins were induced by addition of 0.5 mM IPTG for 3 more hours at 30°C,

shaking at 160 rpm. Finally, cells were harvested at 4500 x g for 10 min at 4°C and cell pellet was stored at -20°C until use.

2.4.7.2 Isolation of *E.coli* membranes

Cell pellets were resuspended in 150 ml of 50 mM Tris-HCl, 250 mM NaCl, 20 mM imidazole, 4 mM β -mercaptoethanol, 1 mM PMSF, pH 8.0. Cells were broken mechanically using high-pressure homogenizer at max pressure (18,000 psi) with three passes on ice. A clarification centrifuge was applied at 27,200 x g for 20 min at 4°C. Then, cell membranes were harvested at 186,000 x g for 2 h at 4°C and homogenized in 20 ml of cell resuspension buffer using Dounce-homogenizer. Protein concentration of homogenized membranes was measured using Bradford assay (section 2.4.1.3) and the membranes were flash frozen using liquid-N₂ and stored at -80°C.

2.4.7.3 Purification of recombinant membrane Tim17-Tim23 complex from isolated membranes

Isolated membranes were solubilized in 50 mM Tris-HCl, 250 mM NaCl, 20 mM imidazole, 1 mM PMSF, 0.75% (w/v) Fos-choline 12 (FC12), pH 8.0 at 15 mg/ml final protein concentration in cold room by stirring for 1.5 h. Insoluble material was removed by centrifugation at 257,000 x g for 40 min at 4°C. Supernatant was loaded on NiNTA agarose column equilibrated with 50 mM Tris-HCl, 250 mM NaCl, 20 mM imidazole, 0.05% (w/v) FC12, pH 8.0. Then, NiNTA column was washed with at least 10 column volume (CV) of same buffer and histidine tagged proteins were eluted with 50 mM Tris-HCl, 250 mM NaCl, 300 mM imidazole, 0.05% (w/v) FC12, pH 8.0 as 1 ml fractions. Protein content of the fractions were quickly checked by dropping 2 μ l from each on a nitrocellulose membrane and staining with Ponceau S (see section 2.4.1.2 for recipe). The most intense fractions were combined and loaded on Strep-tactin column equilibrated with 20 mM HEPES-KOH, 100 mM KCl, 0.05% (w/v) FC12, pH 8.0. Streptactin column was washed again with 10 CV of the same buffer and strep-tagged proteins were eluted with the same buffer containing 2.5 mM desthiobiotin. Protein concentration of the fractions were measured using Bradford assay (section 2.4.1.3) and purified proteins were flash frozen and stored at -80°C until use.

All of the purification steps mentioned above were performed at 4°C.

2.4.8 Reconstitution of recombinant Tim17-Tim23 in proteoliposomes

E. coli polar lipid extract (Avanti) and cardiolipin (1,1'2,2'-Tetraoleoyl Cardiolipin from Avanti), both in chloroform, were mixed in a glass tube to obtain a mixture containing 10% (mol/mol) final cardiolipin. Lipid mix was dried slowly by rotating under a stream of N₂. Dried lipids were resuspended in liposome storage buffer (20 mM HEPES-KOH, 50 mM KCl, 2 mM DTT, pH 8.0) at 20 mg/ml and the suspension was homogenized by using a bath sonicator for 10 min at max frequency. Four times freeze-thaw cycles were applied using liquid N₂ and room temperature. Following an incubation at 65°C for 1h, resulting suspension was passed 11 times through a mini extruder with 400 nm pore sized membrane. Suspension was diluted to 4 mg/ml using buffer R (20 mM HEPES-KOH, 100 mM KCl, 1 mM DTT, pH 8.0). 400 µl of liposome suspension was mixed with 400 µl purified complex (75 µg of protein) (section 2.4.7.3) and incubated by shaking head-over-head for 30 min in cold room. 400 µl of buffer R was added to the mixture and the detergent was removed gradually by incubating with Bio-beads SM-2 (Bio-Rad), pre-equilibrated in buffer R. Bio-Beads SM2 (50 mg) were added to the samples and incubated with shaking on an overhead shaker 2 h at 4°C. This step was repeated once again and finally 100 mg of Bio-Beads SM2 were added for an overnight incubation in cold room. After each step, used Bio-Beads were rinsed with 100 µl of buffer R and the rinsed volume was added to liposome suspension. Next morning, the proteoliposomes were collected at 200,000 x g for 30 min at 4°C, resuspended in 1ml buffer R for washing and the centrifugation repeated. Pellet was resuspended in 200 µl of buffer R containing 1.4 M sucrose, overlayed with 500 µl of buffer R containing 1 M sucrose and subsequently overlayed with 200 µl of buffer R to form a gradient. Proteoliposomes were floated at 225,000 x g for 45 min at 4°C. Floated liposomes were collected carefully and diluted 5 times with buffer R. Following centrifugation at 200,000 x g for 30 min at 4°C, pellet was resuspended in 1 ml of Na⁺-import buffer (20 mM HEPES-NaOH, 100 mM NaCl, 1 mM DTT, pH 7.5) and centrifugation was repeated. Finally, proteoliposomes were resuspended in 250 µl of Na⁺-import buffer and used immediately or kept 1-2 days at 4°C for further experiments.

Control liposomes were made in parallel, using Streptactin elution buffer, instead of purified proteins.

2.4.8.1 Na₂CO₃ extraction

50 µl of ice-cold Na₂CO₃ (0.1 M, pH 11.5) was added onto 50 µl of purified protein (2 µg in Streptactin elution buffer, section 2.4.7.3) and proteoliposome suspension (2 µg protein in Na⁺-import buffer, section 2.4.8). After incubation for 20 min on ice, samples were pellet by ultracentrifugation at 166,500 x g for 1 h. Supernatants were mixed with 20 µl of 72% trichloroacetic acid (TCA). Samples were mixed thoroughly and then incubated at -20°C for 20 min. Precipitated proteins were collected by centrifugation at 36,700 x g for 20 min at 4°C. The pellet was washed with 200 µl of ice-cold acetone and the centrifugation step repeated for 10 min. Precipitated proteins from the supernatant fractions and pellets from ultracentrifugation were resuspended in Laemmli buffer with β-mercaptoethanol and analyzed by SDS-PAGE (section 2.4.1.1) and Western blotting (section 2.4.1.2).

2.4.8.2 Precursor binding to proteoliposomes

10 µl of liposome suspension and 2 µl of radioactive lysate were mixed in 200 µl of Na⁺-import buffer containing 2 mM ATP and incubated together for 10 min at 25°C. 90 µl of the sample was kept as total and the other 90 µl aliquot was centrifuged at 50,000 x g for 20 min at 4°C to separate bound from unbound fractions. 20 µl of 72% (w/v) TCA were added to total and the supernatant (unbound fraction) samples. After 20 min incubation at -20°C, samples were centrifuged (36,700 x g, 20 min at 4°C), pellets were washed with 200 µl ice-cold acetone and the centrifugation step repeated for 10 min. Following removal of acetone, pellets were resuspended in Laemmli buffer with β-mercaptoethanol. For the bound fraction, the pellet from the first centrifugation step was resuspended in 500 µl Na⁺-import buffer containing 1.4 M and transferred to a SW60 rotor tube. The sample was overlaid with 1 ml of Na⁺-import buffer containing 1 M sucrose and then with 500 µl Na⁺-import buffer without sucrose. Liposomes were floated by ultracentrifugation at 200,000 x g for 1 h at 4°C. Area between Na⁺-import buffer and Na⁺-import buffer containing 1 M sucrose was collected and diluted 5X with Na⁺-import buffer. Ultracentrifugation step was repeated and the pellets

were resuspended in Laemmli buffer with β -mercaptoethanol. Finally, all samples were cooked for 5 min at 95°C and analyzed by SDS-PAGE and autoradiography.

3. RESULTS

Tim17 and Tim23 are two homologous proteins that form the core of the TIM23 complex onto which all other subunits of the complex assemble (Dekker et al., 1997; Kozany et al., 2004). Both Tim17 and Tim23 are anchored to the inner mitochondrial membrane with 4 predicted transmembrane segments (Figure 3.1). In addition, Tim23 has a ca. 100 amino acid residues long segment that is exposed to the IMS. In the first part of my thesis, I dissected Tim23 *in vivo*.

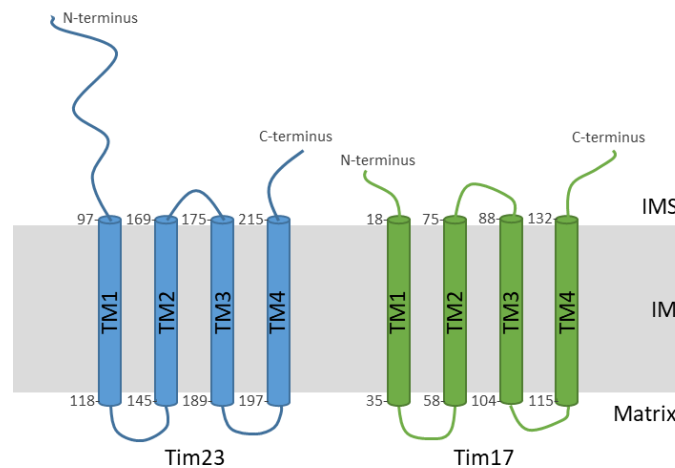


Figure 3.1 Schematic representation of Tim23 and Tim17. Predicted TM segments of Tim23 (blue) and Tim17 (green) are indicated with the residue numbers in the IMS and the matrix side of the IM (grey).

3.1 *In vivo* dissection of Tim23

3.1.1 Evolutionary conservation of Tim23

Sequence conservation analysis of 795 Tim23 sequences identified in the work of Zarsky and Dolezal (2016) showed that the C-terminal region of Tim23, which contains the predicted TMs, is well conserved over the entire region (Figure 3.2). On the other hand, the N-terminal, IMS-exposed region of Tim23 shows a relatively poor sequence conservation especially over the first 50 residues.

The ca. 100 amino acid residues long IMS domain of Tim23 is predicted to be intrinsically disordered and the purified domain indeed shows little, if any, structural features (de la Cruz et al., 2010; Gevorgyan-Airapetov et al., 2009). Still, this domain was shown to be

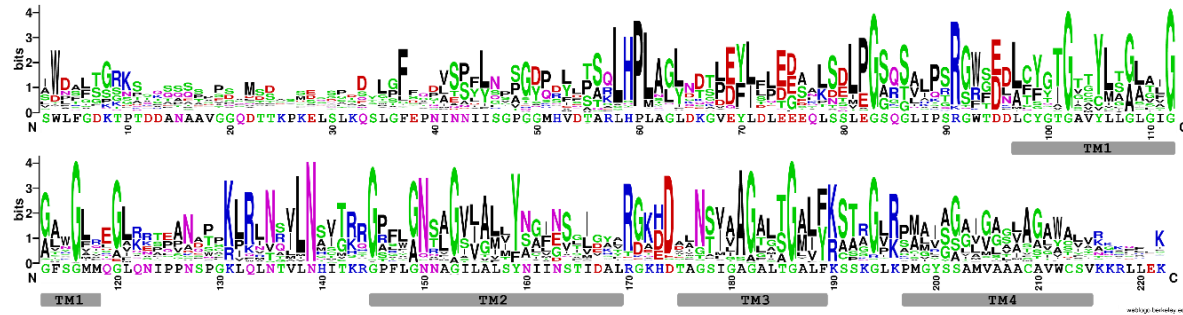


Figure 3.2 Sequence conservation of yeast Tim23. Multiple sequence alignment of Tim23 was converted to logo chart via WebLogo creation tool at weblogo.berkeley.edu/logo.cgi. Size of the letters depicts the conservation of the individual residues. X-axis shows the sequence of *Saccharomyces cerevisiae* Tim23. Predicted TM segments are indicated with grey bars. Y-axis shows the conservation (Max value: $\log_2 20 = 4.3$ for 20 possible amino acids).

involved in many interactions (Bajaj et al., 2014a; Bajaj et al., 2014b; Bauer et al., 1996; de la Cruz et al., 2010; Gevorgyan-Airapetov et al., 2009; Lytovchenko et al., 2013; Marom et al., 2011; Tamura et al., 2009). These interactions, summarized in Figure 3.3, were mostly demonstrated in *in vitro* studies using purified protein domains and the significance of many of the identified interaction sites was never analyzed *in vivo*. In this part of my thesis, a systematic, *in vivo* mutational analysis was carried out to understand the function of the IMS domain of Tim23.

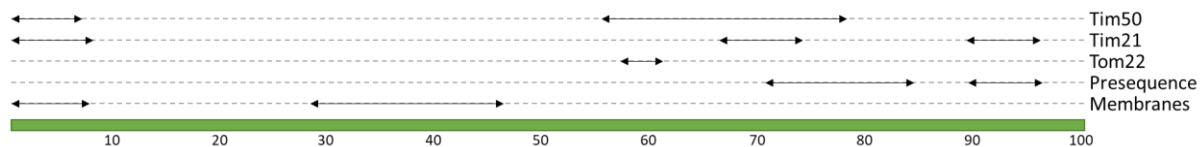


Figure 3.3 Schematic representation of Tim23_{IMS} with its proposed interaction regions. Previously proposed interaction regions are indicated as straight horizontal double-sided arrows. Interaction partners are indicated on the right. See text for details.

3.1.2 Deletion of the first 70 residues of Tim23 can be tolerated by yeast cells

To understand the importance of the IMS domain of Tim23, truncated versions from the N-terminus were generated in a centromeric plasmid with the endogenous *TIM23* promoter and 3'UTR (section 2.1.8.1) and their ability to support the function of the full length protein was analyzed by plasmid shuffling (section 2.2.3). Tim23 shuffling strain is a haploid yeast strain in which the chromosomal copy of the *TIM23* gene is replaced with a KAN cassette. Since deletion of *TIM23* is lethal, a *URA3* plasmid containing wild-type (WT) Tim23 is introduced to make the strain viable. Upon transformation of the shuffling strain with

plasmids encoding truncated versions of Tim23, 5-FOA selection is used to eliminate cells with the *URA3* plasmid, and thereby the WT *TIM23* encoded on it. In this way, only cells with a functional copy of Tim23 present on the transformed plasmid remain alive.

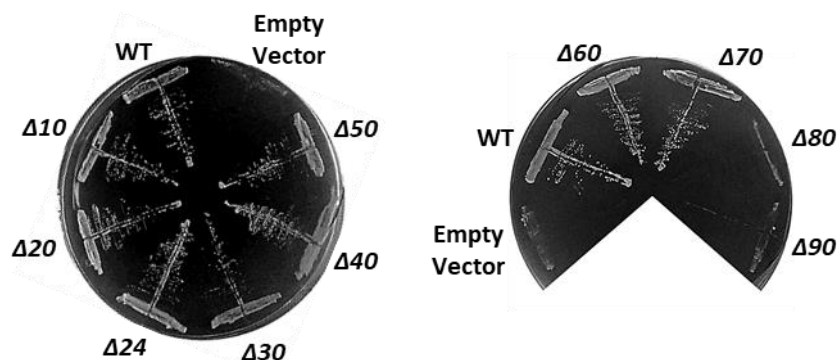


Figure 3.4 Rescue of the function of Tim23 by N-terminally truncated versions of Tim23. Tim23 shuffling strain was transformed with the plasmids encoding indicated truncated versions of Tim23 and the viability of the cells was analyzed on 5-FOA selection plates. FL construct (WT) and the empty vector were used as positive and negative controls, respectively.

The cells expressing the wild-type (WT) Tim23 were viable on plates containing 5-FOA, whereas cells transformed with an empty plasmid were not (Figure 3.4). N-terminal truncations encompassing up to 70 residues were able to support the function of the FL Tim23, but further deletions ($\Delta 80$ and $\Delta 90$) were not. This result demonstrates that a large portion of the IMS-exposed segment of Tim23 is dispensable for cell viability.

To test whether the deletions of up to 50 residues support the function of Tim23 fully or only partially, serial dilution spot assay (section 2.3.3.1) was performed on fermentable

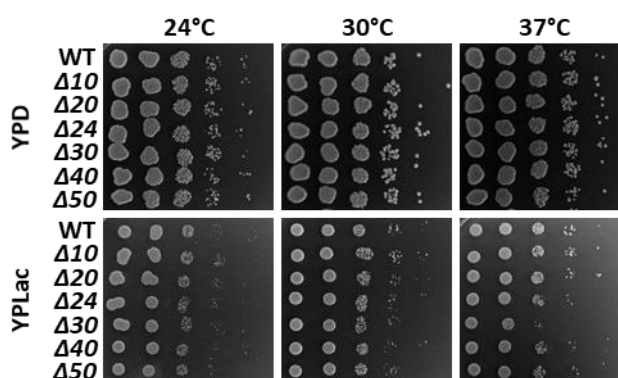


Figure 3.5 Growth phenotype of N-terminal truncations of Tim23. WT and the mutants with N-terminally truncated versions of Tim23 were grown to same OD in YPD and 10-fold serially diluted cells were dropped onto YPD and YPLac plates. The plates were incubated at indicated temperatures for 2-5 days.

(YPD) and non-fermentable (YPLac) media at three different temperatures (24, 30 and 37°C) (Figure 3.5). None of the mutants showed any obvious growth defect on YPD medium at any of the tested temperatures. This is in agreement with the fact that, on glucose-containing medium, yeast cells can use glycolysis for ATP production and therefore do not rely heavily on mitochondria for this purpose. YPLac medium, on the other hand, does not contain a fermentable carbon source and yeast cells require mitochondria to produce ATP they need by oxidative phosphorylation. On a non-fermentable medium, $\Delta 10$ and $\Delta 20$ grew like WT and the growth of $\Delta 24$ was only marginally defective at 37°C. Interestingly, $\Delta 30$ showed a relatively strong temperature sensitive growth defect, compared to other truncations. This result is particularly interesting since longer truncations ($\Delta 40$ and $\Delta 50$), covering the deletion of the first 30 residues, showed a milder phenotype compared to $\Delta 30$.

3.1.3 Deletion of the first 30 residues of Tim23 reduces levels of Tim23 protein

To understand the molecular basis of the impaired growth, expression levels of Tim23 were analyzed with antibodies against the C-terminal peptide of Tim23 after SDS-PAGE analysis of mitochondria isolated from the truncation mutants (Figure 3.6). Tim23 levels were severely reduced in $\Delta 30$ compared to WT and to the other N-terminal truncation mutants. In addition, a slight decrease in $\Delta 50$ was observed but this decrease apparently did not cause as strong growth defect as seen with $\Delta 30$ (Figure 3.5).

If the growth phenotype was caused by the reduced levels of the protein, then the overexpression of the protein should rescue the growth defect, at least to a certain degree.

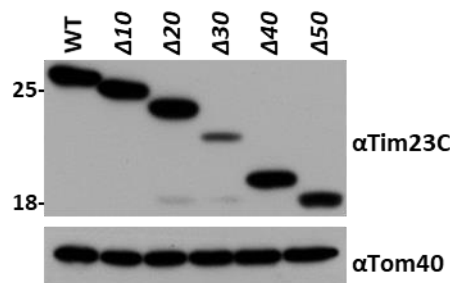


Figure 3.6 Expression of N-terminal truncations of Tim23 in isolated mitochondria. Mitochondria isolated from WT and the mutant strains were analyzed by SDS-PAGE and immunostaining. Antibodies against the C-terminal peptide of Tim23 were used to detect WT and the N-terminally truncated proteins; from left to right WT, $\Delta 10$, $\Delta 20$, $\Delta 24$, $\Delta 30$, $\Delta 40$ and $\Delta 50$. Tom40 was used as control.

To test this hypothesis, *tim23Δ30* was cloned into a yeast expression plasmid with a GPD promoter and the growth of the yeast strains expressing *tim23Δ30* under different promoters was analyzed by the serial dilution spot assay (section 2.3.3.1). The overexpression strain ($\Delta30\uparrow$) grew better than the strain expressing *tim23Δ30* under the endogenous promoter ($\Delta30$) (Figure 3.7a). The level of Tim23 $\Delta30$ expression under GPD promoter was higher than of the WT (Figure 3.7b) and an additional band of around 18 kDa (indicated as *), which likely corresponds to a degradation product, was observed. This result suggests that the impaired growth of *tim23Δ30* is likely caused by the reduced levels of truncated Tim23.

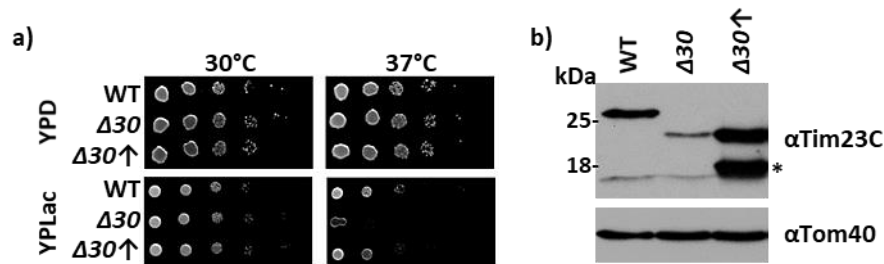


Figure 3.7 Overexpression of Tim23 $\Delta30$ largely rescues the growth defect. a) The growth of $\Delta30$ strains expressing Tim23 $\Delta30$ under endogenous and GPD promoter was compared in serial dilution spot assay. b) Protein levels of Tim23 $\Delta30$ were detected by immunostaining with antibodies against the C-terminal part of Tim23. Tom40 was used as a loading control. *-degradation product of Tim23 $\Delta30$.

3.1.4 Removal of the first 10 residues from Tim23 does not impair binding of Tim50 and Tim21 to the TIM23 complex

I observed no effect on growth when the first 10 residues of Tim23 were deleted, however, this segment was previously implicated in binding of Tim50 and Tim21 when binding between recombinant proteins was analyzed *in vitro* (Figure 3.3) (Bajaj et al., 2014a). To analyze whether the first 10 residues of Tim23 play a role in either Tim50 or Tim21 binding also *in organello*, a co-immunoprecipitation experiment (section 2.4.4) from digitonin-solubilized mitochondria was performed. Since the antibody against the C-terminal part of Tim23 does not work in immunoprecipitation (data not shown) and the N-terminal antibody does not recognize the mutants with N-terminal truncations, antibodies against Tim17 were used instead for immunoprecipitation. As seen in Figure 3.8, antibodies against Tim17 depleted both Tim17 and Tim23 from the supernatants and both proteins were found in the immunoprecipitated fractions (Pel.) when WT mitochondria were analyzed. Fractions of

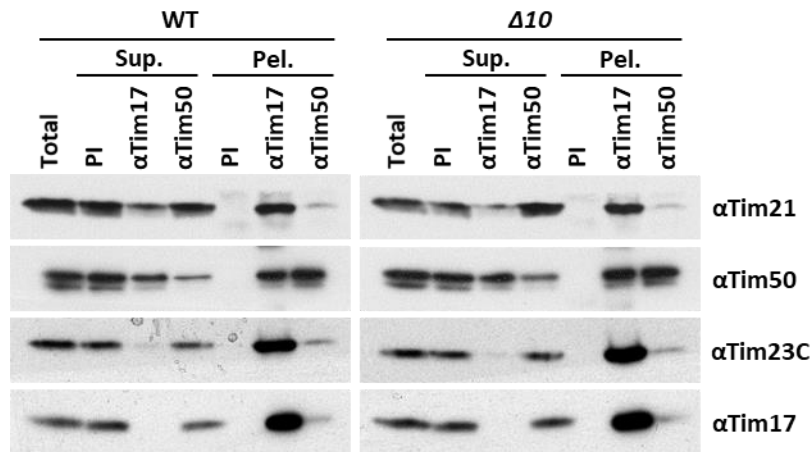


Figure 3.8 Immunoprecipitation of Tim21 and Tim50 with Tim23 Δ 10. Isolated mitochondria from WT and Δ 10 cells were solubilized with digitonin containing buffer and subjected to immunoprecipitation using antibodies against Tim17 and Tim50. Samples were analyzed by SDS-PAGE and immunostaining. PI: Pre-immune serum, Sup.: Supernatant, Pel.: Pellet. Totals and Supernatants- 20% and Pellets- 100%.

Tim21 and of Tim50 were also co-immunoprecipitated. In Δ 10 mitochondria, no alteration in the levels of co-immunoprecipitated Tim50 or Tim21 was observed compared to WT. Similarly, the amounts of Tim17 and Tim23 co-immunoprecipitated with antibodies against Tim50 were also essentially the same in WT and Δ 10 mitochondria. These results suggest that the first 10 residues of Tim23 may contribute to but are not essential for either Tim21 or Tim50 binding.

3.1.5 Protein import into mitochondria from Δ 10 is slightly reduced

In order to see directly whether deletion of the first 10 residues of Tim23 affects import of proteins via the TIM23 pathway, the ability of mitochondria isolated from WT and Δ 10 cells to import *in vitro* translated and 35 S-labeled precursors was analyzed. Figure 3.9 shows that mitochondria isolated from Δ 10 cells imported both matrix-targeted, Su9(1-69)DHFR and Jac1, and laterally sorted, DLD, precursors slightly less efficiently. Import of Tim23, which uses the TIM22 complex for its import, was not affected, suggesting a TIM23 complex-specific import defect in Δ 10. However, the observed import defect was apparently not rate limiting for cell growth under any of the conditions tested (Figure 3.5).

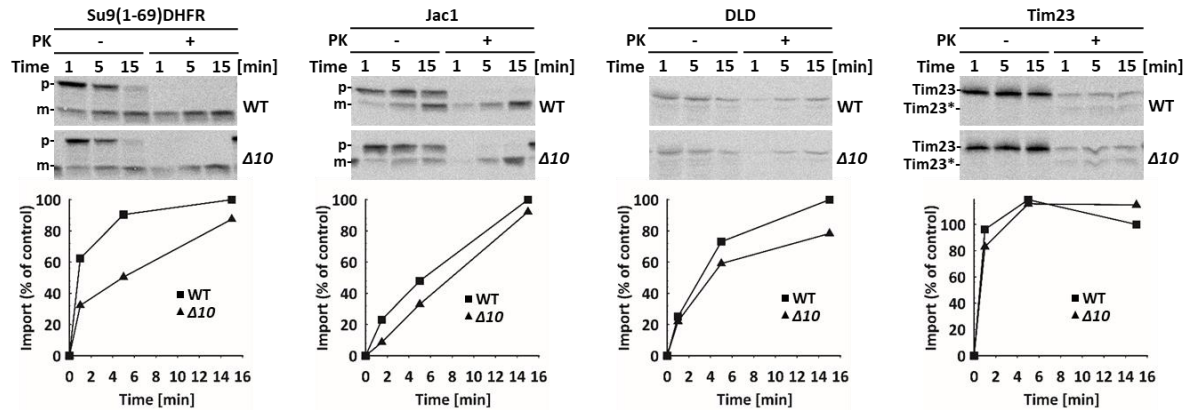


Figure 3.9 *In vitro* protein import into $\Delta 10$ mitochondria. Isolated mitochondria were incubated with *in vitro* translated, radioactively labeled precursor proteins in an import buffer. Import reactions were stopped at indicated time points and half of the samples were treated with proteinase K (PK) to degrade non-imported precursors. After re-isolation of mitochondria, mitochondrial lysates were analyzed by SDS-PAGE and autoradiography. p- precursor and m- mature forms of precursor proteins. Tim23*- clipped version of Tim23 generated in intact mitochondria by externally added PK (Donzeau et al., 2000). Lower panels represent quantifications of the import reactions. The amount of PK-protected mature form in the longest time point of import into WT mitochondria was set to 100%. For quantification of Tim23 import, total amount of Tim23 and Tim23* was used.

3.1.6 Alanine scanning mutagenesis of the region between amino acid residues 51 and 100 of Tim23 identifies three distinct functionally important regions

Since the second half of the IMS-exposed region of Tim23 shows a higher degree of sequence conservation (see Figure 3.2, residues 51-100), a more conservative approach was used for its analysis. The plasmid encoding WT Tim23 under the control of its endogenous promoter and 3'UTR was mutated so that patches of 2 to 7 amino acid residues at the time were changed to alanines (section 2.1.8.2). Thirteen different mutants, with or without overlapping residues, were generated. Overlapping mutations were designed to obtain a better resolution when assigning the effects to individual residues towards the end of the domain in the screening procedure. All of the mutants created were viable after 5-FOA selection (data not shown), demonstrating that they are able to support the function of Tim23. When analyzed by serial dilution spot assay (Figure 3.10), only one of the mutants, V68A5 (indicated with red star), showed a very severe growth defect in all tested conditions, pointing towards an essential role of this region. The analysis of the C-terminal region of the

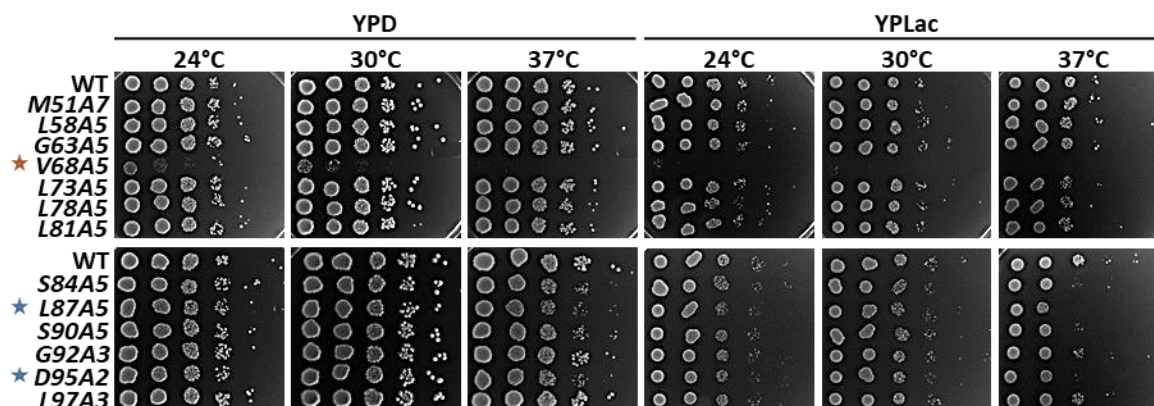


Figure 3.10 Alanine scanning mutagenesis of the region 51 to 100 of Tim23. Growth of WT and indicated mutant cells were analyzed by serial dilution spot assay on YPD and YPLac plates at indicated temperatures. **Nomenclature:** The first number and letter define the first mutated residue in the patch, the second number defines the number of residues mutated from the first residue and the letter in between specifies what they were mutated to (e.g. V68A5: 5 residues from V68 to D72 were mutated to Alanine).

domain identified several overlapping mutants with impaired growth that mapped to two distinct regions, separated by residues 92-94. Two mutants from this region, *L87A5* and *D95A2* (indicated with blue stars) were chosen for further analysis due to their strongest growth defects.

3.1.7 The region around amino acid residue 40 of Tim23 is in close proximity to Tom22

The first 50 residues of Tim23 also contain a site where Tim23 can be crosslinked to Tom22. Namely, using site-specific photocrosslinking, Endo group previously showed that position 41 of Tim23 is in close vicinity to Tom22 (Tamura et al., 2009). This approach is based on introduction of a non-natural amino acid, Bpa (p-benzoyl-L-phenylalanine) which crosslinks to the nearby molecules upon illumination with UV light (Chen et al., 2007). In order to introduce Bpa residue into specific positions of a C-terminally Histidine tagged-Tim23, the endogenous codons at the chosen positions were individually mutated to amber stop codons, TAG. The amber stop codon can be suppressed *in vivo* by co-transforming yeast cells with an engineered plasmid encoding an orthogonal tRNA/aminoacyl-tRNA synthetase pair specific for Bpa. When these cells are grown in the presence of Bpa, Bpa will be incorporated in Tim23 at the position defined by the amber stop codon.

To understand the interaction between Tim23 and Tom22 in more detail and to map it more precisely, Bpa was introduced at eleven different positions within the first 40 residues of Tim23 (Trp3, Lys8, Thr11, Asn15, Val18, Gln21, Lys25, Leu29, Gln33, Phe37 and Asn40). Upon exposure of cells to UV light, total cell extracts (section 2.3.3.3) were prepared and analyzed by SDS-PAGE and immunoblotting. Antibodies against Tom22 showed an additional, UV-specific band at around 50 kDa for positions 37 and 40 (Figure 3.11). These residues are in the immediate neighborhood of residue Ile41 identified by Tamura et al. (2009). Thus, a more central region of the IMS-exposed domain of Tim23, rather than its more N-terminal part, is in contact with Tom22.

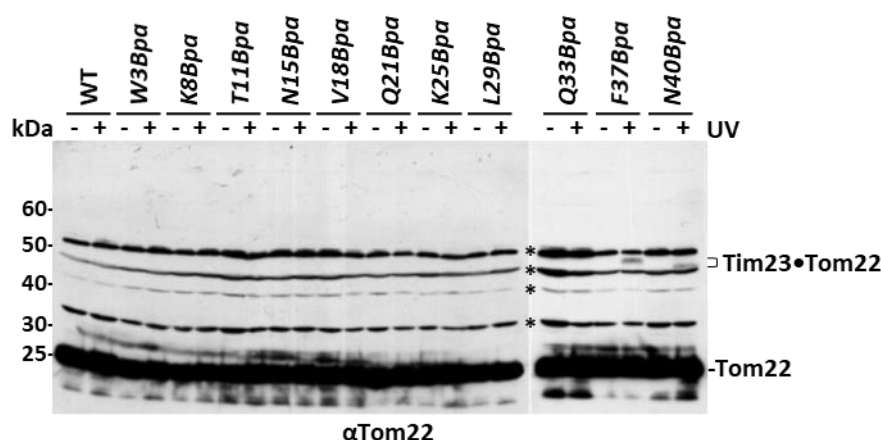


Figure 3.11 Site specific photo-crosslinking of IMS exposed segment of Tim23 with Tom22. Yeast cells expressing C-terminally His-tagged Tim23 and carrying an amber stop codon for Bpa incorporation at the indicated positions were grown in the presence of 1mM Bpa. Cells were harvested and one half was illuminated with UV while the other half was kept in dark. Total cell extracts were made and samples were analyzed by SDS-PAGE and immunostaining with α Tom22. Non-specific bands are indicated with *.

Tom22-Tim23 interaction was also previously analyzed using recombinant proteins (Bajaj et al., 2014a). This study suggested that the region between residues 58 and 62 of Tim23 was involved in the interaction with Tom22. To analyze the importance of this segment for Tim23-Tom22 interaction *in vivo*, Bpa was introduced into *L58A5* in which the segment between residues 58 and 62 is mutated to alanines. Figure 3.12 shows that the Tim23-Tom22 photocrosslinks were not dramatically reduced in *L58A5* mutant, neither when Bpa was in position *F37Bpa* nor in *N40Bpa* (see *F37Bpa/L58A5*, +UV lane at Figure 3.12a and *N40Bpa/L58A5*, +UV lane at Figure 3.12b). These results suggest that amino acid residues 58 to 61 may not be essential for Tim23 interaction with Tom22.

The same approach was used to analyze a potential effect of Tim23-Tim50 interaction on Tim23-Tom22 interaction by combining F37Bpa and N40Bpa with a mutant in which residues Tyr70 and Leu71 were mutated to alanines (Y70A2) (Figure 3.12a and b, last lanes). This mutation abolishes the interaction between Tim23 and Tim50 (Gevorkyan-Airapetov et al., 2009). Also in this case, no major effect of the mutation was observed, suggesting that Tim23 interactions with Tom22 and Tim50 may be independent of each other.

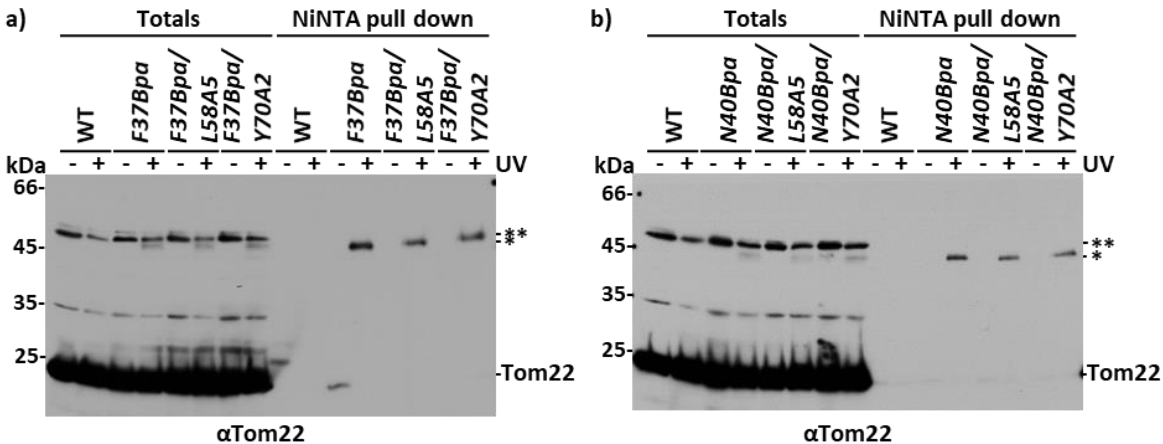


Figure 3.12 Tim23-Tom22 crosslinks in *L58A5* and *Y70A2* backgrounds. Yeast cells expressing C-terminally His-tagged Tim23 with an amber stop codon at **a)** Phe37 and **b)** Asn40 for Bpa incorporation and additional mutations indicated, were grown in the presence of 1mM Bpa. Cells were harvested and one half was illuminated with UV while the other half was kept in dark. Following cell lysis, NiNTA pull down was carried out to enrich His-tagged products. Total (7%) and the NiNTA-bound (100%) fractions were analyzed by SDS-PAGE followed by immunostaining with α Tom22. * - Tim23-Tom22 crosslinks. ** - non-specific bands.

3.1.8 Tim50 binding region on Tim23 is larger than described previously

V68A5 mutant contains two conserved residues, Tyr70 and Leu71, which were previously found to be important for the interaction of Tim23 with the main receptor Tim50 (Gevorkyan-Airapetov et al., 2009; Tamura et al., 2009). Still, while mutation of these two residues cause a temperature sensitive growth defect at 37°C on a non-fermentable medium, *V68A5* mutant made here showed a much stronger growth defect, implying the importance of the other residues in Tim50 binding, or possibly, an additional role for them.

The alignment in Figure 3.2 shows that the adjacent residue, Glu69, is as conserved as Tyr70 and Leu71. Therefore, a detailed mutational analysis for this region was carried out using single, double or triple mutants (Figure 3.13). None of the single mutants, including

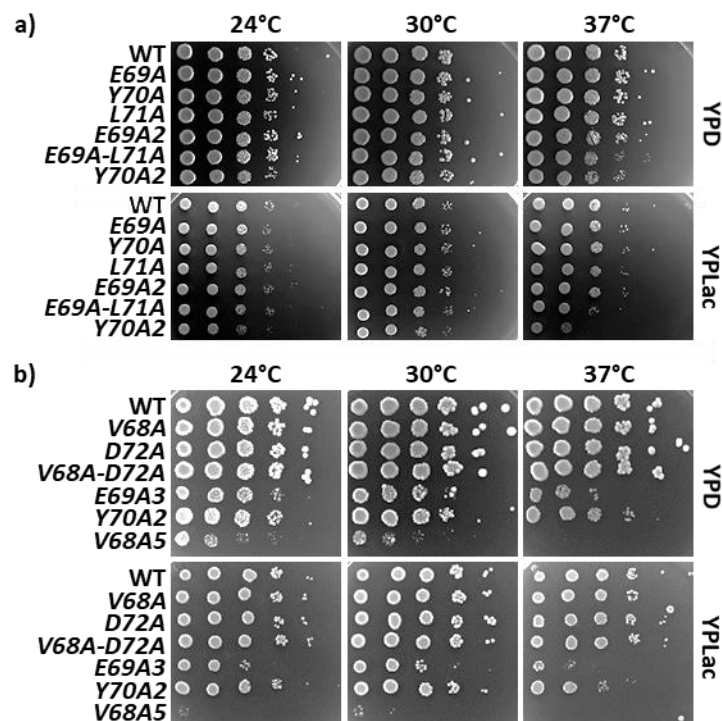


Figure 3.13 Detailed analysis of residues 68 to 72 of Tim23. Contributions of **a)** the conserved amino acid residues 69 to 71 and **b)** neighbouring residues Val68 and Asp72 to the growth phenotype of V68A5 were analyzed as single, double or triple mutations by serial dilution spot assay on YPD and YPLac plates at indicated temperatures. See Figure 3.10 for the nomenclature.

E69A, showed any obvious growth phenotype, in agreement with what was previously shown for Y70A and L71A mutants (Gevorkyan-Airapetov et al., 2009). The double mutant *E69A2* also grew like WT while *Y70A2* and *E69A/L71A* showed temperature sensitive growth (Figure 3.13a). The effect in the latter was slightly less pronounced. Combination of all three mutations in the *E69A3* mutant affected the cell growth even more but not as much as in *V68A5*. This shows that all five residues contribute to the observed phenotype. Mutating Val68 and Asp72, individually or together, did not lead to any growth phenotype (Figure 3.13b). Thus, the effects of the individual mutations on cell growth can be ordered as Leu71>Tyr70>Glu69>Val68 and Asp72.

In order to determine whether Glu69 also plays a role in Tim50 binding, isolated mitochondria were analyzed by co-immunoprecipitation (Figure 3.14). As shown previously, Tim50 binding to Tim23 in the *Y70A2* double mutant was completely abolished (Gevorkyan-Airapetov et al., 2009). I observed the same in *L71A* mitochondria. Yet in *E69A*, the Tim23-

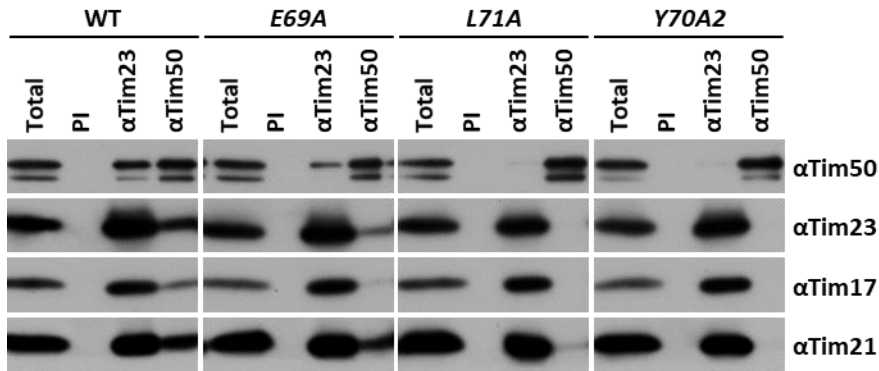


Figure 3.14 The effect of E69A and L71A mutations on Tim23-Tim50 interaction. Isolated mitochondria from WT and E69A, L71A and Y70A2 mutants were solubilized with digitonin-containing buffer and antibodies against Tim23 and Tim50 were used for immunoprecipitation of the TIM23 complex. Samples were analyzed by SDS-PAGE and immunostaining. Totals are 20% of the immunoprecipitated fractions. PI: Pre-immune serum.

Tim50 interaction was reduced, but not completely abolished. These results suggest that the interaction site on Tim23 for Tim50 is larger than previously reported. The interaction appears to mainly rely on hydrophobic interactions and residue Leu71 in particular.

3.1.9 TIM23-mediated protein import is impaired in the *tim23L87A5* mutant

The next mutant identified in the alanine scanning mutagenesis approach and analyzed here is the *L87A5* mutant. To understand the molecular basis of the observed growth defect, mitochondria were isolated from the mutant cells, and WT as a control, and protein levels of a number of mitochondrial proteins were analyzed by immunodecoration. The levels of all tested proteins from different subcompartments of mitochondria were comparable between the mutant and WT (Figure 3.15). The only observed difference was the

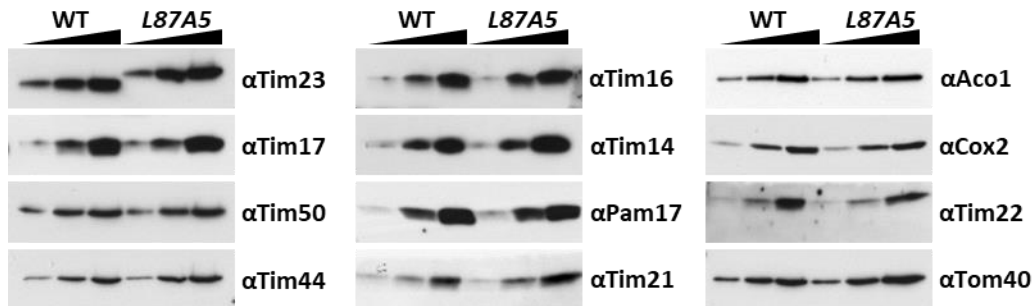


Figure 3.15 Comparison of protein profiles of isolated mitochondria from WT and *L87A5* cells. Increasing amounts of mitochondria were analyzed by SDS-PAGE and immunostaining with antibodies against subunits of the TIM23 complex and various other proteins from different compartments of mitochondria.

altered migration of mutant Tim23. This demonstrates that the changed protein levels or altered protein stability are not the reason behind the impaired growth.

To test whether reduced import via the TIM23 pathway is responsible for the growth impairment, the ability of isolated mitochondria to import matrix targeted precursors, $b_2(1-167)\Delta DHFR$, Su9(1-69)DHFR, Jac1, $F_1\beta$ and Tim44, and laterally sorted precursor, $b_2(1-167)DHFR$, was analyzed (Figure 3.16). In addition, a carrier protein of the IM, AAC, which is imported via the TIM22 complex, was used as a control. All tested clients of the TIM23 complex, matrix targeted ones in particular, were imported poorly into mitochondria isolated from *L87A5* mutant cells. On the other hand, import of AAC was as efficient as in WT

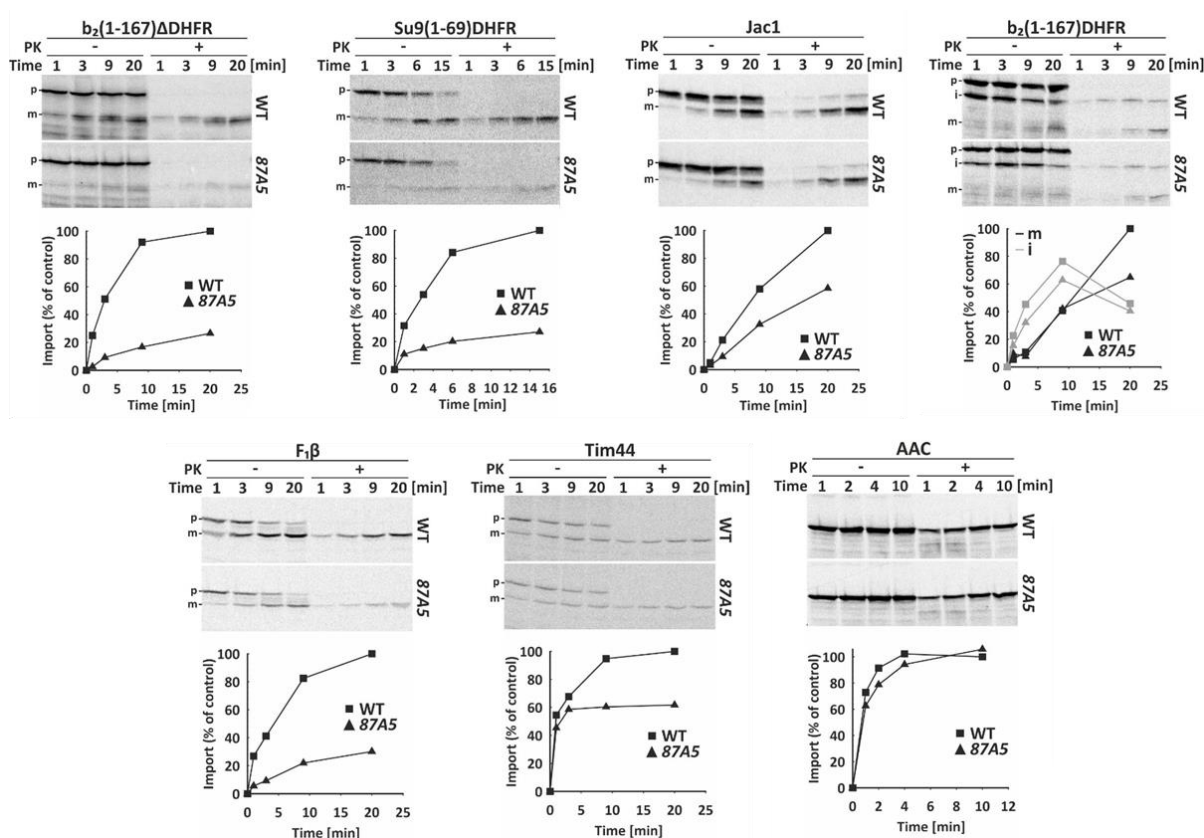


Figure 3.16 *In vitro* protein import into mitochondria isolated from *L87A5* mutant cells. Isolated mitochondria were incubated with *in vitro* translated, radioactively labeled precursor proteins in an import buffer. Import reactions were stopped at indicated time points and, where indicated, samples were treated with proteinase K (PK) to digest non-imported precursors. Following re-isolation of mitochondria, samples were analyzed by SDS-PAGE and autoradiography. p- precursor, i- intermediate and m- mature forms of precursor proteins. Graphs show quantifications of the import reactions. Amount of PK-protected mature form at the longest time point of import into WT mitochondria was set to 100%.

mitochondria. These results show that there is no general problem with mutant mitochondria but rather that the TIM23-mediated import is affected, revealing the reason behind the growth defect.

To further exclude general effects of the mutation on mitochondria, the ability of the mutant mitochondria to generate $\Delta\Psi$ was tested by using a potentiometric, fluorescent dye, DiSC₃(5) (3,3'-dipropylthiadicarbocyanine iodide) (section 2.4.3.1). Figure 3.17 shows that mitochondria isolated from *L87A5* cells can generate $\Delta\Psi$ as efficiently as the ones isolated from WT cells. Therefore, the observed import defect of TIM23-dependent precursors is due to a direct effect of the mutation.

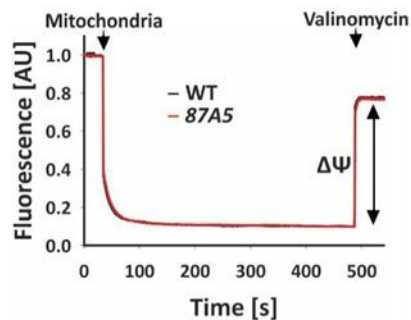


Figure 3.17 $\Delta\Psi$ measurement of mitochondria isolated from WT and *L87A5*. Isolated mitochondria were added to the buffer containing NADH and the fluorescent dye DiSC₃(5). Fluorescence was observed at excitation and emission wavelengths 622 and 670 nm, respectively. $\Delta\Psi$ was dissipated by addition of a K⁺ transporter, valinomycin. Down arrows indicate when mitochondria and valinomycin were added to the sample.

3.1.10 Interaction of Pam17 with Tim23 is reduced in *L87A5* mutant

In order to investigate the reason for the import defect in mitochondria isolated from *L87A5* cells, the assembly of the TIM23 complex was examined by co-immunoprecipitation using antibodies against Tim23 and Tim50 (Figure 3.18). Both antibodies co-precipitated all subunits of the TIM23 complex in similar amounts from WT and the mutant mitochondria, except for Pam17. The amount of Pam17 co-precipitated with antibodies against Tim23 was reduced in the mutant, suggesting that the impaired Tim23-Pam17 interaction may be the reason behind the impaired import into mutant mitochondria.

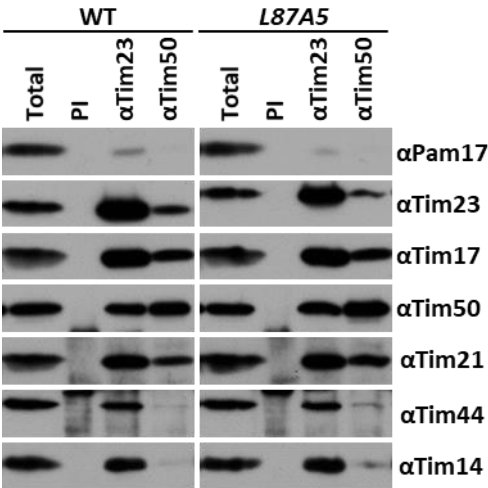


Figure 3.18 Assembly of the TIM23 complex in *L87A5*. Isolated mitochondria from WT and *L87A5* solubilized with digitonin-containing buffer and antibodies against Tim23 and Tim50 were used for immunoprecipitation. Samples were analyzed with SDS-PAGE and immunostaining. Totals are 20% of the immunoprecipitated fractions. PI: Pre-immune serum.

Another way to analyze the interaction between Tim23 and Pam17 is chemical crosslinking in isolated mitochondria with an amino group specific homobifunctional crosslinker, DSG (disuccinimidyl glutarate) (section 2.4.5). When DSG crosslinking is performed with isolated WT mitochondria and analyzed with antibodies against Tim23, two crosslinking products are observed – Tim23 dimers and Tim23-Pam17 crosslink (Popov-Celeketic et al., 2008). Consistent with the co-immunoprecipitation experiment, in *L87A5*, the crosslink between Tim23 and Pam17 was diminished while the Tim23 dimers were not

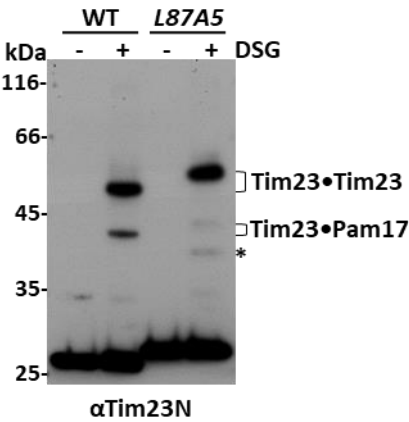


Figure 3.19 DSG crosslinking of Tim23 in *L87A5*. Isolated mitochondria were incubated on ice in the absence or presence of the crosslinker, DSG. Following quenching of the crosslinker and reisolation of mitochondria by centrifugation, the samples were analyzed by SDS-PAGE and immunostaining with αTim23N antibody. *- Unknown crosslinking product.

affected (Figure 3.19). In addition, an unknown DSG-specific crosslink band was observed below Tim23-Pam17 crosslink (indicated with *) for mitochondria isolated from *L87A5* cells.

3.1.11 Pam17 is in direct contact with Tim23 in the IMS

Pam17 has only a small loop exposed to the IMS and this loop does not contain any amino group (van der Laan et al., 2005), suggesting that the DSG crosslinking must take place at the matrix side of the IM. To address whether Pam17 and Tim23 are in close contact also in the IMS, site-specific photo crosslinking approach (section 2.3.3.3) was used. Four different positions (Gln85, Leu87, Ile88 and Arg91) were chosen to introduce Bpa around residues 87-91 of Tim23. After growing yeast cells in Bpa-containing medium and exposure to UV light, total cell extracts were made and His-tagged Tim23 and its crosslinks were enriched on NiNTA-agarose. A crosslinking product between Tim23I88Bpa and Pam17 was detected with an antibody against Pam17 (Black arrowhead in Figure 3.20). The *in vivo* site-specific crosslinking in *I88Bpa* mutant suggests that, indeed, Pam17 is in close contact with Tim23 on the IMS side of the IM. Interestingly, this implies that changes in the IMS can be transduced from the IMS, across the IM, into the matrix.

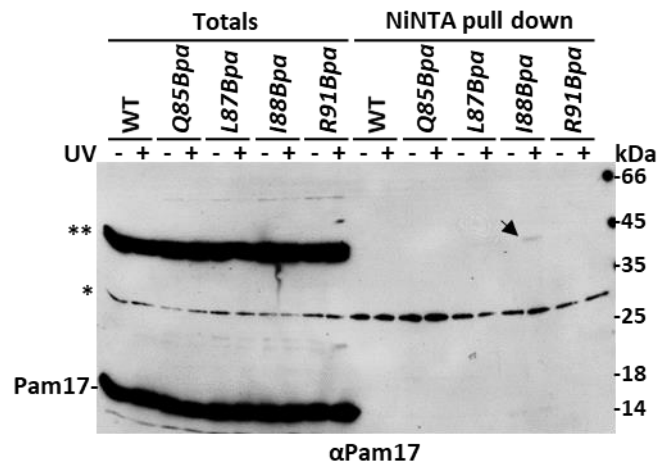


Figure 3.20 Direct interaction of Tim23 with Pam17 in the IMS. The yeast cells expressing His-tagged Tim23 at the C-terminus and carrying an amber stop codon for Bpa incorporation at the indicated positions were grown in the presence of 1mM Bpa. Cells were harvested and one half was illuminated with UV while the other half was kept in the dark. After cell lysis, His-tagged Tim23 and its crosslinks were enriched by binding to the NiNTA-agarose. Totals (7%) and NiNTA-bound (100%) fractions analyzed by SDS-PAGE followed by immunostaining with αPam17. * and ** indicate non-specific bands and black arrow indicates the UV specific Tim23-Pam17 crosslink.

3.1.12 Negative charges at positions 95 and 96 are required for optimal cell growth

The last mutant that was identified by alanine scanning and analyzed here is *D95A2*. The negatively charged residues towards the end of the IMS domain of Tim23 at position 95 and 96 are relatively well conserved and mutating them to alanine caused a temperature sensitive growth defect at 37°C on YPLac medium (Figure 3.10). In order to understand the importance of the two negative charges, in addition to the alanine mutants, the two residues were also mutated to positively charged lysine. Reversing the charges caused an additional stress on the cells and the growth phenotype of *D95K2* was clearly worse than that of *D95A2* (Figure 3.21). This suggests that the negative charges in these positions are essential for optimal cell growth.

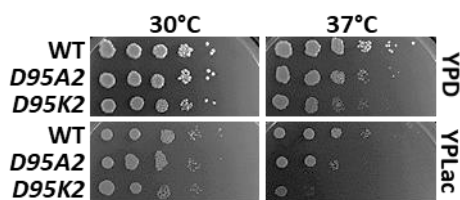


Figure 3.21 Importance of negative charges at positions 95 and 96 of Tim23. Alanine and lysine mutants together with WT Tim23 were grown to same OD in YPGal and analyzed by serial dilution spot assay at indicated temperatures on YPD and YPLac plates.

3.1.13 Protein import is impaired in *D95A2* and *D95K2* mutant mitochondria

Isolated mitochondria showed similar amounts of various mitochondrial proteins from different compartments, suggesting no major changes caused by the mutations (Figure 3.22). In order to see the effect of the mutations directly on protein import, isolated mitochondria from *D95A2* and *D95K2* mutant cells were analyzed in *in vitro* import experiments. Import of precursors using the TIM23 complex was impaired in mutant mitochondria (Figure 3.23). Matrix targeted precursors, $b_2(1-167)\Delta\text{DHFR}$, F1 β and Tim44, and laterally sorted precursors, DLD and $b_2(1-167)\text{DHFR}$, were imported less efficiently in the mutant mitochondria. In all cases, imports in the charge-reversal mutant mitochondria were impaired more than in the alanine mutant, in agreement with the observed growth phenotypes. Control precursor AAC was imported equally efficiently into both types of mutant mitochondria as in WT. Additionally, $\Delta\Psi$ measurements showed that both types of

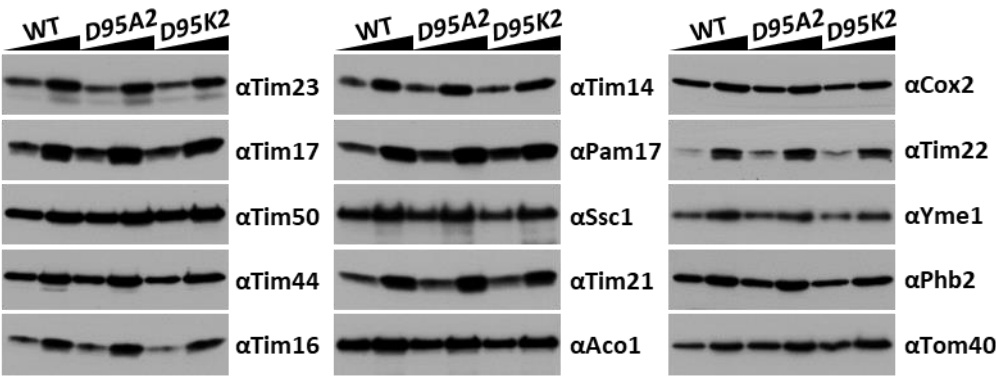


Figure 3.22 Comparison of isolated mitochondria from WT, D95A2 and D95K2. Increasing amounts of mitochondria were lysed in 2X Laemmli buffer, separated via SDS-PAGE and analyzed by immunostaining with antibodies against the TIM23 complex subunits and other mitochondrial proteins.

mutant mitochondria were able to generate membrane potential as efficiently as WT mitochondria (Figure 3.24), suggesting that the observed import defects are the direct effect

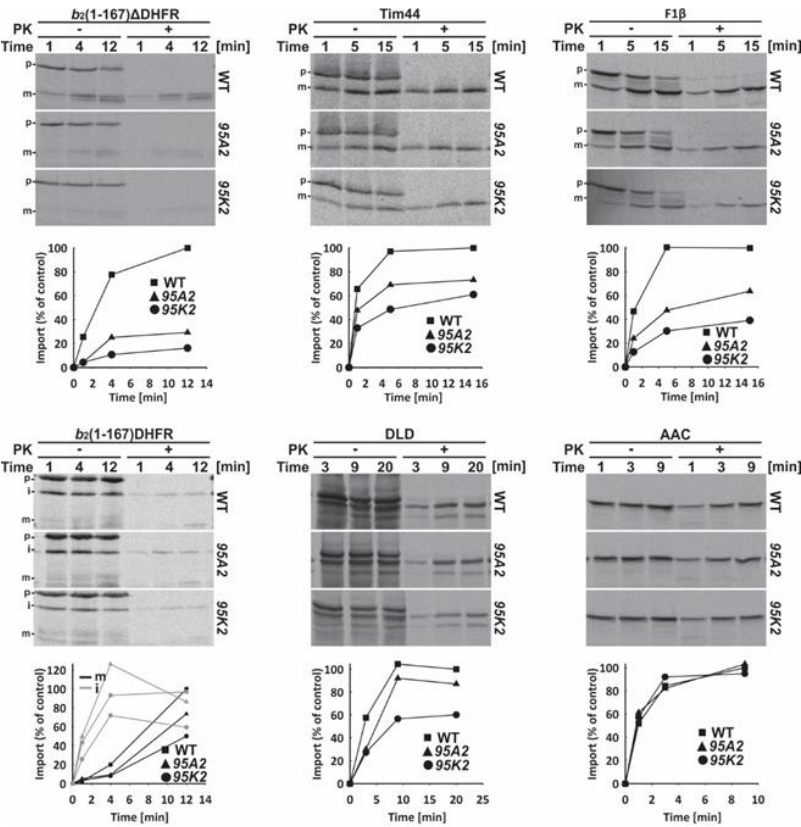


Figure 3.23 *In vitro* protein import into mitochondria from D95A2 and D95K2. Isolated mitochondria were subjected to an *in vitro* import assay with *in vitro* translated, radioactively labeled precursor proteins. Samples were analyzed by SDS-PAGE and autoradiography. p- precursor, i- intermediate and m- mature forms of precursor proteins. Quantifications of import reactions were shown in the lower panels. Amount of PK-protected mature form at the longest time point of import into WT mitochondria was set to 100%.

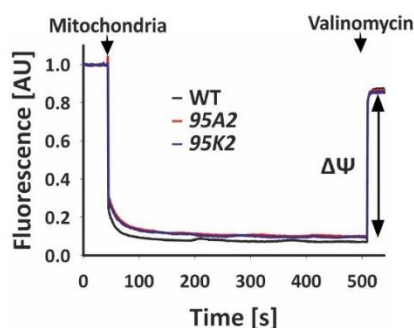


Figure 3.24 $\Delta\Psi$ measurement of WT, *D95A2* and *D95K2* mitochondria. Isolated mitochondria were incubated with the fluorescent dye, DiSC₃(5), and NADH. The kinetics of dye uptake was observed at excitation and emission wavelengths, 622 and 670 nm. Dissipation of $\Delta\Psi$ was provided with addition of a K⁺ transporter, valinomycin. Down arrows indicate the time points of the addition of respective component.

of the mutation on the activity of the TIM23 complex.

3.1.14 Residues 95 and 96 alter conformation of Tim23 in the IMS

To reveal the molecular reason behind the growth defects and the impaired mitochondrial import in *D95A2* and *D95K2* mutants, the composition and the conformation of the TIM23 complex were analyzed. DSG crosslinking in mitochondria from *D95A2* and *D95K2* demonstrated different crosslinking patterns compared to WT (Figure 3.25). Interestingly, Tim23 dimers were highly reduced in *D95A2* and essentially absent in *D95K2*, recapitulating the severity of their growth phenotypes. Additionally, the crosslinks between Tim23 and Pam17 were slightly reduced in both mutants. However, neither of the mutations affected interaction of Tim23 with any other subunit of the TIM23 complex, as judged by the co-immunoprecipitation experiment (Figure 3.26). All tested subunits of the TIM23 complex

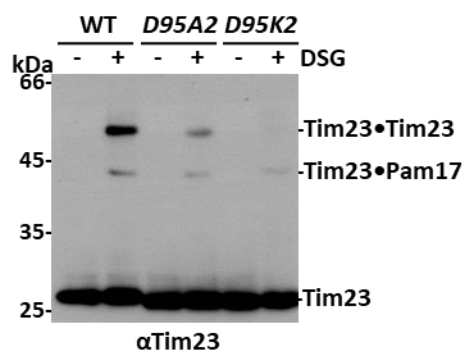


Figure 3.25 DSG crosslinking of Tim23 in *D95A2* and *D95K2* mitochondria. Isolated mitochondria were incubated on ice in the presence or absence with the crosslinker, DSG. Following quenching of the crosslinker and reisolation of mitochondria, samples were analyzed by SDS-PAGE and immunostaining with α Tim23N antibody.

were coprecipitated by the antibody against Tim23 in comparable amounts as in WT. These results suggest that, when the residues 95 and 96 are mutated, conformation or dynamics of the IMS domain of Tim23 may change in a way that does not allow the transfer of the precursors to the translocation channel in the IM.

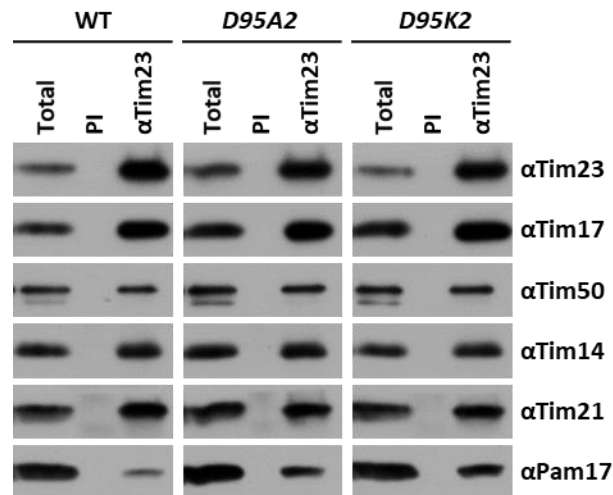


Figure 3.26 Assembly of the TIM23 complex in *D95A2* and *D95K2* mutant mitochondria. Isolated mitochondria from WT, *D95A2* and *D95K2* were solubilized with digitonin-containing buffer and incubated with antibodies against Tim23 and Tim50. Samples were analyzed with SDS-PAGE and immunostaining. Totals are 20% of the immunoprecipitated fractions. PI: Pre-immune serum.

3.1.15 TMs 3 and 4 of Tim23 are not essential for cell viability

Residues 95 and 96 are predicted to be in the immediate vicinity of the translocation channel of the TIM23 complex, which is at least in part formed by the C-terminal domain of Tim23. The C-terminal domain of Tim23 is embedded in the IM with four predicted TM segments (Figure 3.1). The first two TMs of Tim23 were implicated in the channel formation (Alder et al., 2008b; Demishtein-Zohary et al., 2015) whereas a recent random mutagenesis screen suggested that TM3 and TM4 may not be essential for Tim23 function (Pareek et al., 2013).

To check whether the last two TMs of Tim23 are indeed not essential for Tim23 function, plasmids expressing Tim23 truncated by the TM4 alone ($\Delta TM4$) and by both TM3 and TM4 ($\Delta TM3-4$) under endogenous promoter were transformed into Tim23 shuffling strain. $\Delta TM4$ and $\Delta TM3-4$ were generated by adding a stop codon after Ser192 and Leu169, respectively. 5-FOA selection plates showed that both mutants were indeed viable,

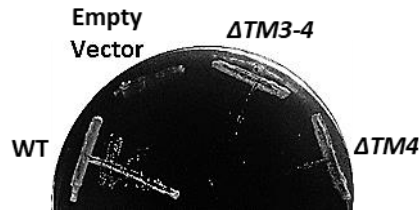


Figure 3.27 C-terminal truncations of Tim23 rescues the function of the FL Tim23 (WT). Tim23 shuffling strains was transformed with the C-terminally truncated versions of Tim23 ($\Delta TM4$ and $\Delta TM3-4$) and the viability of the cells were analyzed on 5-FOA selection plates. FL construct and the empty vector were used as positive and negative controls, respectively.

confirming the previously published data (Pareek et al., 2013). However, only a few colonies survived the selection procedure, suggesting a severe functional defect of the TIM23 complex (Figure 3.27). The growth of the C-terminally truncated mutants of Tim23 was analyzed by serial dilution spot assay (Figure 3.28). Both mutants showed severe temperature sensitive growth defects and were inviable at 37°C on either fermentable or non-fermentable carbon source. On a non-fermentable carbon source, they were growing very poorly even at 30°C.

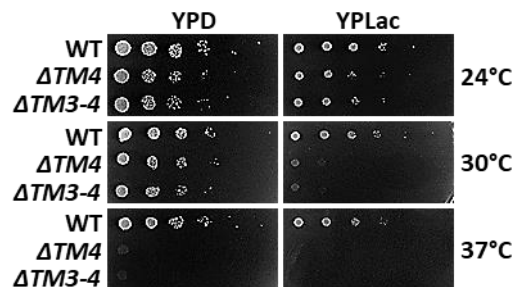


Figure 3.28 Growth of C-terminal truncation mutants of Tim23. WT and C-terminally truncated versions of Tim23 were grown to same OD in YPGal and serially diluted cells were dropped onto YPD and YPLac plates. The plates were incubated at the indicated temperatures.

3.1.16 Import into $\Delta TM4$ and $\Delta TM3-4$ is impaired

To understand whether impaired growth is due to the reduced efficiency of import via the TIM23 complex, isolated mitochondria from WT and the mutant strains were analyzed in *in vitro* import experiments. Import efficiencies of matrix targeted precursors, $b_2(1-167)\Delta DHFR$ and Jac1, and of a laterally sorted substrate, DLD, were drastically reduced in mitochondria expressing the C-terminally truncated versions of Tim23 (Figure 3.29). However, import of Tim23, used as a control precursor, which uses the TIM22 pathway for its import, was similar to WT. This demonstrates that mitochondria isolated from $\Delta TM4$ and

$\Delta TM3-4$ were specifically defective in import via the TIM23 pathway. Interestingly, the clipped version of the imported Tim23 (Tim23*) was more prominent after import into the mutant mitochondria than into WT. This result suggests that newly imported WT Tim23 can assemble more easily into the TIM23 complex in mutant than in WT mitochondria. A similar observation was previously made when WT version of Tim23 was imported into mitochondria containing a mutant version of Tim23 that cannot assemble with Tim17 (Dekker et al., 1997), raising the possibility that the assembly of the TIM23 complex may be impaired in the mutants.

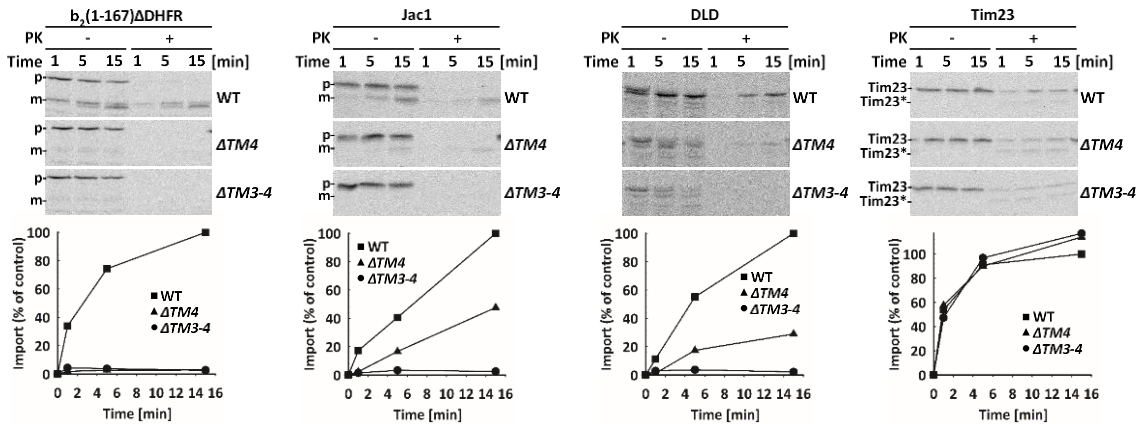


Figure 3.29 *In vitro* protein import into $\Delta TM4$ and $\Delta TM3-4$ mitochondria. Isolated mitochondria were subjected to *in vitro* import experiments as described previously. Samples were analyzed by SDS-PAGE and autoradiography. p-precursor, i-intermediate and m-mature forms of precursor proteins. Tim23*- clipped version of Tim23. Quantifications of import reactions were shown in the lower panels. Amount of PK-protected mature form at the longest time point of import into WT mitochondria was set to 100%.

3.1.17 Last two transmembrane segments of Tim23 are important for stabilization of Tim23 interaction with Tim17

To address whether the impaired assembly of the TIM23 complex is the reason behind the impaired import into the mitochondria carrying the C-terminally truncated versions of Tim23, the expression levels of the C-terminally truncated mutants of Tim23 were analyzed first. Even though it was previously reported that C-terminal truncations did not affect the expression levels of Tim23 (Pareek et al., 2013), an analysis of total cell extracts using antibodies against the N-terminal part of Tim23 showed that Tim23 levels were reduced in both mutants (Figure 3.30). Thus, newly imported Tim23 could probably assemble with the surplus of available Tim17.

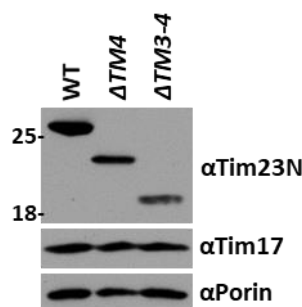


Figure 3.30 Expression of C-terminally truncated versions of Tim23. Total cell extracts of WT and the mutant strains were analyzed by SDS-PAGE and immunostaining. Antibodies against the N-terminal peptide of Tim23 were used to detect WT and the C-terminally truncated proteins. Tim17 and Porin were used as loading controls.

The mitochondrial import signal of Tim23 was previously shown to reside in its C-terminal domain (Davis et al., 1998). Therefore, localization of the truncated Tim23 proteins was checked in subcellular localization experiment using crude mitochondria isolated by differential centrifugation and the corresponding cytosolic fractions (section 2.3.3.4). Figure 3.31 demonstrates that both C-terminally truncated versions of Tim23 were exclusively present in mitochondria. Whether the reduced levels of Tim23 arose from lower transcription, translation, increased degradation, within or outside of mitochondria, or reduced import efficiency of C-terminally truncated Tim23 remains currently unclear.

The lower expression levels of Tim23 could explain the observed phenotypes. However, it is still possible that the assembly of the TIM23 complex is impaired in cells expressing the C-terminally truncated versions of Tim23. To study the assembly of the TIM23 complex in $\Delta TM4$ and $\Delta TM3-4$, co-immunoprecipitation experiment was done with digitonin-

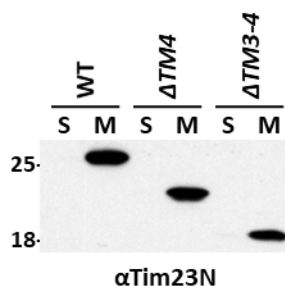


Figure 3.31 Localization of the C-terminal truncation mutants of Tim23. Mitochondrial localization of the proteins was assessed by isolating crude mitochondria from yeast cells. The cells were lysed mechanically by vigorous vortexing with glass beads and mitochondria were isolated by differential centrifugation. Supernatant (S) fraction remaining after pelleting of mitochondria, which corresponds to the cytosol, and mitochondrial (M) fractions were analyzed by SDS-PAGE and immunoblotting against α Tim23N.

solubilized mitochondria using antibodies against Tim17 and Tim23. The analysis of the input samples (Total) revealed that, except for the reduced levels of truncated versions of Tim23 in the mutant mitochondria, all other analyzed subunits of the TIM23 complex were present in comparable amounts as in WT. When the precipitated fractions were analyzed, similar results were obtained with mitochondria isolated from $\Delta TM4$ (Figure 3.32a) and $\Delta TM3-4$ (Figure 3.32b) mutants. Most prominently, both C-terminally truncated versions of Tim23 showed an impaired interaction with Tim17. This can be most easily seen when comparing the amounts of Tim17 and Tim23 co-precipitated with the antibody against the other protein. In WT mitochondria, both Tim17 and Tim23 antibodies immunoprecipitated both proteins in similar amounts. In contrast, in the mutant, each antibody immunoprecipitated prominently only its own target. Though reduced levels of Tim17 co-precipitated with antibodies against Tim23 could potentially be explained by lower endogenous Tim23 levels, the fact that also antibodies against Tim17 co-precipitated less of Tim23 in mutant mitochondria clearly shows that Tim17-Tim23 interaction is impaired when the last or the last two TMs of Tim23 are missing. Consistent with previous observations that the interaction of Tim50 with the rest of the TIM23 complex is mediated mainly through Tim23 (Geissler et al., 2002; Mokranjac et al., 2003a; Mokranjac et al., 2009; Yamamoto et al., 2002), antibodies against Tim17 co-precipitated less of Tim50 from mutant mitochondria than did antibodies against Tim23, further supporting the notion that the interaction between Tim17 and Tim23 is impaired in

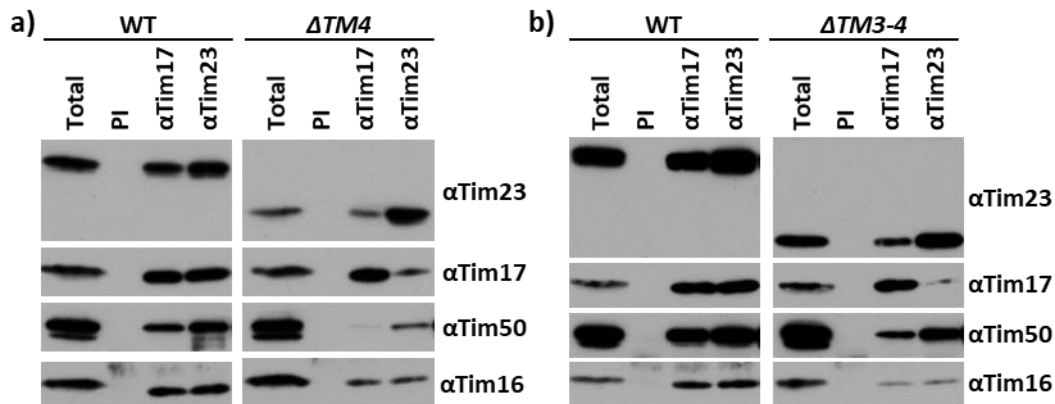


Figure 3.32 Assembly of the TIM23 complex in $\Delta TM4$ and $\Delta TM3-4$. Isolated mitochondria from WT, a) $\Delta TM4$ and b) $\Delta TM3-4$ were solubilized with digitonin-containing buffer and antibodies against Tim17 and Tim23 were used for immunoprecipitation. Samples were analyzed with SDS-PAGE and immunostaining with indicated antibodies. Totals are 20% of immunoprecipitated samples. PI: Pre-immune serum.

the mutants. On the other hand, within one type of mitochondria, import motor subunit, Tim16, was co-precipitated equally efficiently with both Tim17 and Tim23 antibodies, confirming the previous finding that the import motor binds only to the assembled Tim17-Tim23 core of the TIM23 complex. The levels of co-precipitated import motor subunit were, however reduced in the mutants, again speaking for the impaired interaction between Tim17 and Tim23 in the Tim23 C-terminally truncated mutants.

In summary, *in vivo* dissection of Tim23 showed that distinct regions in the IMS domain of Tim23 play different roles during protein import by the TIM23 complex. Tim50 binding region was found larger than previously proposed and mutation of the region dramatically impaired growth of yeast cells. Detection of an unexpected interaction in the IMS with Pam17 pointed out that the IMS domain not only acts as a hub for the initiation for the import process, but also it regulates the later stages of it. The conserved negative charges at positions 95 and 96 were found to be important for the function of Tim23. In addition, dissection of the TM domain of Tim23 demonstrated that the last two TMs of Tim23 are required for stable interaction with Tim17 and, thus, also import motor recruitment.

3.2 *In vivo* dissection of Tim17

3.2.1 TMs of Tim17 are essential

Since Tim23 and Tim17 belong to the same family of proteins and the deletion of the last two TMs of Tim23 can be tolerated by yeast cells, role of the TMs of Tim17 was analyzed.

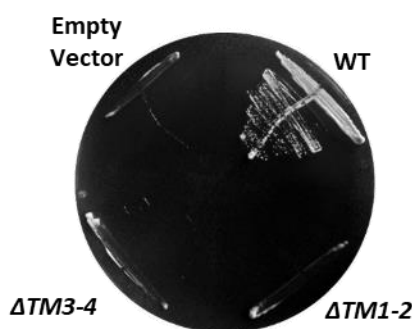


Figure 3.33 Rescue of the function of Tim17 by the truncated versions of Tim17. Tim17 shuffling strain was transformed with plasmids encoding the truncated versions of Tim17 (Δ TM3-4 and Δ TM1-2) and the cell viability was checked on 5-FOA selection plates. Plasmid encoding the wild-type version of Tim17 (WT) and the empty vector were used as positive and negative controls, respectively.

Constructs were generated in which either the last two or the first two TMs of Tim17 were deleted, and the truncated proteins were expressed under the control of the endogenous *TIM17* promoter and 3'UTR in a Tim17 shuffling strain. Neither of the truncated versions of Tim17 gave viable cells on a 5-FOA selection plate (Figure 3.33), suggesting that all the TMs of Tim17 are essential, unlike the ones in Tim23.

3.2.2 Mutations in GxxxG motifs in the first 3 TMs of Tim17 result in defective import via the TIM23 complex

Sequence alignment of 920 Tim17 sequences (Zarsky and Dolezal, 2016) revealed highly conserved GxxxG motifs in first three transmembrane segments of Tim17 (indicated with red stars in Figure 3.34). GxxxG motifs in the TMs of membrane proteins function as the structural contact sites to maintain inter- or intra-molecular tight packing of the TMs (Teese and Langosch, 2015). By replacing the glycine residues in the motifs with bulky residues such as leucine, the effects of TM packing in Tim17 were analyzed in collaboration with the group of Prof. Azem at the Tel Aviv University, as it was done previously for Tim23 (Demishtein-Zohary et al., 2015; Pareek et al., 2013). Azem group observed temperature sensitive growth phenotype when several glycine residues in TM1, TM2 and TM3 were replaced with bulky leucine residues (Demishtein-Zohary et al., 2017). In agreement with the growth phenotypes, all of the mutants demonstrated impaired import of both matrix-targeted, $b_2(1-167)\Delta\text{DHFR}$, and laterally sorted, $b_2(1-167)\text{DHFR}$ and $b_2(1-220)\text{DHFR}$, precursor proteins (Figure 3.35). The

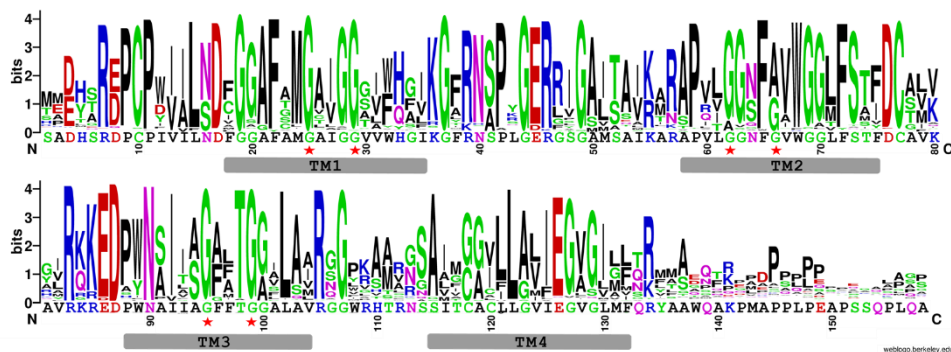


Figure 3.34 Sequence conservation of yeast Tim17. Multiple sequence alignment of Tim17 was converted to logo chart via WebLogo creation tool at weblogo.berkeley.edu/logo.cgi. Sizes of the letters depict the conservation of the residues. X-axis shows the sequence of *Saccharomyces cerevisiae* Tim17. TM segments are indicated with grey bars. Y-axis shows the conservation (Max value: $\log_2 20 = 4.3$ for 20 possible amino acids). Red stars indicate residues in GxxxG motifs that were analyzed here.

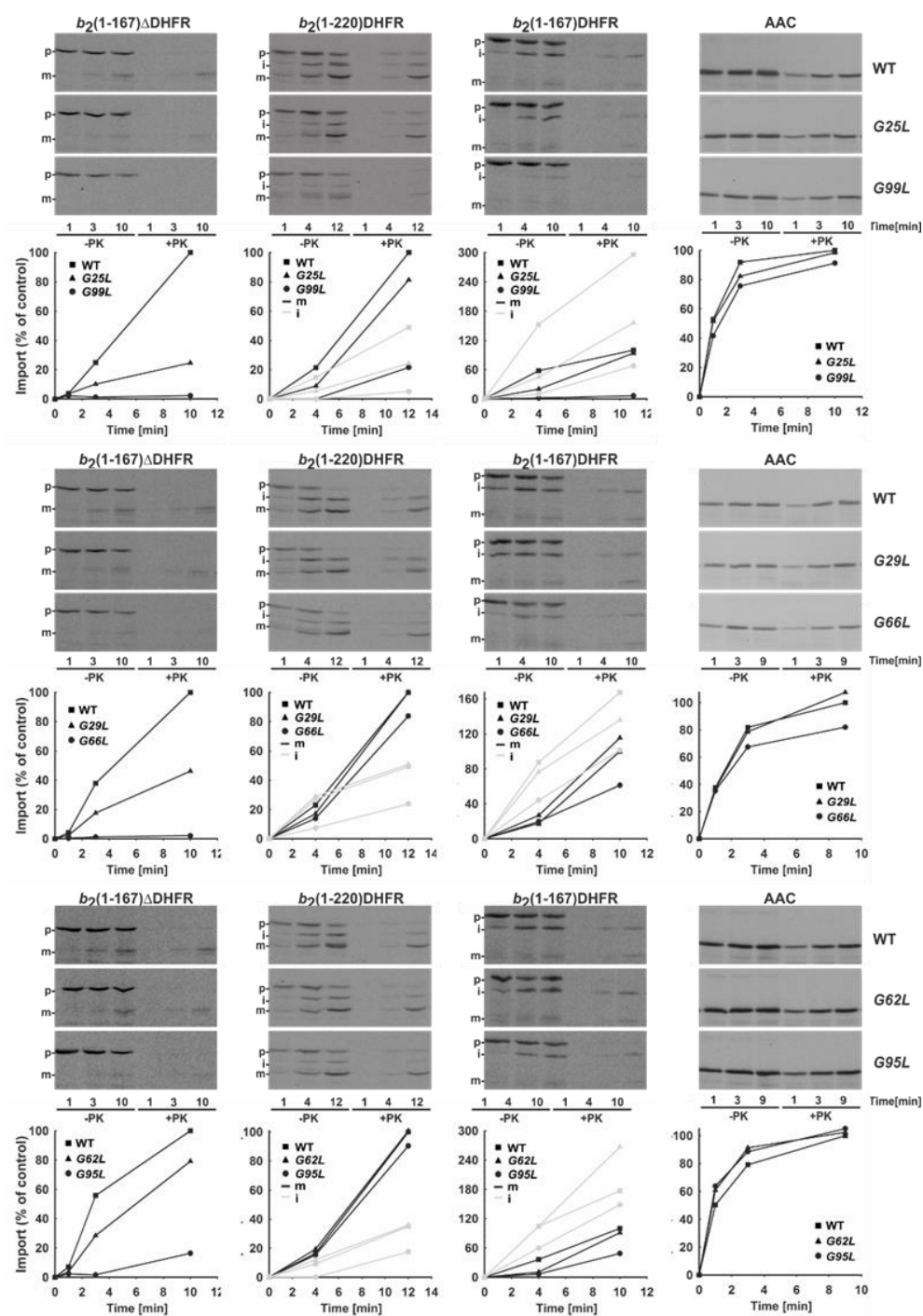


Figure 3.35 Protein import into GxxxG motif mutants of Tim17. Isolated mitochondria were incubated with *in vitro* translated, radioactively labeled precursor proteins in an import buffer. Import reactions were stopped at indicated time points and samples were treated with proteinase K (PK), where indicated. PK removes precursors which are not imported. After re-isolation of mitochondria, mitochondrial lysates were analyzed by SDS-PAGE and autoradiography. p-precursor and m-mature forms of precursor proteins. Quantifications of import reactions are shown in the lower panels (PK-protected mature form at the longest time point of import into WT mitochondria was set to 100%).

import defect of matrix-targeted precursor was more prominent than of the laterally sorted ones. Import of AAC, on the other hand, was not affected in any of the mutants, showing that the effect is specific for the TIM23 complex clients.

3.2.3 Mutations of GxxxG motifs in TM segments of Tim17 differently affect assembly of the TIM23 complex

To understand the reason behind the impaired growth and defective import via the TIM23 complex, the effects of the mutations on the assembly of the TIM23 complex were analyzed. Isolated mitochondria were solubilized with digitonin and analyzed for the assembly of the TIM23 complex by BN-PAGE and for protein levels by SDS-PAGE (Figure 3.36). SDS-PAGE analysis revealed that all analyzed subunits of the TIM23 complex, Tim17, Tim23, Tim44, Tim50 and Tim16 were present in similar amounts in all mutants, as compared to WT. BN-PAGE analysis indicated that the Tim17-Tim23 complex formation was impaired in mutants mapping to TM1 and TM2 (G25L and G29L on TM1 and G62L and G66L on TM2). However, mutations in the GxxxG motif in TM3 (G95L and G99L) did not affect the Tim17-Tim23 complex formation. Thus, import defects and growth phenotypes of TM1 and TM2

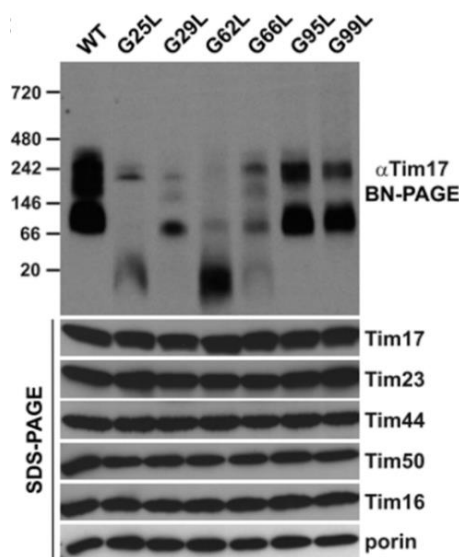


Figure 3.36 Assembly of the TIM23 complex in GxxxG motif mutants of Tim17. Isolated mitochondria from WT and the GxxxG motif mutants were solubilized with digitonin and the samples were analyzed by BlueNative (upper panel) and SDS-PAGE (lower panel) followed by immunoblotting.

mutants could be explained by defective formation of the Tim17-Tim23 core of the TIM23 complex but not in the TM3 mutants.

3.2.4 N-terminal part of loop 3 of Tim17 is essential for cell viability

Co-immunoprecipitation experiments done with the GxxxG motif mutants confirmed the results obtained by BN-PAGE that mutations in TM1 and TM2 of Tim17 impair Tim17-Tim23 interaction and showed that TM3 mutants are impaired in import motor recruitment (Demishtein-Zohary et al., 2017). In the light of these results and considering previous finding from our group that Tim17 directly interacts with Tim44 (Banerjee et al., 2015) and that Ting et al. (2014) found no interaction of Tim44 with the loop 1 of Tim17, an analysis on the matrix exposed loop between TM3 and TM4 (loop 3) of Tim17 was done in order to identify a possible Tim44-binding site. Two alanine mutants of this loop were created in which five consecutive residues were mutated to alanines (*V104A5* and *R109A5*). Interestingly, *V104A5* mutant produced no viable clones upon 5-FOA selection, suggesting an essential role for this region (Figure 3.37).

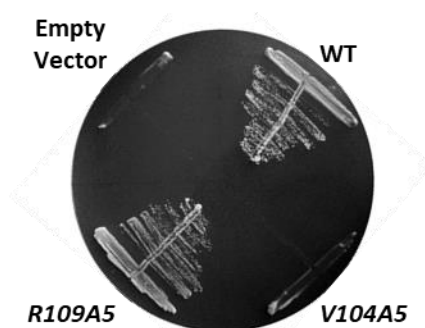


Figure 3.37 Alanine scanning of matrix exposed loop 3 of Tim17. Tim17 shuffling strain was transformed with plasmids encoding alanine mutants of Tim17 (*V104A5* and *R109A5*) and the viability of the corresponding cells was checked on 5-FOA selection plates. WT construct and the empty vector were used as positive and negative controls, respectively.

3.2.5 Conserved residue Arg105 is important for cell viability

Alignment of Tim17 from different species demonstrated a highly conserved arginine residue at position 105 within the first alanine patch (residues 104-108) (Figure 3.34). Therefore, a R105A mutant was generated and a serial dilution spot assay of the single mutant together with the second alanine patch mutant, which was viable on 5-FOA plate (Figure 3.37), was done (Figure 3.38). The *R109A5* mutant did not cause any growth defect at any of the tested condition. Mutating Arg105 to alanine, on the other hand, caused a very

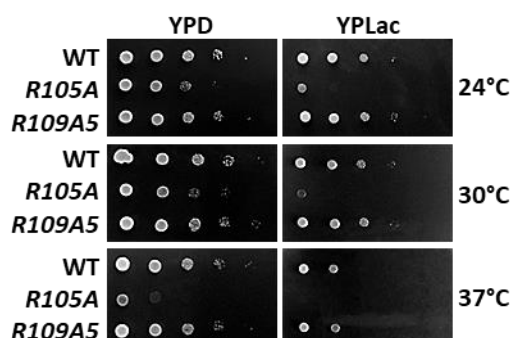


Figure 3.38 The effect of mutating conserved Arg105 on growth of yeast cells. WT and the indicated mutants were grown to same OD in YPGal. 10-fold serial dilution of cells were made and cells were spotted onto YPD and YPLac plates. The plates were incubated at indicated temperatures.

severe growth defect and the mutant was essentially inviable on a non-fermentable medium. To address the importance of the positive charge at position 105, the arginine residue was mutated to a lysine, keeping the charge and the length of the residue very similar. However, this conservative mutation (R105K) could improve the growth only marginally and only on a fermentable medium (Figure 3.39), demonstrating that the charge of the residue is not the most important feature for this position.

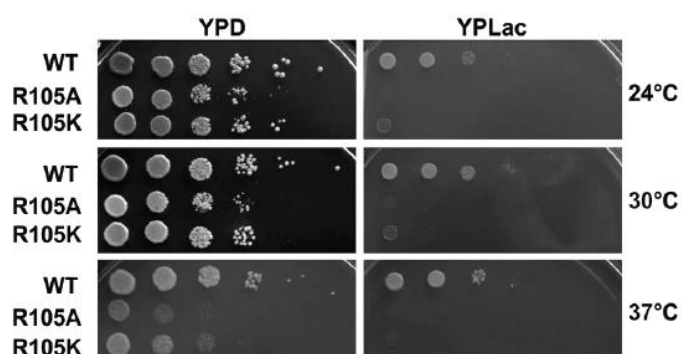


Figure 3.39 The effect of positive charge at position 105 of Tim17 on growth of yeast cells. WT, R105A and R105K were tested by serial dilution spot assay at indicated temperatures. The cells were grown in YPGal medium prior to dropping on YPD and YPLac plates.

3.2.6 Protein import via the TIM23 complex is defective in R105A mutant

For further analysis, mitochondria were isolated from WT and R105A cells. To assess whether mitochondrial protein profiles were affected by the mutation, a number of mitochondrial proteins were immunostained after SDS-PAGE. No major difference between mitochondria isolated from WT and R105A cells was found (Figure 3.40). Still, precursors using the TIM23 complex were imported into R105A mitochondria with reduced efficiencies

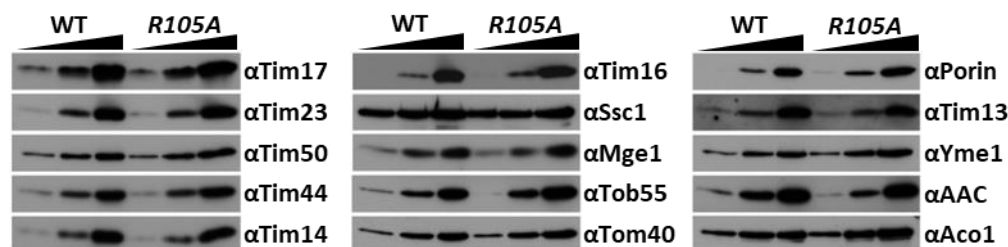


Figure 3.40 Comparison of isolated mitochondria from WT and *R105A* cells. Increasing amounts of mitochondria were lysed in 2X Laemmli buffer, separated by SDS-PAGE and analyzed by immunostaining with antibodies against the TIM23 complex subunits and the various other mitochondrial proteins.

compared to WT, irrespective whether matrix targeted or laterally sorted ones were analyzed. However, a TIM23-independent precursor AAC was imported in mutant mitochondria as efficiently as in WT (Figure 3.41), confirming a TIM23-specific defect.

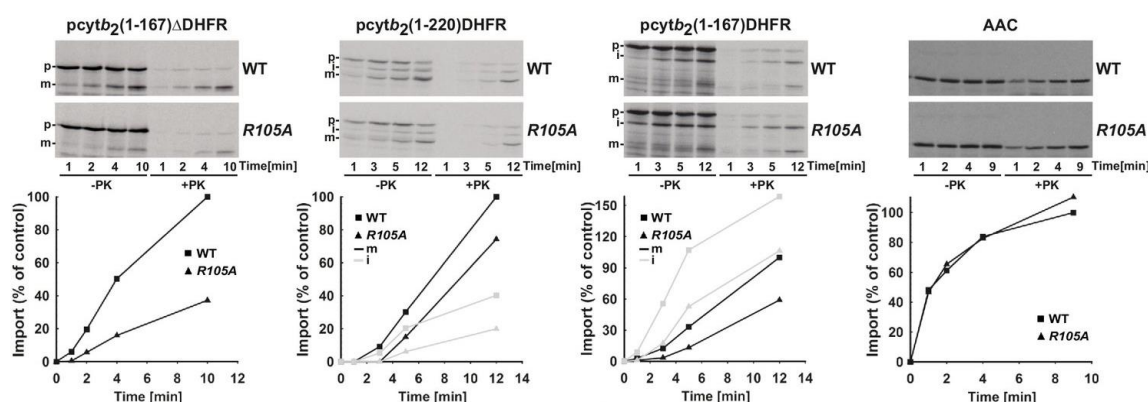


Figure 3.41 *In vitro* protein import into *R105A*. Mitochondria isolated from WT and *R105A* cells were subjected to *in vitro* import experiment using *in vitro* translated, radioactively labeled precursor proteins as described in section 2.4.2. p-precursor, i-intermediate and m-mature forms of precursor proteins. Quantifications of PK-protected samples were shown in lower panels. Amount of PK-protected mature form at the longest time point of import into WT mitochondria was set to 100%.

3.2.7 Import motor interaction in *R105A* mutant is impaired

To analyze the assembly of the TIM23 complex in *R105A*, a co-immunoprecipitation experiment was carried out (Figure 3.42). Similar to the glycine mutants of TM3, import motor subunits could not be co-precipitated using antibodies against Tim17 and Tim23. In addition, antibodies against Tim16 could not co-precipitate Tim17-Tim23 core of the TIM23 complex. All these results are in agreement with that the notion that the loop 3 of Tim17 and residue Arg105 in particular are crucial for import motor recruitment.

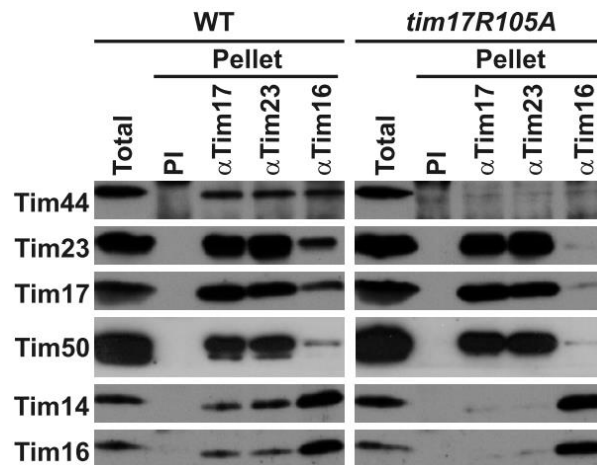


Figure 3.42 Assembly of the TIM23 complex in *tim17R105A* mutant. Isolated mitochondria from WT and *R105A* cells were solubilized with digitonin and antibodies against Tim17, Tim23 and Tim16 were used for immunoprecipitation. Samples were analyzed with SDS-PAGE and immunostaining. Totals are 20% of the pellet fractions PI: Pre-immune serum.

3.2.8 Loop 3 of Tim17 is in direct contact with Tim44

To analyze whether there is a direct contact between loop 3 of Tim17 and Tim44, three Bpa mutants at positions 104, 106 and 108 of Tim17 were generated. Only when Bpa was incorporated at position 106, a direct interaction was observed with antibodies against Tim44 (Demishtein-Zohary et al., 2017). To test whether this contact is dependent on Arg105, the site specific crosslinking was done in the *R105A* background. Therefore, a version of Tim17 was made in which Bpa at position 106 was combined with R105A mutation. As the respective plasmid gave no viable clones in Tim17 shuffling strain (data not shown), it was analyzed in WT background. Whereas the plasmid-borne version of Tim17 carrying Bpa at position 106 gave a prominent crosslink to Tim44 also in WT background, no Tim44-Tim17 crosslink was observed when the Tim17 version carrying the R105A mutation in addition was used. This confirms the role of Arg105 in Tim17-Tim44 interaction (Figure 3.43).

Taken together, *in vivo* dissection of Tim17 revealed that all its TM segments are essential for the function of the protein – the first two are important for Tim17-Tim23 interaction and the last two, and the matrix-exposed loop between them in particular, for recruitment of the import motor.

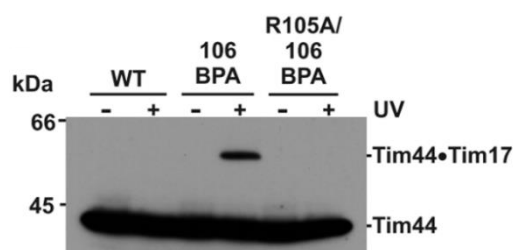


Figure 3.43 Requirement of Arg105 for the interaction between Tim17 and Tim44. WT cells were transformed with plasmids expressing C-terminally His-tagged Tim17 and carrying a premature stop-codon at position 106 in the presence or absence of R105A mutation. The cells were grown in the presence of 1mM Bpa. Cells were harvested and one half was illuminated with UV light while the other half was kept in dark. Total cell extracts were analyzed by SDS-PAGE and immunostaining with α Tim44.

3.3 Purification and reconstitution of the recombinant Tim17-Tim23 core of the TIM23 complex

3.3.1 Expression and purification of the recombinant Tim17-Tim23 complex

Experiments described so far identified many functionally important segments of Tim17 and Tim23 and revealed the previously unknown contacts within the TIM23 complex. However, mechanistic understanding of the function of the TIM23 complex would require the availability of a robust *in vitro* system reconstituted from recombinantly expressed subunits. To this end, a C-terminally His-tagged version of Tim23 (Tim23_{his9}) and a Strep-tagged version of Tim17 (Tim17_{strep}) were cloned into two multiple cloning sites of pET-Duet1 vector. Following transformation of the plasmid into *E. coli* C43(DE3) cells, expression of the proteins was induced by addition of IPTG. Indeed, Tim23 and Tim17 can be co-expressed recombinantly in *E. coli* cells (Figure 3.44).

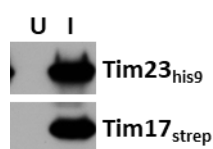


Figure 3.44 Recombinant expression of Tim23_{his9} and Tim17_{strep} in *E. coli* cells. Total cell extracts of *E. coli* C43(DE3) cells transformed with the plasmid encoding Tim17_{strep} and Tim23_{his9} were made before and after induction (U- Uninduced, I- Induced) with IPTG. Samples were analyzed by SDS-PAGE and western blot using antibodies against Histidine-tag and Tim17.

Localization of Tim17 and Tim23 in bacterial cells was tested by differential centrifugation. After lysing the cells mechanically, a low-speed clarification centrifugation step was applied to remove unbroken cells, large cellular debris and inclusion bodies. Cytosolic and membrane fractions were subsequently separated by ultracentrifugation.

Recombinantly expressed Tim23 and Tim17 were predominantly co-localized with an *E. coli* membrane protein, membrane protein insertase, YidC (Figure 3.45). The cytosolic *E. coli* Hsp70 chaperone, DnaK, on the other hand, was predominantly present in the soluble fraction after ultracentrifugation. This result shows that eukaryotic mitochondrial inner membrane proteins, Tim23 and Tim17, were correctly targeted to membranes in prokaryotic *E. coli* cells.

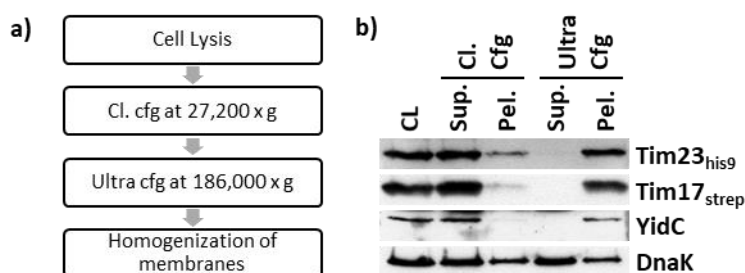


Figure 3.45 Membrane isolation from *E. coli* cells expressing recombinant Tim17 and Tim23. **a)** Scheme of membrane isolation protocol (see section 2.4.7.2). **b)** Samples from each step were analyzed by SDS-PAGE and immunostaining using antibodies against Histidine-tag, Tim17, YidC and DnaK. CL- Cell lysate, Cl. cfg- Clarification centrifuge, sup.- supernatant and pel.- pellet fractions.

To check whether Tim17 and Tim23 also form a complex in *E. coli* membranes, isolated membranes were solubilized in a buffer containing Fos-choline 12 (FC12) and the proteins were purified using two affinity chromatography steps (Figure 3.46). A previous postdoctoral researcher in the group identified FC12 as the optimal detergent for solubilization of *E. coli* membranes without disrupting Tim17-Tim23 interaction (Du Plessis, unpublished observation). The identity of Tim17 and Tim23 in the elution fractions from Streptactin-Sepharose column was confirmed by western blotting (data not shown). The CBB-staining of the same fractions demonstrated that Tim23 and Tim17 were the only proteins present in the fractions, showing that a certain fraction of the expressed proteins formed the complex in *E. coli* membranes and could successfully be purified as the recombinant Tim17-Tim23 complex. A large fraction of Tim23 was, however, present in the flow-through fraction of the Streptactin column (see FT lane of Streptactin purification), suggesting that Tim17-Tim23

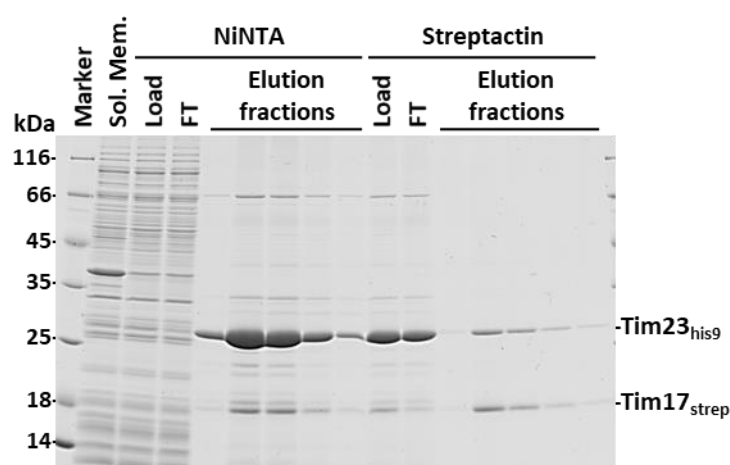


Figure 3.46 Purification of recombinant Tim17-Tim23 complex from *E. coli* membranes. The Tim17-Tim23 complex was purified via two affinity chromatography steps, using NiNTA-Agarose and Streptactin Sepharose beads, after solubilization of isolated membranes in a buffer containing Fos-choline 12. Samples were analyzed by SDS-PAGE and visualized by CBB staining. FT- Flow through.

complex formation is not as efficient as in mitochondria. Nonetheless, the final amount of the eluted complex was sufficient for further experiments.

3.3.2 Reconstitution of the recombinant Tim17-Tim23 complex in liposomes

To reconstitute, recombinant Tim17-Tim23 complex into proteoliposomes, the purified complex was mixed with the liposomes and the detergent was removed gradually from the solution (see section 2.4.8 for details). To mimic the lipid composition of the mitochondrial inner membrane, liposomes with 10% (mol/mol) cardiolipin were generated by mixing *E. coli* polar lipid extract with cardiolipin. Figure 3.47 follows the distribution of Tim17 and Tim23 during the various steps of reconstitution protocol, from the starting mix to the final proteoliposome suspension. Comparison of the band intensities in the starting mix and in the pellet after the final wash indicates that most of the core complex was reconstituted in proteoliposomes.

To test the integration of the proteins in the lipid bilayer, a carbonate extraction method was employed (section 2.4.8.1). In this assay, membranes are incubated with Na_2CO_3 solution. The high pH (11.5) extracts peripheral membrane proteins and sometimes membrane proteins with a single TM whereas integral membrane proteins with multiple TM segments cannot be extracted out of the membranes (Fujiki et al., 1982). When the purified

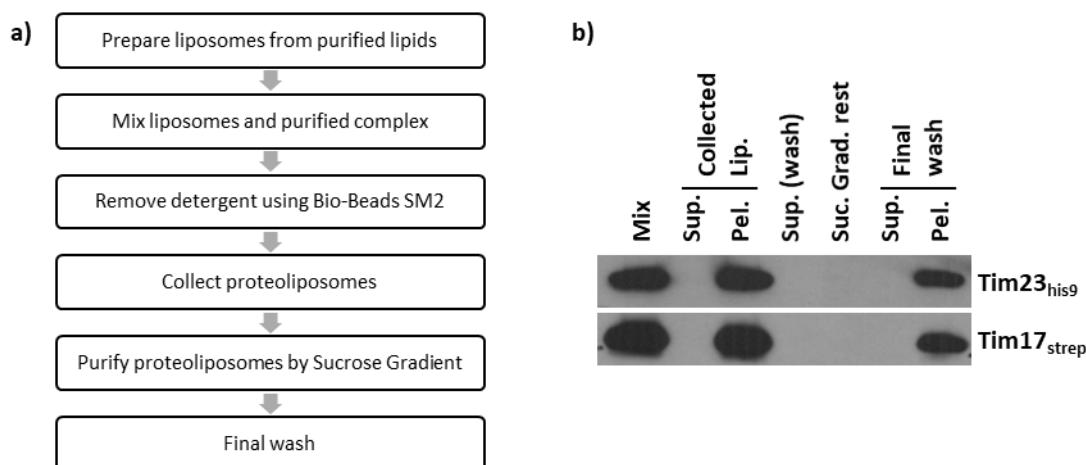


Figure 3.47 Reconstitution of the Tim17-Tim23 complex into proteoliposomes. **a)** A scheme for reconstitution protocol (see section 2.4.8 for details). **b)** Liposomes and the purified recombinant Tim17-Tim23 complex were mixed 1:1 (V:V) ratio and FC12 was removed gradually for assembly of the proteoliposomes. Proteoliposomes were collected by ultracentrifugation, washed once and then purified by floatation through a sucrose density gradient. Floated proteoliposomes were collected and washed again. Finally, they were resuspended in Na⁺-import buffer. Suc. Grad. rest indicates the sample from the rest of floatation solution. Samples were loaded as equivalent amounts from the respective volumes. Sup.- supernatant and Pel.- Pellet.

Tim17-Tim23 complex was subjected to Na₂CO₃ extraction, the majority of Tim17 and Tim23 stayed in the supernatant. However, the Tim17-Tim23 complex reconstituted in the proteoliposomes remained in the pellet fraction after carbonate extraction (Figure 3.48), suggesting that it got integrated in the membrane during reconstitution procedures.

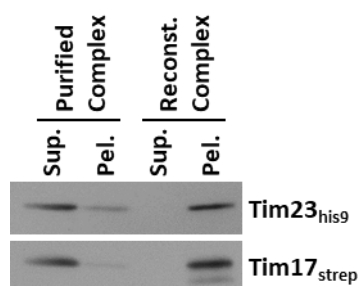


Figure 3.48 Integration of Tim17-Tim23 complex in proteoliposomes. Purified complex was subjected to Na₂CO₃ extraction before and after reconstitution to test integration of proteins in the lipid bilayer (section 2.4.8.1). Sup.- supernatant and Pel.- Pellet. * indicates degradation product of Tim17.

3.3.3 Reconstituted Tim17 and Tim23 complex can specifically recognize presequences

To test the biological activity of the reconstituted complex, binding of radiolabeled presequence containing-proteins to empty liposomes and Tim17-Tim23 proteoliposomes

was analyzed (Figure 3.49). All precursors with a presequence (Su9(1-69)DHFR, Cox4(1-25)DHFR, b₂(1-167) Δ DHFR and b₂(1-55)DHFR), were specifically bound by the proteoliposomes containing reconstituted Tim17 and Tim23. Importantly, DHFR, which does not contain a presequence, and SynB2DHFR, which contain a scrambled and therefore non-functional presequence (Allison and Schatz, 1986), did not bind to proteoliposomes. These results indicate that the recombinant Tim17-Tim23 complex reconstituted in proteoliposomes can recognize precursor proteins in a presequence-specific manner.

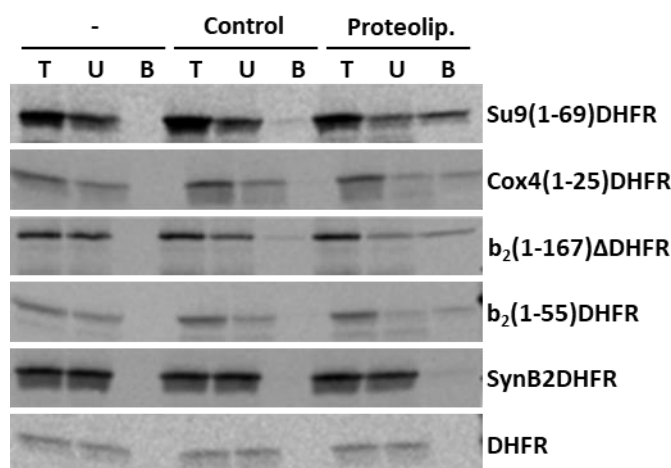


Figure 3.49 Binding of presequence-containing precursor proteins to Tim17-Tim23 proteoliposomes. Proteoliposomes containing reconstituted Tim17-Tim23 complex (Proteolip.) and empty liposomes (Control) were incubated with indicated radiolabeled proteins. Liposomes were collected by centrifugation, purified via sucrose gradient floatation and reisolated by centrifugation. Samples were analyzed by SDS-PAGE and autoradiography. “-” samples did not contain any liposomes. T- total, B- bound and U- unbound fractions. Unbound fraction is the supernatant after collection of proteoliposomes in the first centrifugation step.

3.3.4 Reconstituted proteoliposomes can generate membrane potential

The TIM23 complex requires $\Delta\Psi$ for its function. In mitochondria, $\Delta\Psi$ is generated through the activity of the respiratory chain complexes. Interestingly, protein import into mitochondria can also be driven by the valinomycin-induced K⁺ diffusion potential (Pfanner and Neupert, 1985). Hence, to generate $\Delta\Psi$ across lipid bilayer of proteoliposomes, the proteoliposomes were prepared in a buffer containing K⁺ and resuspended in a Na⁺-containing buffer. Valinomycin is an ionophore that allows passage of K⁺ ions across lipid bilayer, but not of Na⁺. Since interior of the liposomes contain K⁺ ions and exterior contain Na⁺ ions, addition of valinomycin causes the release of K⁺ from the interior volume, and thus,

makes the exterior more positive than the interior. Like with isolated mitochondria, generation of $\Delta\Psi$ in the liposomes can be monitored by DiSC₃(5) uptake (Figure 3.50) (see section 2.4.3.2 for details). Both empty liposomes as well as Tim17-Tim23 proteoliposomes generated $\Delta\Psi$. Addition of NaCl did not affect the generated $\Delta\Psi$ but addition of KCl dissipated it by abolishing the ion imbalance.

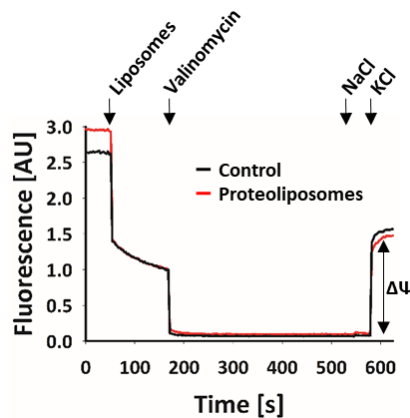


Figure 3.50 $\Delta\Psi$ measurement of liposomes. Liposomes, with or without reconstituted Tim17-Tim23 complex were added to Na⁺-import buffer containing DiSC₃(5). $\Delta\Psi$ was generated by addition of valinomycin and the kinetics of the uptake of the dye was observed at excitation and emission wavelengths 622 and 670 nm, respectively. $\Delta\Psi$ was dissipated by addition of KCl. Down arrows indicate the time point of addition of respective component. Control samples do not contain reconstituted complex. Proteoliposomes contain reconstituted Tim17-Tim23 complex.

Taken together, the presented data demonstrate that Tim17 and Tim23 can be recombinantly expressed and purified Tim23 and Tim17 as a complex. Furthermore, the complex can be reconstituted into proteoliposomes. These proteoliposomes can generate membrane potential and specifically recognize presequence-containing proteins, providing the solid basis for future import experiments.

4. DISCUSSION

4.1 IMS domain of Tim23 does more than orchestrating the IMS part of the TIM23 complex

Mitochondrial proteins, which are translated in the cytosol, use specialized translocases to reach their specific subcompartment within mitochondria. About 70% of mitochondrial proteins contain N-terminal matrix targeting signals (MTS), also called presequences, and use the TIM23 complex to reach the final place of their function within mitochondria. Therefore, understanding the molecular mechanisms of function of the TIM23 complex in protein translocation is essential for uncovering the mechanisms of mitochondrial biogenesis and diseases associated with them. In this thesis, I have dissected the channel forming subunits of the TIM23 complex, Tim23 and Tim17, *in vivo* to gain a better mechanistic understanding of function of the complex.

Tim23 is the central subunit of the TIM23 complex and consists of an N-terminal mostly unstructured domain in the IMS and a C-terminal domain embedded in the IM. While the TM segments anchor the protein in the IM with matrix and IMS exposed loops, the IMS domain can extend to the cytosol spanning the OM (Donzeau et al., 2000). Thus, the topology of Tim23 is unique among mitochondrial proteins – it is exposed to all four subcompartments of mitochondria and to the cytosol. Previous experiments showed that the exposure of Tim23 on the cytosolic surface of mitochondria is a dynamic process that depends on Tim23 interaction with Tim50, the dynamics of the TOM complex and the translocation activity of the TIM23 complex (Gevorkyan-Airapetov et al., 2009; Popov-Celeketic et al., 2008; Tamura et al., 2009; Waagemann et al., 2015). Furthermore, the IMS domain of Tim23 was shown to interact with many components of the TOM and TIM23 complexes, summarized in Figure 3.3, and many of the proposed interaction sites overlapped with each other. These results suggest that the IMS domain of Tim23 needs to alter its conformation to provide efficient transfer of precursor proteins. Multiple sequence alignment of Tim23 showed that the IMS domain is not highly conserved, especially over the first 50 residues. All the characteristics of the domain of Tim23 in the IMS thus reflect properties of classical intrinsically disordered

proteins (IDPs). They do not form a defined and properly folded 3D structure and they can adapt their structure for different binding states (Kim et al., 2008). Here, an *in vivo* mutational approach combined with biochemical experiments was used to study the function of the IMS domain of Tim23. Presented data demonstrate that even though a large portion of this domain is not essential for cell viability, different regions of the IMS domain of Tim23 have different functions and, more importantly, that this domain not only acts as a hub in the IMS for initiation of the import process but also regulates later stages of the import process (Figure 4.1).

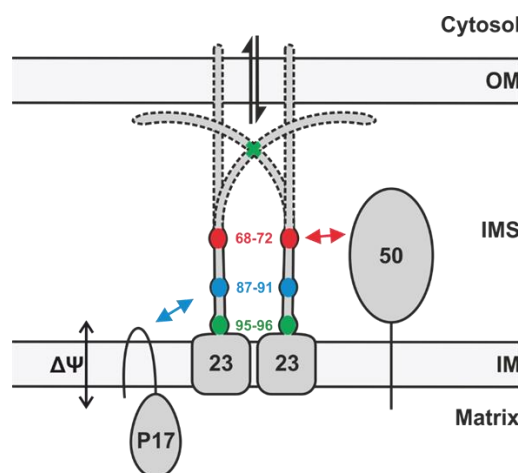


Figure 4.1 Three distinct functional regions of the IMS domain of Tim23 identified in this thesis. The region between residues 68-72 (red) is essential for Tim50 binding while the region between residues 87-91 (blue) interacts with Pam17 and the negative residues at positions 95 and 96 (green) affects the conformation of the IMS domain of Tim23.

My *in vivo* analysis could not confirm the involvement of the first 10 residues of Tim23 in interaction with Tim21 and Tim50 that was previously suggested based on an NMR analysis (Bajaj et al., 2014a). Deletion of the first 10 residues of Tim23 neither impaired growth of yeast cells nor affected Tim23 interaction with Tim21 and Tim50. Since NMR measurements require highly concentrated purified proteins, it is possible that non-physiological interactions may have been detected. However, it is also possible that the importance of the first 10 residues for the interactions may be overlooked *in vivo* due to the stabilizing effects of other interaction points between the proteins. Still, it is clear that this segment of Tim23 is not essential for the interaction with either Tim21 or Tim50, though its involvement in the interaction cannot be excluded.

The analysis of N-terminally truncated mutants of Tim23 revealed different effects on the stability of the protein. Truncating the first 30 residues of Tim23 resulted in a temperature sensitive growth phenotype with highly reduced protein amounts within mitochondria. Interestingly, further truncations did not result in such a defect, even though they also contain the deletion of the first 30 residues. The 'N-end rule', which determines the half-life of proteins depending on their N-terminal amino acid residues adjacent to the initiator methionine (Bachmair et al., 1986), may be a possible explanation for enhanced degradation of Tim23 Δ 30. This rule works differently in different organisms and, in mitochondria, prokaryotic rules may apply (Tobias et al., 1991; Vogtle et al., 2009). According to the 'N-end rule', WT protein, Δ 10, Δ 20, Δ 40 and Δ 50 are predicted to be stable because they have Ser, Thr, Gln, Ile and His, respectively, adjacent to the initiator methionine. On the other hand, Δ 24 and Δ 30 have Lys and Leu, respectively, and these residues are considered as destabilizing signals, marking the proteins for faster degradation either in the cytosol before their translocation or in mitochondria after complete translocation. However, lysine residue for Δ 24, in this case, did not cause a growth phenotype as defective as Δ 30, but only slightly. Thus, the growth phenotype observed for these specific mutants could be caused by destabilization of the respective Tim23 variants according to the N-end rule.

The essential interaction of the IMS domain of Tim23 is with the major receptor of the TIM23 complex – subunit Tim50. Although this interaction was previously studied in some detail (Geissler et al., 2002; Gevorgyan-Airapetov et al., 2009; Mokranjac et al., 2009; Tamura et al., 2009; Yamamoto et al., 2002), alanine scanning mutagenesis performed in this work showed that the binding site for Tim50 on Tim23 is larger than previously proposed (Tyr70 and Leu71). Using the genetic approach, we found that the more residues in this region were mutated, the stronger the growth phenotype became, with V68A5 having the most severe growth defect. Especially the three conserved residues, Glu69, Tyr70 and Leu71, seem to be the important ones for Tim50 binding (Figure 3.13). However, unlike Tyr70 and Leu71 (Gevorgyan-Airapetov et al., 2009), E69A did not show complete impairment of Tim50 binding. It seems that the interaction between Tim23 and Tim50 is mainly mediated through hydrophobic interactions and partly through negatively charged Glu69.

The alanine scanning mutagenesis screen also revealed novel interactions of Tim23 in the IMS. A particularly interesting one is a direct interaction with Pam17. Though initially identified as a component of the import motor (van der Laan et al., 2005), subsequent experiments showed that Pam17, structurally and functionally, interacts with the Tim17-Tim23 core of the TIM23 complex (Hutu et al., 2008; Popov-Celeketi et al., 2011; Schilke et al., 2012; Ting et al., 2014). Still, all so far known direct interactions of Pam17 with Tim17 and Tim23 were mapped to the matrix, where the major part of Pam17 resides (Hutu et al., 2008; Popov-Celeketi et al., 2008; Ting et al., 2014). Here, a direct interaction of Pam17 with Tim23 at the IMS side of the IM membrane was identified for the first time. Even though the exact role of Pam17 is still not clear, the results presented here suggest another level of regulation of function of the TIM23 complex mediated by the IMS-exposed domain of Tim23 through Pam17. Interestingly, Schendzielorz et al. (2017) recently showed that Pam17 might have a role in the $\Delta\Psi$ -dependent import of mature parts of translocating precursors. iMTS-Ls (internal MTS-like signals), which share common features with presequences, may be responsible for this phenomenon (Backes et al., 2018). Import experiments performed here with mitochondria isolated from the 87A5 mutant recapitulated the observations made by Schendzielorz et al. (2017), suggesting that the effects of Pam17 may be initiated by Tim23 in the IMS. Taken together, the IMS domain of Tim23 seems to have an active role in regulating $\Delta\Psi$ -dependent and import motor-dependent steps of the import process by communicating with the subunits in the matrix side of the IM through Pam17 interaction. It is tempting to speculate that the conformational changes of the TIM23 complex occurring at different stages of the import process need to be reset or catalyzed depending on the requirements for translocation of specific regions of the incoming polypeptide chains.

Lastly, another mutant identified in the screen encompasses two conserved negatively charged residues, Asp95 and Asp96. Although sequence-wise, *D95A2* and *D95K2* mutants map very close to the 87A5 mutant, they showed clearly different characteristics. Crosslinking and import experiments showed that the interaction with Pam17 was largely unaffected in *D95A2* and *D95K2* mutants. In contrast, the crosslinked dimers were reduced dramatically. It seems that the mutation of the negatively charged residues affects the conformation of the

complex without making major changes in the composition of the complex, at least within the monomers. Another intriguing possibility is that the alteration of the negative charges may affect the interaction of Tim23 with positively charged presequences. It has been hypothesized that positively charged presequences sequentially bind to the acidic patches on the subunits of the TOM and TIM23 complexes on their way into the mitochondrial matrix (Komiya et al., 1998). Since Asp95 and Asp96 are predicted to be at the entrance of the translocation channel of the TIM23 complex, they may have a role in properly directing the precursor proteins into the channel. Reverting the charges may cause a repulsive effect on the presequences at the entrance. It will be interesting to see in the future whether the two residues have a direct role in recognition and binding of presequences and guiding them to the translocation channel in the inner membrane.

4.2 Last two TMs of Tim23 are required for stabilization of Tim17-Tim23 interaction

The translocation channel of the TIM23 complex is likely formed by the IM embedded domains of both Tim23 and Tim17. Both proteins belong to the same protein family and contain four predicted TM segments. It has been shown before that TM1 and TM2 of Tim23 are essential for the formation of the aqueous channel (Alder et al., 2008a) whereas TM3 and TM4 were dispensable for the function of the protein (Pareek et al., 2013). The analysis presented here confirmed that the last two TMs of Tim23 are indeed dispensable for viability of yeast cells. However, the C-terminal truncation mutants described here showed strong growth defects, in contrast to the previous report (Pareek et al., 2013). Moreover, in the same publication, protein levels of Tim23 and the interaction between Tim17 and Tim23 were not affected by the absence of last two TMs of Tim23. Different genetic backgrounds of the parental yeast strains could be a possible explanation for the differences in growth phenotypes and expression levels of Tim23 observed in the two studies. Recently, it has also been revealed that certain motifs, called C-degrons, at the C-terminus of proteins determine half-life of proteins in mammalian cells (Koren et al., 2018). Even though such motifs await to be explored in yeast, C-terminal degron of the mouse ornithine decarboxylase was shown to

destabilize proteins also in yeast when it was added to the C-terminus of proteins (Hoyt et al., 2003), showing conservation of the mechanism. Therefore, it is tempting to speculate that a change in the C-terminus of Tim23 may alter the stability of the C-terminally truncated versions of Tim23, resulting in reduced level of the mutant protein observed in this thesis. Still, on the molecular level, the interaction between Tim23 and Tim17 should have been affected in the same way in both studies. Whether the different buffer compositions used for immunoprecipitation may be the reason behind observed differences remains currently unclear. Taken together, TM3 and TM4 of Tim23 are not essential for the function of the protein and thereby for cell viability but they considerably contribute to the stabilization of the Tim17-Tim23 interaction. However, how this contribution takes place – via direct contact or allosteric effects – awaits a high-resolution structure of the TIM23 complex.

4.3 Tim17 has a role in coupling the import motor complex to the translocation channel of the TIM23 complex

Despite belonging to the same protein family and sharing a considerable sequence homology in the transmembrane segments, Tim17 and Tim23 cannot substitute for each other (Ryan et al., 1994). This finding is further supported by the result reported here that, unlike in Tim23, all TMs of Tim17 are essential for cell viability. Our data, presented here and in Demishtein-Zohary et al. (2017), suggests that, like in Tim23, the first two TMs of Tim17 are involved in Tim17-Tim23 interaction. It is tempting to speculate that TM1 and TM2 of Tim17 also contribute to the formation of the translocation channel of the TIM23 complex, however, there is currently no experimental evidence available to support this notion. Interestingly, the experiments shown here demonstrate that the last two TMs of Tim17, and the loop between them in particular, play an essential role in recruiting the import motor to the translocation channel. Using a combination of alanine scanning mutagenesis and *in vivo* site-specific photocrosslinking, a conserved arginine residue at position 105, in the matrix-exposed loop of Tim17, was identified as a direct interaction point between Tim17 and Tim44. This result is in line with the previous finding of our group that the C-terminal domain of Tim44 directly binds to Tim17 (Banerjee et al., 2015). Furthermore, subsequently published

report identified surface exposed residues on the C-terminal domain of Tim44 that are in direct contact with Tim17 and also Tim23 (Ting et al., 2017). Taken together, the data presented here support a model in which Tim17 recruits the import motor complex to the exit of translocating channel by interacting with Tim23 through its two TMs and with Tim44 through the loop between its last two TMs (Figure 4.2).

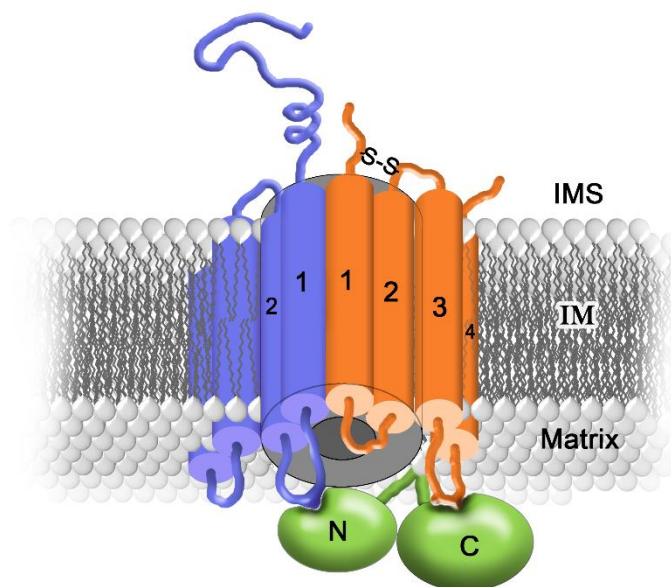


Figure 4.2 A model for the bridging role of Tim17 in recruitment of the import motor to the core channel. Tim17 (orange) interacts with Tim23 (blue) in the IM and the matrix exposed loops of both recruit Tim44 (green).

Overall, presented data in this thesis provides new molecular insights into the structure and function of the TIM23 complex. The current model of function of the TIM23 complex suggests that the presequence containing precursor proteins are recognized in the IMS by the receptor subunits of the complex, after their emergence from the TOM complex. Then, the precursors are transferred to the translocation channel in the inner membrane by a coordinated action of the subunits in the IMS and, in a $\Delta\Psi$ -dependent step, driven through the translocation channel. At the matrix face of the channel, import motor captures incoming precursors to complete the translocation process using the energy from ATP. The data presented here update this model in the way that novel interaction of the IMS-exposed domain of Tim23 were identified, revealing a role of this domain as a hub that not only regulates initial recognition of presequences in the IMS but also contributes to later stages of protein translocation across inner membrane through an interaction with Pam17. Also, an

essential role of Tim17 in coupling the import motor to the translocation channel was uncovered.

4.4 The Tim17-Tim23 core of the TIM23 complex can be purified recombinantly and reconstituted in proteoliposomes

Testing of any model of function of the TIM23 complex would be greatly simplified by the availability of a biochemically defined system consisting of recombinant proteins. Except for Tim17-Tim23 core, all other essential subunits of the TIM23 complex are already available in their recombinant forms (Mokranjac et al., 2006; Qian et al., 2011; Sichting et al., 2005; Weiss et al., 1999). To fill this gap, a recombinant expression and purification system of the Tim17-Tim23 core of the complex was developed here. The two proteins can indeed be co-expressed and co-purified as a complex. The complex was also successfully reconstituted in proteoliposomes, which could specifically bind presequence-containing precursors (Figure 3.49). Thus, the initial steps of the import process by the TIM23 complex were successfully reconstituted. I also showed that $\Delta\Psi$ could be generated in proteoliposomes (Figure 3.50). These experiments lay a solid foundation for the future investigations to address the channel activity of the reconstituted complex as well as the actual translocation process across and into the membrane. It is likely that incorporation of other essential subunits of the TIM23 complex into the system will be necessary to observe any translocation activity.

5. Summary

Protein import into mitochondria is an essential process for all eukaryotic cells because 99% of proteins that function in mitochondria are made in the cytosol as precursor proteins. About 70% of them are targeted to the organelle by N-terminal, positively charged presequences. The TIM23 complex is the major protein translocase of the mitochondrial inner membrane that recognizes precursor proteins with presequences, as they appear at the outlet of the TOM complex in the outer membrane, and mediates their translocation across and insertion into the inner membrane in a membrane potential- and ATP-dependent manner. This highly evolutionary conserved complex is comprised of at least 11 subunits and can be divided into three functional units - the receptor part facing the intermembrane space, the translocation channel in the inner membrane and the import motor facing the matrix. This study provides new insights into the structure and function of Tim23 and Tim17, the inner membrane-embedded subunits of the translocation channel of the TIM23 complex.

Both Tim23 and Tim17 contain four predicted transmembrane segments in the inner membrane, which likely together form the translocation channel of the TIM23 complex. Tim23 has an additional, intrinsically disordered domain exposed to the intermembrane space. *In vivo* dissection of the intermembrane space-exposed domain of Tim23 performed here identified its novel interaction partners and crystallized this domain as an organizational hub that not only coordinates transfer of proteins between TOM and TIM23 complexes but also regulates later stages of protein translocation across mitochondrial inner membrane. The analysis of membrane embedded segments of Tim23 revealed that the last two transmembrane segments, though not essential for cell viability, contribute to the stability of Tim17-Tim23 interaction and thus to the import process. On the other hand, the first two transmembrane segments of Tim17 are required for Tim17-Tim23 interaction and the last two, and in particular, the matrix exposed loop between them, for recruitment of the import motor. Thus, the data suggest an essential role of Tim17 in transferring the precursor proteins from the translocation channel in the inner membrane to the import motor during their translocation into mitochondria.

In addition to the *in vivo* analyses, a system for recombinant expression and purification of Tim17 and Tim23 was established. The purified Tim17-Tim23 complex was reconstituted in proteoliposomes, which specifically recognized presequence-containing precursor proteins. Thus, a solid basis has been laid for future experiments towards establishing a simple, robust and biochemically defined system needed to obtain a mechanistic understanding of protein translocation across mitochondrial inner membrane and biogenesis of mitochondria.

6. Zusammenfassung

Proteintransport in Mitochondrien ist ein essentieller Prozess aller eukaryotischer Zellen, da 99% der Proteine, die ihre Funktionen in Mitochondrien entfalten, im Zytosol als Vorläuferproteine synthetisiert werden. Rund 70% dieser Proteine werden durch N-terminale, positiv geladene Präsequenzen zum Organell dirigiert. Der TIM23 Komplex ist die Hauptproteintranslokase der mitochondrialen Innenmembran. Er erkennt Vorläuferproteine mit Präsequenzen, nachdem diese durch den TOM Komplex die mitochondriale Außenmembran durchquert haben, und vermittelt die membranpotential- und ATP-abhängige Translokation durch, sowie die Insertion in die Innenmembran. Dieser evolutionär hoch konservierte Komplex besteht aus mindestens 11 Komponenten und kann in drei funktionelle Einheiten eingeteilt werden: der Rezeptorteil, welcher dem Intermembranraum zugewandt ist, der Translokationskanal in der Innenmembran und der Importmotor in der Matrix. In dieser Arbeit werden neue Erkenntnisse über die Struktur und Funktion von Tim23 und Tim17, die Untereinheiten des Translokationskanals des TIM23 Komplexes in der Innenmembran, beleuchtet.

Sowohl Tim23 als auch Tim17 besitzen vier vorhergesagte Transmembransegmente in der mitochondrialen Innenmembran, welche vermutlich den Translokationskanal des TIM23 Komplexes bilden. Tim23 verfügt zusätzlich über eine intrinsisch ungeordnete Domäne, die dem Intermembranraum zugewandt ist. Mittels *in vivo* Analyse der Tim23-Domäne im Intermembranraum konnten neue Interaktionspartner identifiziert werden. Dies bekräftigt die Rolle von Tim23 als organisatorisches Element im Intermembranraum, welches sowohl den Proteintransfer zwischen TOM und TIM23 Komplexen koordiniert als auch spätere Phasen der Proteintranslokation durch die mitochondriale Innenmembran reguliert. Die Analyse der in der Membran integrierten Tim23 Segmente zeigte, dass die beiden letzten Transmembransegmente zur Stabilität der Tim17-Tim23 Interaktion sowie zum Proteintransport beitragen, obwohl diese für das Überleben der Zelle nicht essentiell sind. Dahingegen werden die beiden ersten Transmembransegmente von Tim17 für die Interaktion zwischen Tim17 und Tim23 benötigt. Die beiden Letzten, vor allem der zur Matrix gewandte

Loop dazwischen, vermitteln die Rekrutierung des Importmotors. Diese Ergebnisse deuten auf eine essentielle Rolle von Tim17 beim Transport von Vorläuferproteinen vom Translokationskanal in der Innenmembran bis zum Importmotor in der Matrix während der Proteintranslokation in Mitochondrien.

Zusätzlich zur *in vivo* Analyse wurde eine Methode zur rekombinanten Expression und Aufreinigung von Tim17 und Tim23 etabliert. Der aufgereinigte Tim17-Tim23 Komplex wurde in Proteoliposomen rekonstituiert, welcher spezifisch Vorläuferproteine mit Präsequenzen erkannte. Dadurch konnte eine solide Grundlage für zukünftige Experimente gelegt werden, um ein einfaches und biochemisch definiertes System zu entwickeln, dass eine mechanistische Untersuchung der Proteintranslokation durch die mitochondriale Innenmembran und Biogenese der Mitochondrien ermöglicht.

7. REFERENCES

- Ahting, U., Floss, T., Uez, N., Schneider-Lohmar, I., Becker, L., Kling, E., Iuso, A., Bender, A., de Angelis, M.H., Gailus-Durner, V., *et al.* (2009). Neurological phenotype and reduced lifespan in heterozygous Tim23 knockout mice, the first mouse model of defective mitochondrial import. *Biochim Biophys Acta* 1787, 371-376.
- Alder, N.N., Jensen, R.E., and Johnson, A.E. (2008a). Fluorescence mapping of mitochondrial TIM23 complex reveals a water-facing, substrate-interacting helix surface. *Cell* 134, 439-450.
- Alder, N.N., Sutherland, J., Buhning, A.I., Jensen, R.E., and Johnson, A.E. (2008b). Quaternary structure of the mitochondrial TIM23 complex reveals dynamic association between Tim23p and other subunits. *Mol Biol Cell* 19, 159-170.
- Allison, D.S., and Schatz, G. (1986). Artificial mitochondrial presequences. *Proc Natl Acad Sci U S A* 83, 9011-9015.
- Araiso, Y., Tsutsumi, A., Qiu, J., Imai, K., Shiota, T., Song, J., Lindau, C., Wenz, L.S., Sakaue, H., Yunoki, K., *et al.* (2019). Structure of the mitochondrial import gate reveals distinct preprotein paths. *Nature* 575, 395-401.
- Bachmair, A., Finley, D., and Varshavsky, A. (1986). In vivo half-life of a protein is a function of its amino-terminal residue. *Science* 234, 179-186.
- Backes, S., Hess, S., Boos, F., Woellhaf, M.W., Godel, S., Jung, M., Muhlhaus, T., and Herrmann, J.M. (2018). Tom70 enhances mitochondrial preprotein import efficiency by binding to internal targeting sequences. *J Cell Biol* 217, 1369-1382.
- Bajaj, R., Jaremko, L., Jaremko, M., Becker, S., and Zweckstetter, M. (2014a). Molecular basis of the dynamic structure of the TIM23 complex in the mitochondrial intermembrane space. *Structure* 22, 1501-1511.
- Bajaj, R., Munari, F., Becker, S., and Zweckstetter, M. (2014b). Interaction of the intermembrane space domain of Tim23 protein with mitochondrial membranes. *J Biol Chem* 289, 34620-34626.
- Banerjee, R., Gladkova, C., Mapa, K., Witte, G., and Mokranjac, D. (2015). Protein translocation channel of mitochondrial inner membrane and matrix-exposed import motor communicate via two-domain coupling protein. *Elife* 4, e11897.
- Banerjee, R., Gunsell, U., and Mokranjac, D. (2017). Chemical Crosslinking in Intact Mitochondria. *Methods Mol Biol* 1567, 139-154.
- Bauer, M.F., Sirrenberg, C., Neupert, W., and Brunner, M. (1996). Role of Tim23 as voltage sensor and presequence receptor in protein import into mitochondria. *Cell* 87, 33-41.
- Blobel, G. (1980). Intracellular protein topogenesis. *Proc Natl Acad Sci U S A* 77, 1496-1500.
- Bohnert, M., Rehling, P., Guiard, B., Herrmann, J.M., Pfanner, N., and van der Laan, M. (2010). Cooperation of stop-transfer and conservative sorting mechanisms in mitochondrial protein transport. *Curr Biol* 20, 1227-1232.
- Bonora, E., Evangelisti, C., Bonichon, F., Tallini, G., and Romeo, G. (2006). Novel germline variants identified in the inner mitochondrial membrane transporter TIMM44 and their role in predisposition to oncocytic thyroid carcinomas. *Br J Cancer* 95, 1529-1536.
- Bradford, M.M. (1976). A rapid and sensitive method for the quantitation of microgram quantities of protein utilizing the principle of protein-dye binding. *Anal Biochem* 72, 248-254.

- Burbulla, L.F., Schelling, C., Kato, H., Rapaport, D., Voitalla, D., Schiesling, C., Schulte, C., Sharma, M., Illig, T., Bauer, P., *et al.* (2010). Dissecting the role of the mitochondrial chaperone mortalin in Parkinson's disease: functional impact of disease-related variants on mitochondrial homeostasis. *Hum Mol Genet* 19, 4437-4452.
- Casadaban, M.J., and Cohen, S.N. (1980). Analysis of gene control signals by DNA fusion and cloning in *Escherichia coli*. *J Mol Biol* 138, 179-207.
- Chacinska, A., Koehler, C.M., Milenkovic, D., Lithgow, T., and Pfanner, N. (2009). Importing mitochondrial proteins: machineries and mechanisms. *Cell* 138, 628-644.
- Chacinska, A., Lind, M., Frazier, A.E., Dudek, J., Meisinger, C., Geissler, A., Sickmann, A., Meyer, H.E., Truscott, K.N., Guiard, B., *et al.* (2005). Mitochondrial presequence translocase: switching between TOM tethering and motor recruitment involves Tim21 and Tim17. *Cell* 120, 817-829.
- Chen, S., Schultz, P.G., and Brock, A. (2007). An improved system for the generation and analysis of mutant proteins containing unnatural amino acids in *Saccharomyces cerevisiae*. *J Mol Biol* 371, 112-122.
- D'Silva, P.D., Schilke, B., Walter, W., Andrew, A., and Craig, E.A. (2003). J protein cochaperone of the mitochondrial inner membrane required for protein import into the mitochondrial matrix. *Proc Natl Acad Sci U S A* 100, 13839-13844.
- D'Silva, P.R., Schilke, B., Walter, W., and Craig, E.A. (2005). Role of Pam16's degenerate J domain in protein import across the mitochondrial inner membrane. *Proc Natl Acad Sci U S A* 102, 12419-12424.
- Davey, K.M., Parboosingh, J.S., McLeod, D.R., Chan, A., Casey, R., Ferreira, P., Snyder, F.F., Bridge, P.J., and Bernier, F.P. (2006). Mutation of DNAJC19, a human homologue of yeast inner mitochondrial membrane co-chaperones, causes DCMA syndrome, a novel autosomal recessive Barth syndrome-like condition. *J Med Genet* 43, 385-393.
- Davis, A.J., Ryan, K.R., and Jensen, R.E. (1998). Tim23p contains separate and distinct signals for targeting to mitochondria and insertion into the inner membrane. *Mol Biol Cell* 9, 2577-2593.
- Dayan, D., Bandel, M., Gunsel, U., Nussbaum, I., Prag, G., Mokranjac, D., Neupert, W., and Azem, A. (2019). A mutagenesis analysis of Tim50, the major receptor of the TIM23 complex, identifies regions that affect its interaction with Tim23. *Sci Rep* 9, 2012.
- de la Cruz, L., Bajaj, R., Becker, S., and Zweckstetter, M. (2010). The intermembrane space domain of Tim23 is intrinsically disordered with a distinct binding region for presequences. *Protein Sci* 19, 2045-2054.
- Dekker, P.J., Martin, F., Maarse, A.C., Bomer, U., Muller, H., Guiard, B., Meijer, M., Rassow, J., and Pfanner, N. (1997). The Tim core complex defines the number of mitochondrial translocation contact sites and can hold arrested preproteins in the absence of matrix Hsp70-Tim44. *Embo j* 16, 5408-5419.
- Demishtein-Zohary, K., and Azem, A. (2017). The TIM23 mitochondrial protein import complex: function and dysfunction. *Cell Tissue Res* 367, 33-41.
- Demishtein-Zohary, K., Gunsel, U., Marom, M., Banerjee, R., Neupert, W., Azem, A., and Mokranjac, D. (2017). Role of Tim17 in coupling the import motor to the translocation channel of the mitochondrial presequence translocase. *Elife* 6.

- Demishtein-Zohary, K., Marom, M., Neupert, W., Mokranjac, D., and Azem, A. (2015). GxxxG motifs hold the TIM23 complex together. *FEBS J* 282, 2178-2186.
- Donzeau, M., Kaldi, K., Adam, A., Paschen, S., Wanner, G., Guiard, B., Bauer, M.F., Neupert, W., and Brunner, M. (2000). Tim23 links the inner and outer mitochondrial membranes. *Cell* 101, 401-412.
- Endo, T., Yamano, K., and Kawano, S. (2011). Structural insight into the mitochondrial protein import system. *Biochim. Biophys. Acta-Biomembr.* 1808, 955-970.
- Folsch, H., Guiard, B., Neupert, W., and Stuart, R.A. (1996). Internal targeting signal of the BCS1 protein: a novel mechanism of import into mitochondria. *EMBO J* 15, 479-487.
- Frazier, A.E., Dudek, J., Guiard, B., Voos, W., Li, Y., Lind, M., Meisinger, C., Geissler, A., Sickmann, A., Meyer, H.E., *et al.* (2004). Pam16 has an essential role in the mitochondrial protein import motor. *Nat Struct Mol Biol* 11, 226-233.
- Fujiki, Y., Hubbard, A.L., Fowler, S., and Lazarow, P.B. (1982). Isolation of intracellular membranes by means of sodium carbonate treatment: application to endoplasmic reticulum. *J Cell Biol* 93, 97-102.
- Gao, S.P., Sun, H.F., Jiang, H.L., Li, L.D., Hu, X., Xu, X.E., and Jin, W. (2016). Loss of TIM50 suppresses proliferation and induces apoptosis in breast cancer. *Tumour Biol* 37, 1279-1287.
- Geissler, A., Chacinska, A., Truscott, K.N., Wiedemann, N., Brandner, K., Sickmann, A., Meyer, H.E., Meisinger, C., Pfanner, N., and Rehling, P. (2002). The mitochondrial presequence translocase: an essential role of Tim50 in directing preproteins to the import channel. *Cell* 111, 507-518.
- Gevorkyan-Airapetov, L., Zohary, K., Popov-Celeketic, D., Mapa, K., Hell, K., Neupert, W., Azem, A., and Mokranjac, D. (2009). Interaction of Tim23 with Tim50 is essential for protein translocation by the mitochondrial TIM23 complex. *J Biol Chem* 284, 4865-4872.
- Gunsel, U., Paz, E., Gupta, R., Mathes, I., Azem, A., and Mokranjac, D. (2020). InVivo Dissection of the Intrinsically Disordered Receptor Domain of Tim23. *J Mol Biol* 432, 3326-3337.
- Guo, Y., Cheong, N., Zhang, Z., De Rose, R., Deng, Y., Farber, S.A., Fernandes-Alnemri, T., and Alnemri, E.S. (2004). Tim50, a component of the mitochondrial translocator, regulates mitochondrial integrity and cell death. *J Biol Chem* 279, 24813-24825.
- Hansen, K.G., and Herrmann, J.M. (2019). Transport of Proteins into Mitochondria. *Protein J* 38, 330-342.
- Hell, K., Herrmann, J.M., Pratje, E., Neupert, W., and Stuart, R.A. (1998). Oxa1p, an essential component of the N-tail protein export machinery in mitochondria. In *Proc Natl Acad Sci U S A*, pp. 2250-2255.
- Herzig, S., and Shaw, R.J. (2018). AMPK: guardian of metabolism and mitochondrial homeostasis. *Nat Rev Mol Cell Biol* 19, 121-135.
- Hoyt, M.A., Zhang, M., and Coffino, P. (2003). Ubiquitin-independent mechanisms of mouse ornithine decarboxylase degradation are conserved between mammalian and fungal cells. *J Biol Chem* 278, 12135-12143.
- Hutu, D.P., Guiard, B., Chacinska, A., Becker, D., Pfanner, N., Rehling, P., and van der Laan, M. (2008). Mitochondrial protein import motor: differential role of Tim44 in the recruitment of Pam17 and J-complex to the presequence translocase. *Mol Biol Cell* 19, 2642-2649.

- Ieva, R., Schrempp, S.G., Opalinski, L., Wollweber, F., Hoss, P., Heisswolf, A.K., Gebert, M., Zhang, Y., Guiard, B., Rospert, S., *et al.* (2014). Mgr2 functions as lateral gatekeeper for preprotein sorting in the mitochondrial inner membrane. *Mol Cell* 56, 641-652.
- Josyula, R., Jin, Z., Fu, Z., and Sha, B. (2006). Crystal structure of yeast mitochondrial peripheral membrane protein Tim44p C-terminal domain. *J Mol Biol* 359, 798-804.
- Jubinsky, P.T., Short, M.K., Mutema, G., Morris, R.E., Ciraolo, G.M., and Li, M. (2005). Magmas expression in neoplastic human prostate. *J Mol Histol* 36, 69-75.
- Kang, Y., Fielden, L.F., and Stojanovski, D. (2018). Mitochondrial protein transport in health and disease. *Semin Cell Dev Biol* 76, 142-153.
- Kim, P.M., Sboner, A., Xia, Y., and Gerstein, M. (2008). The role of disorder in interaction networks: a structural analysis. *Mol Syst Biol* 4, 179.
- Komiya, T., Rospert, S., Koehler, C., Looser, R., Schatz, G., and Mihara, K. (1998). Interaction of mitochondrial targeting signals with acidic receptor domains along the protein import pathway: evidence for the 'acid chain' hypothesis. *EMBO J* 17, 3886-3898.
- Koren, I., Timms, R.T., Kula, T., Xu, Q., Li, M.Z., and Elledge, S.J. (2018). The Eukaryotic Proteome Is Shaped by E3 Ubiquitin Ligases Targeting C-Terminal Degrons. *Cell* 173, 1622-1635.e1614.
- Kozany, C., Mokranjac, D., Sichting, M., Neupert, W., and Hell, K. (2004). The J domain-related cochaperone Tim16 is a constituent of the mitochondrial TIM23 preprotein translocase. *Nat Struct Mol Biol* 11, 234-241.
- Laemmli, U.K. (1970). Cleavage of structural proteins during the assembly of the head of bacteriophage T4. *Nature* 227, 680-685.
- Li, Y., Dudek, J., Guiard, B., Pfanner, N., Rehling, P., and Voos, W. (2004). The presequence translocase-associated protein import motor of mitochondria. Pam16 functions in an antagonistic manner to Pam18. *J Biol Chem* 279, 38047-38054.
- Lu, W.J., Lee, N.P., Kaul, S.C., Lan, F., Poon, R.T., Wadhwa, R., and Luk, J.M. (2011). Mortalin-p53 interaction in cancer cells is stress dependent and constitutes a selective target for cancer therapy. *Cell Death Differ* 18, 1046-1056.
- Lytovchenko, O., Melin, J., Schulz, C., Kilisch, M., Hutu, D.P., and Rehling, P. (2013). Signal recognition initiates reorganization of the presequence translocase during protein import. *EMBO J* 32, 886-898.
- Malhotra, K., Modak, A., Nangia, S., Daman, T.H., Gunsel, U., Robinson, V.L., Mokranjac, D., May, E.R., and Alder, N.N. (2017). Cardiolipin mediates membrane and channel interactions of the mitochondrial TIM23 protein import complex receptor Tim50. *Sci Adv* 3, e1700532.
- Malhotra, K., Sathappa, M., Landin, J.S., Johnson, A.E., and Alder, N.N. (2013). Structural changes in the mitochondrial Tim23 channel are coupled to the proton-motive force. *Nat Struct Mol Biol* 20, 965-972.
- Marom, M., Dayan, D., Demishtein-Zohary, K., Mokranjac, D., Neupert, W., and Azem, A. (2011). Direct interaction of mitochondrial targeting presequences with purified components of the TIM23 protein complex. *J Biol Chem* 286, 43809-43815.
- Martinez-Caballero, S., Grigoriev, S.M., Herrmann, J.M., Campo, M.L., and Kinnally, K.W. (2007). Tim17p regulates the twin pore structure and voltage gating of the mitochondrial protein import complex TIM23. *J Biol Chem* 282, 3584-3593.

- Mehawej, C., Delahodde, A., Legeai-Mallet, L., Delague, V., Kaci, N., Desvignes, J.P., Kibar, Z., Capo-Chichi, J.M., Chouery, E., Munnich, A., *et al.* (2014). The impairment of MAGMAS function in human is responsible for a severe skeletal dysplasia. *PLoS Genet* **10**, e1004311.
- Meier, S., Neupert, W., and Herrmann, J.M. (2005a). Conserved N-terminal negative charges in the Tim17 subunit of the TIM23 translocase play a critical role in the import of preproteins into mitochondria. *J Biol Chem* **280**, 7777-7785.
- Meier, S., Neupert, W., and Herrmann, J.M. (2005b). Proline residues of transmembrane domains determine the sorting of inner membrane proteins in mitochondria. *J Cell Biol* **170**, 881-888.
- Meinecke, M., Wagner, R., Kovermann, P., Guiard, B., Mick, D.U., Hutu, D.P., Voos, W., Truscott, K.N., Chacinska, A., Pfanner, N., *et al.* (2006). Tim50 maintains the permeability barrier of the mitochondrial inner membrane. *Science* **312**, 1523-1526.
- Melton, D.A., Krieg, P.A., Rebagliati, M.R., Maniatis, T., Zinn, K., and Green, M.R. (1984). Efficient in vitro synthesis of biologically active RNA and RNA hybridization probes from plasmids containing a bacteriophage SP6 promoter. *Nucleic Acids Res* **12**, 7035-7056.
- Miroux, B., and Walker, J.E. (1996). Over-production of proteins in *Escherichia coli*: mutant hosts that allow synthesis of some membrane proteins and globular proteins at high levels. *J Mol Biol* **260**, 289-298.
- Mokranjac, D., Bourenkov, G., Hell, K., Neupert, W., and Groll, M. (2006). Structure and function of Tim14 and Tim16, the J and J-like components of the mitochondrial protein import motor. *EMBO J* **25**, 4675-4685.
- Mokranjac, D., and Neupert, W. (2009). Thirty years of protein translocation into mitochondria: Unexpectedly complex and still puzzling. *Biochim. Biophys. Acta-Mol. Cell Res.* **1793**, 33-41.
- Mokranjac, D., Paschen, S.A., Kozany, C., Prokisch, H., Hoppins, S.C., Nargang, F.E., Neupert, W., and Hell, K. (2003a). Tim50, a novel component of the TIM23 preprotein translocase of mitochondria. *EMBO J* **22**, 816-825.
- Mokranjac, D., Popov-Celeketic, D., Hell, K., and Neupert, W. (2005a). Role of Tim21 in mitochondrial translocation contact sites. *J Biol Chem* **280**, 23437-23440.
- Mokranjac, D., Sichting, M., Neupert, W., and Hell, K. (2003b). Tim14, a novel key component of the import motor of the TIM23 protein translocase of mitochondria. *EMBO J* **22**, 4945-4956.
- Mokranjac, D., Sichting, M., Popov-Celeketic, D., Berg, A., Hell, K., and Neupert, W. (2005b). The import motor of the yeast mitochondrial TIM23 preprotein translocase contains two different J proteins, Tim14 and Mdj2. *J Biol Chem* **280**, 31608-31614.
- Mokranjac, D., Sichting, M., Popov-Celeketic, D., Mapa, K., Gevorgyan-Airapetov, L., Zohary, K., Hell, K., Azem, A., and Neupert, W. (2009). Role of Tim50 in the transfer of precursor proteins from the outer to the inner membrane of mitochondria. *Mol Biol Cell* **20**, 1400-1407.
- Mossmann, D., Meisinger, C., and Vogtle, F.N. (2012). Processing of mitochondrial presequences. *Biochim Biophys Acta* **1819**, 1098-1106.
- Neupert, W. (2015). A perspective on transport of proteins into mitochondria: a myriad of open questions. *J Mol Biol* **427**, 1135-1158.
- Nunnari, J., and Suomalainen, A. (2012). Mitochondria: in sickness and in health. *Cell* **148**, 1145-1159.

- Pareek, G., Krishnamoorthy, V., and D'Silva, P. (2013). Molecular insights revealing interaction of Tim23 and channel subunits of presequence translocase. *Mol Cell Biol* 33, 4641-4659.
- Pelham, H.R.B., and Jackson, R.M. (1976). An efficient mRNA-dependent translation system from reticulocyte lysates. *Eur. J. Biochem.* 67, 247-256.
- Pfanner, N., and Neupert, W. (1985). Transport of proteins into mitochondria: a potassium diffusion potential is able to drive the import of ADP/ATP carrier. *Embo j* 4, 2819-2825.
- Popov-Celeketic, D., Mapa, K., Neupert, W., and Mokranjac, D. (2008). Active remodelling of the TIM23 complex during translocation of preproteins into mitochondria. *EMBO J* 27, 1469-1480.
- Popov-Celeketic, D., Waegemann, K., Mapa, K., Neupert, W., and Mokranjac, D. (2011). Role of the import motor in insertion of transmembrane segments by the mitochondrial TIM23 complex. *EMBO Rep* 12, 542-548.
- Qian, X., Gebert, M., Hopker, J., Yan, M., Li, J., Wiedemann, N., van der Laan, M., Pfanner, N., and Sha, B. (2011). Structural basis for the function of Tim50 in the mitochondrial presequence translocase. *J Mol Biol* 411, 513-519.
- Rahman, B., Kawano, S., Yunoki-Esaki, K., Anzai, T., and Endo, T. (2014). NMR analyses on the interactions of the yeast Tim50 C-terminal region with the presequence and Tim50 core domain. *FEBS Lett* 588, 678-684.
- Ramesh, A., Peleh, V., Martinez-Caballero, S., Wollweber, F., Sommer, F., van der Laan, M., Schroda, M., Alexander, R.T., Campo, M.L., and Herrmann, J.M. (2016). A disulfide bond in the TIM23 complex is crucial for voltage gating and mitochondrial protein import. *J Cell Biol* 214, 417-431.
- Reyes, A., Melchionda, L., Burlina, A., Robinson, A.J., Ghezzi, D., and Zeviani, M. (2018). Mutations in TIMM50 compromise cell survival in OxPhos-dependent metabolic conditions. *EMBO Mol Med* 10.
- Roise, D., and Schatz, G. (1988). Mitochondrial presequences. *J Biol Chem* 263, 4509-4511.
- Rosenzweig, R., Nillegoda, N.B., Mayer, M.P., and Bukau, B. (2019). The Hsp70 chaperone network. *Nat Rev Mol Cell Biol*.
- Royer-Bertrand, B., Castillo-Taucher, S., Moreno-Salinas, R., Cho, T.J., Chae, J.H., Choi, M., Kim, O.H., Dikoglu, E., Campos-Xavier, B., Girardi, E., *et al.* (2015). Mutations in the heat-shock protein A9 (HSPA9) gene cause the EVEN-PLUS syndrome of congenital malformations and skeletal dysplasia. *Sci Rep* 5, 17154.
- Ryan, K.R., Menold, M.M., Garrett, S., and Jensen, R.E. (1994). SMS1, a high-copy suppressor of the yeast mas6 mutant, encodes an essential inner membrane protein required for mitochondrial protein import. *Molecular Biology of the Cell* 5, 529-538.
- Schendzielorz, A.B., Bragoszewski, P., Naumenko, N., Gomkale, R., Schulz, C., Guiard, B., Chacinska, A., and Rehling, P. (2018). Motor recruitment to the TIM23 channel's lateral gate restricts polypeptide release into the inner membrane. *Nature Communications* 9, 4028.
- Schendzielorz, A.B., Schulz, C., Lytovchenko, O., Clancy, A., Guiard, B., Ieva, R., van der Laan, M., and Rehling, P. (2017). Two distinct membrane potential-dependent steps drive mitochondrial matrix protein translocation. *J Cell Biol* 216, 83-92.
- Schilke, B.A., Hayashi, M., and Craig, E.A. (2012). Genetic analysis of complex interactions among components of the mitochondrial import motor and translocon in *Saccharomyces cerevisiae*. *Genetics* 190, 1341-1353.

- Schiller, D., Cheng, Y.C., Liu, Q., Walter, W., and Craig, E.A. (2008). Residues of Tim44 involved in both association with the translocon of the inner mitochondrial membrane and regulation of mitochondrial Hsp70 tethering. *Mol Cell Biol* 28, 4424-4433.
- Schusdziarra, C., Blamowska, M., Azem, A., and Hell, K. (2013). Methylation-controlled J-protein MCJ acts in the import of proteins into human mitochondria. *Hum Mol Genet* 22, 1348-1357.
- Shahrour, M.A., Staretz-Chacham, O., Dayan, D., Stephen, J., Weech, A., Damseh, N., Pri Chen, H., Edvardson, S., Mazaheri, S., Saada, A., *et al.* (2017). Mitochondrial epileptic encephalopathy, 3-methylglutaconic aciduria and variable complex V deficiency associated with TIMM50 mutations. *Clin Genet* 91, 690-696.
- Shiota, T., Mabuchi, H., Tanaka-Yamano, S., Yamano, K., and Endo, T. (2011). In vivo protein-interaction mapping of a mitochondrial translocator protein Tom22 at work. *Proc Natl Acad Sci U S A* 108, 15179-15183.
- Sichting, M., Mokranjac, D., Azem, A., Neupert, W., and Hell, K. (2005). Maintenance of structure and function of mitochondrial Hsp70 chaperones requires the chaperone Hep1. *EMBO J* 24, 1046-1056.
- Sikorski, R.S., and Hieter, P. (1989). A system of shuttle vectors and yeast host strains designed for efficient manipulation of DNA in *Saccharomyces cerevisiae*. *Genetics* 122, 19-27.
- Sinha, D., Joshi, N., Chittoor, B., Samji, P., and D'Silva, P. (2010). Role of Magmas in protein transport and human mitochondria biogenesis. In *Hum Mol Genet*, pp. 1248-1262.
- Sinha, D., Srivastava, S., Krishna, L., and D'Silva, P. (2014). Unraveling the intricate organization of mammalian mitochondrial presequence translocases: existence of multiple translocases for maintenance of mitochondrial function. *Mol Cell Biol* 34, 1757-1775.
- Sinzel, M., Tan, T., Wendling, P., Kalbacher, H., Ozbalci, C., Chelius, X., Westermann, B., Brugger, B., Rapaport, D., and Dimer, K.S. (2016). Mcp3 is a novel mitochondrial outer membrane protein that follows a unique IMP-dependent biogenesis pathway. *EMBO Rep* 17, 965-981.
- Song, J., Tamura, Y., Yoshihisa, T., and Endo, T. (2014). A novel import route for an N-anchor mitochondrial outer membrane protein aided by the TIM23 complex. *EMBO Rep* 15, 670-677.
- Tamura, Y., Harada, Y., Shiota, T., Yamano, K., Watanabe, K., Yokota, M., Yamamoto, H., Sesaki, H., and Endo, T. (2009). Tim23-Tim50 pair coordinates functions of translocators and motor proteins in mitochondrial protein import. *J Cell Biol* 184, 129-141.
- Tamura, Y., Harada, Y., Yamano, K., Watanabe, K., Ishikawa, D., Ohshima, C., Nishikawa, S., Yamamoto, H., and Endo, T. (2006). Identification of Tam41 maintaining integrity of the TIM23 protein translocator complex in mitochondria. *J Cell Biol* 174, 631-637.
- Teese, M.G., and Langosch, D. (2015). Role of GxxxG Motifs in Transmembrane Domain Interactions. *Biochemistry* 54, 5125-5135.
- Ting, S.Y., Schilke, B.A., Hayashi, M., and Craig, E.A. (2014). Architecture of the TIM23 inner mitochondrial translocon and interactions with the matrix import motor. *J Biol Chem* 289, 28689-28696.
- Ting, S.Y., Yan, N.L., Schilke, B.A., and Craig, E.A. (2017). Dual interaction of scaffold protein Tim44 of mitochondrial import motor with channel-forming translocase subunit Tim23. *Elife* 6.

- Tobias, J., Shrader, T., Rocap, G., and Varshavsky, A. (1991). The N-end rule in bacteria. *Science* 254, 1374-1377.
- Truscott, K.N., Kovermann, P., Geissler, A., Merlin, A., Meijer, M., Driessen, A.J., Rassow, J., Pfanner, N., and Wagner, R. (2001). A presequence- and voltage-sensitive channel of the mitochondrial preprotein translocase formed by Tim23. *Nat Struct Biol* 8, 1074-1082.
- Truscott, K.N., Voos, W., Frazier, A.E., Lind, M., Li, Y., Geissler, A., Dudek, J., Muller, H., Sickmann, A., Meyer, H.E., *et al.* (2003). A J-protein is an essential subunit of the presequence translocase-associated protein import motor of mitochondria. *J Cell Biol* 163, 707-713.
- van der Laan, M., Chacinska, A., Lind, M., Perschil, I., Sickmann, A., Meyer, H.E., Guiard, B., Meisinger, C., Pfanner, N., and Rehling, P. (2005). Pam17 is required for architecture and translocation activity of the mitochondrial protein import motor. *Mol Cell Biol* 25, 7449-7458.
- van der Laan, M., Wiedemann, N., Mick, D.U., Guiard, B., Rehling, P., and Pfanner, N. (2006). A role for Tim21 in membrane-potential-dependent preprotein sorting in mitochondria. *Curr Biol* 16, 2271-2276.
- Vogtle, F.N., Wortelkamp, S., Zahedi, R.P., Becker, D., Leidhold, C., Gevaert, K., Kellermann, J., Voos, W., Sickmann, A., Pfanner, N., *et al.* (2009). Global analysis of the mitochondrial N-proteome identifies a processing peptidase critical for protein stability. *Cell* 139, 428-439.
- von Heijne, G. (1986). Mitochondrial targeting sequences may form amphiphilic helices. *Embo j* 5, 1335-1342.
- Waegemann, K., Popov-Celeketi, D., Neupert, W., Azem, A., and Mokranjac, D. (2015). Cooperation of TOM and TIM23 complexes during translocation of proteins into mitochondria. *J Mol Biol* 427, 1075-1084.
- Wagener, N., Ackermann, M., Funes, S., and Neupert, W. (2011). A pathway of protein translocation in mitochondria mediated by the AAA-ATPase Bcs1. *Mol Cell* 44, 191-202.
- Wang, Y., Katayama, A., Terami, T., Han, X., Nunoue, T., Zhang, D., Teshigawara, S., Eguchi, J., Nakatsuka, A., Murakami, K., *et al.* (2015). Translocase of inner mitochondrial membrane 44 alters the mitochondrial fusion and fission dynamics and protects from type 2 diabetes. *Metabolism* 64, 677-688.
- Weiss, C., Oppliger, W., Vergères, G., Demel, R., Jenö, P., Horst, M., de Kruijff, B., Schatz, G., and Azem, A. (1999). Domain structure and lipid interaction of recombinant yeast Tim44. *Proceedings of the National Academy of Sciences* 96, 8890-8894.
- Wenz, L.S., Opalinski, L., Schuler, M.H., Ellenrieder, L., Ieva, R., Bottinger, L., Qiu, J., van der Laan, M., Wiedemann, N., Guiard, B., *et al.* (2014). The presequence pathway is involved in protein sorting to the mitochondrial outer membrane. *EMBO Rep* 15, 678-685.
- Wiedemann, N., and Pfanner, N. (2017). Mitochondrial Machineries for Protein Import and Assembly. *Annu Rev Biochem* 86, 685-714.
- Wrobel, L., Sokol, A.M., Chojnacka, M., and Chacinska, A. (2016). The presence of disulfide bonds reveals an evolutionarily conserved mechanism involved in mitochondrial protein translocase assembly. *Scientific Reports* 6, 27484.
- Xu, X., Qiao, M., Zhang, Y., Jiang, Y., Wei, P., Yao, J., Gu, B., Wang, Y., Lu, J., Wang, Z., *et al.* (2010). Quantitative proteomics study of breast cancer cell lines isolated from a single patient: discovery of TIMM17A as a marker for breast cancer. *Proteomics* 10, 1374-1390.

- Yablonska, S., Ganesan, V., Ferrando, L.M., Kim, J., Pyzel, A., Baranova, O.V., Khattar, N.K., Larkin, T.M., Baranov, S.V., Chen, N., *et al.* (2019). Mutant huntingtin disrupts mitochondrial proteostasis by interacting with TIM23. *Proc Natl Acad Sci U S A* *116*, 16593-16602.
- Yamamoto, H., Esaki, M., Kanamori, T., Tamura, Y., Nishikawa, S., and Endo, T. (2002). Tim50 is a subunit of the TIM23 complex that links protein translocation across the outer and inner mitochondrial membranes. *Cell* *111*, 519-528.
- Zarsky, V., and Dolezal, P. (2016). Evolution of the Tim17 protein family. *Biol Direct* *11*, 54.

Abreviations

5-FOA	5-fluoroorotic acid
AAC	ADP/ATP carrier
ADP	Adenosine diphosphate
Amp	Ampicillin
APS	Ammonium persulfate
ATP	Adenosine triphosphate
BN-PAGE	Blue native polyacrylamide gel electrophoresis
Bpa	p-benzoyl-L-phenylalanine
BSA	Bovine serum albumin
C-	Carboxy-
DHFR	Dihydrofolate reductase
DiSC ₃ (5)	3,3'-Dipropylthiadicarbocyanine Iodide
DMSO	Dimethyl sulfoxide
DNA	Deoxyribonucleic acid
dNTP	Deoxyribonucleoside triphosphate
DSG	Disuccinimidyl glutarate
DTT	Dithiotreitol
<i>E. coli</i>	<i>Escherichia coli</i>
EDTA	Ethylendiaminetetraacetate
F1 β	F1 β subunit of the ATP synthase
FL	Full length
FP	Forward primer
GPD	glyceraldehyde-3-phosphate dehydrogenase
HEPES	4-(2-hydroxyethyl)-1-piperazineethanesulfonic acid
His	Histidine
Hsp	Heat shock protein
Igg	Immunoglobuline G
IM	Inner membrane
IMS	Inter membrane space
IP	Immunoprecipitation
kDa	Kilodalton
LB	Luria Bertani
mtDNA	Mitochondrial DNA
MTS	Mitochondrial targeting sequence
N-	Amino-
NADH	nicotinamide adenine dinucleotide

NBD	Nucleotide binding domain
ncDNA	Nuclear DNA
NEF	Nucleotide exchange factor
NiNTA	Nickel-nitrilotriacetic acid
NMR	Nuclear magnetic resonance
OD _x	Optical density at x nm wavelength
OM	Outer membrane
OXA	Oxidase assembly
PAGE	Polyacrylamide gel electrophoresis
PAS	Protein A sepharose
PCR	Polymerase chain reaction
PEG	Polyethylene glycol
PI	Pre-immune serum
PK	Proteinase K
PMSF	Phenylmethylsulfonyl fluoride
prom-X-flank	promoter-X (gene)-flanking region
PVDF	Polyvinylidene difluoride
RNA	Ribonucleic acid
RNase	Ribonuclease
RP	Reverse primer
RT	Room temperature
<i>S. cerevisiae</i>	<i>Saccharomyces cerevisiae</i>
SAM	Sorting and assembly machinery
SBD	Substrate binding domain
SC	Sub-cloning
SD	Synthetic defined
SDM	Site directed mutagenesis
SDS	Sodium dodecyl sulphate
TAE	Tris base, acetic acid, EDTA
TBS	Tris-buffered saline
TCA	Trichloroacetic acid
TEMED	N,N,N',N'-tetramethylene-1,2-diamine
TIM	Translocase of the inner mitochondrial membrane
TM	Transmembrane segment
TOB	Topogenesis of mitochondrial outer membrane β -barrel proteins
TOM	Translocase of the outer mitochondrial membrane
Tris	Tris(hydroxymethyl)aminomethane
v/v	Volume per volume

w/v	Weight per volume
WT	Wild type
YPD	Yeast extract-Peptone-Dextrose
YPGal	Yeast extract-Peptone-Galactose
YPLac	Yeast extract-Peptone-Lactate
$\Delta\Psi$	Membrane potential

Publications from this thesis

A large part of this thesis has already been published by the author in the publications listed below. There is no specific hint in the text to reveal this point.

Günsel, U., Paz, E., Gupta, R., Mathes, I., Azem, A., and Mokranjac, D. (2020). InVivo Dissection of the Intrinsically Disordered Receptor Domain of Tim23. *J Mol Biol* 432, 3326-3337.

Günsel, U., and Mokranjac, D. (2019). A journey along the TIM23 complex, the major protein translocase of the mitochondrial inner membrane. *Biologia Serbica* 41, 27-35.

Dayan, D., Bandel, M., **Günsel, U.**, Nussbaum, I., Prag, G., Mokranjac, D., Neupert, W., and Azem, A. (2019). A mutagenesis analysis of Tim50, the major receptor of the TIM23 complex, identifies regions that affect its interaction with Tim23. *Sci Rep* 9, 2012.

Malhotra, K., Modak, A., Nangia, S., Daman, T.H., **Günsel, U.**, Robinson, V.L., Mokranjac, D., May, E.R., and Alder, N.N. (2017). Cardiolipin mediates membrane and channel interactions of the mitochondrial TIM23 protein import complex receptor Tim50. *Sci Adv* 3, e1700532.

Demishtein-Zohary, K.*, **Günsel, U.***, Marom, M., Banerjee, R., Neupert, W., Azem, A., and Mokranjac, D. (2017). Role of Tim17 in coupling the import motor to the translocation channel of the mitochondrial presequence translocase. *Elife* 6.

Banerjee, R.*, **Günsel, U.***, and Mokranjac, D. (2017). Chemical crosslinking in intact mitochondria. *Methods Mol Biol.* 1567:139-154.

***Equally contributing authors**

Acknowledgements

Now it has come to thank and to express my gratitude to everyone who has supported and helped me during all these years towards my PhD.

I shall start by expressing my deepest gratitude to my supervisor, PD. Dr. Dejana Mokranjac, for giving me the opportunity to work in her Lab. Her valuable guidance and support was always there whenever I needed. Her expertise in the field and her discipline truly taught me a lot; not only about my project, but also about science in general. I consider myself extremely lucky that I could work in one of the earlier steps of my carrier with a genuinely passionate and dedicated scientist.

I thank my earliest lab mate in this lab, Rupa Banerjee, for being a very helpful colleague and a great friend. We shared many scientific and non-scientific memories together. I also thank to my later lab mate, Marcel Genge, for being a very nice colleague and a helpful friend. I had lots of fun with both and I am sure that the lab would not be the same without them.

I truly appreciate Petra Robisch for her technical assistance in the lab and her helps in general.

I am thankful to Prof. Dr. Andreas Ladurner and all the members of his department for being the part of a cooperative and supportive work atmosphere. I thank to Christine Werner, Dr. Anton Eberharter and Dr. Corey Laverty for making life in the department much easier by taking care of all the administrative work required. I also thank to Zdenka Stanic and Marianne Köber for their technical assistance and services.

I would like to thank all the members of our weekly MitoClub seminars, groups of Prof. Dr. Dr. Walter Neupert, Dr. Kai Hell, Prof. Dr. Barbara Conradt, Prof. Dr. Christof Osman, Dr. Nikola Wagener, Dr. Max Harner and Dr. Stephane Rolland, for their precious valuable discussions and comments.

I would also like to thank to my colleagues and good friends in the department; Julia Preißer, Thomas Pysik, Moritz Resch, Shao-Yen Kao, Hui-Lan Huang and Flavia Söllner, for their generous helps and the precious moments that we had together.

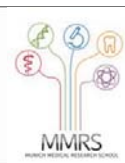
I thank to my students, Ruhita Gupta and William Rivers for their efforts while working with me in the lab.

Sevgili hayat arkadaşım Gizem Güneş Günsel'e doktora çalışmalarım süresince ve günlük hayatta her zaman yanımda olduğu, beni desteklediği ve de bu inişli-çıkışlı yolda zaman zaman da bana katlandığı için derinden teşekkür ederim. Ayrıca Münih'teki kardeşlerime geçirdiğimiz güzel zamanlar için teşekkür ederim.

Son olarak sevgili ailem Cengiz Günsel, Naciye Günsel ve Özer Günsel'e bugünlere gelmemdeki büyük paylarından dolayı ve her zaman beni koşulsuzca maddi, manevi her türlü destekledikleri için sonsuz minnetlerimi sunarım.



Dean's Office
Faculty of Medicine



Affidavit

Günsel, Umut

Surname, first name

[REDACTED]

Street

[REDACTED]

Zip code, town

Germany

Country

I hereby declare, that the submitted thesis entitled

Functional dissection of the Tim17-Tim23 core of the mitochondrial presequence translocase

is my own work. I have only used the sources indicated and have not made unauthorised use of services of a third party. Where the work of others has been quoted or reproduced, the source is always given.

I further declare that the submitted thesis or parts thereof have not been presented as part of an examination degree to any other university.

12.09.2020

Place, date

Umut Günsel

Signature doctoral candidate